PCBBE 2023

XXIII Polish Conference on Biocybernetics
and Biomedical Engineering
Lodz, Poland, 27–29 September 2023

BOOK OF ABSTRACTS

Paweł Strumiłło, Artur Klepaczko, Michał Strzelecki, Dorota Bociąga (editors)

Paweł Strumiłło · Artur Klepaczko · Michał Strzelecki · Dorota Bociąga

Editors

XXXIII Polish Conference on Biocybernetics and Biomedical Engineering

BOOK OF ABSTRACTS

Preface

This book is a collection of abstracts submitted to the XXIII Polish Conference on Biocybernetics and Biomedical Engineering PCBBE 2023 held in Łódź, Poland, from 27 to 29 September 2023. The conference was organized by the Committee of Biocybernetics and Biomedical Engineering of the Polish Academy of Science and hosted by two research units of the Lodz University of Technology – Institute of Electronics, main local organizer, and Institute of Material Science and Engineering, a co-organizer. PCBBE is the biannual event which has been held for over four decades and has gained the status of one of the most important national conferences in computer science and engineering for healthcare. It covers a broad spectrum of fields including artificial intelligence, biomedical image and signal processing, medical physics, computer-assisted intervention, biocybernetics and materials engineering.

The abstracts are grouped into chapters corresponding to a regular track and 9 special thematic tracks and include:

- Applications of Deep Learning in Biomedical Image Analysis
- Biomaterials and Implants
- Biomaterials for Controlled Delivery of Biologically Active Substances
- Biomodelling and Machine Learning in Cancer Diagnosis and Prediction of Metastases
- Electromagnetics in Biology and Medicine
- Hybrid Analysis of Multimodal Medical Data
- Information Content Analysis in Cardiovascular and Respiratory Systems
- Mathematical and Computational Modeling in Physiology, Medicine and Biomedical Engineering
- Texture Analysis in Biomedical Imaging

A separate submission path in the conference was dedicated to authors who wanted to disseminate their research in the form of a full paper. These contributions were published in Volume 746 of the Springer's Lecture Notes in Networks and Systems series (*The Latest Developments and Challenges in Biomedical Engineering*).

We would like to express our deepest gratitude to the reviewers who took the time to evaluate the abstracts and also the full papers. To honor their impact on the substantive value of the conference, a list of all reviewers' names is included at the end of this book. Heartfelt thanks are also due to the chairmen of the special sessions, who invited the authors to submit their works, supported the organizers in the submission process, and thus remarkably contributed to the high scientific output of PCBBE 2023. Their names appear in subtitles of the thematic track chapters. Eventually, congratulations to all the authors for their continuous effort to advance the studies in various fields of biocybernetics and active participation in scientific endeavors of the biomedical engineering community in Poland.

Łódź, Poland

Paweł Strumiłło
Artur Klepaczko
Michał Strzelecki
Dorota Bociąga

The website

For more information about the conference, inlcuding full presentations program, please visit our website: https://pcbbe.p.lodz.pl/.
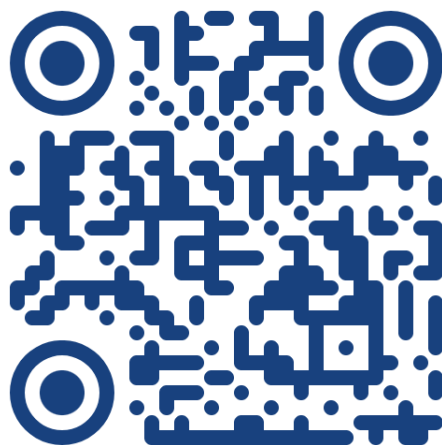
Patronage

HONORARY PATRONAGE

Prof. Marek Konarzewski

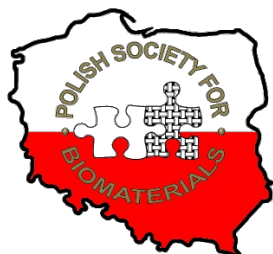PRESIDENT OF THE POLISH ACADEMY OF SCIENCES

Prof. Józef Modelski

UNION RADIO-SCIENTIFIQUE INTERNATIONALE –
INTERNATIONAL UNION OF RADIO SCIENCE
POLISH NATIONAL COMMITTEE

Prof. Elżbieta Pamuła

POLISH SOCIETY FOR BIOMATERIALS (PSB)

MEDIA PATRONAGE

Sponsors

Contents

Regular Track

Applications of Deep Learning in Biomedical Image Analysis

Biomaterials and Implants

Biomaterials for Controlled Delivery of Biologically Active Substances

Biomodelling and Machine Learning in Cancer Diagnosis and Prediction of Metastases

Electromagnetics in Biology and Medicine

Hybrid Analysis of Multimodal Medical Data

Information Content Analysis in Cardiovascular and Respiratory Systems

Mathematical and Computational Modeling in Physiology, Medicine and Biomedical Engineering

Texture Analysis in Biomedical Imaging

Chapter I

Regular Track

Feature extraction and classification of EEG signal in the task of motor activity recognition

Patryk Amsolik[1], Bartłomiej Sztyler[2], Stanisław Zakrzewski[1], Bartłomiej Stasiak[1], Adam Wojciechowski[1]

[1]Institute of Information Technology, al. Politechniki 8, 93-590, Lodz University of Technology

[2]Institute of Electronics, al. Politechniki 10, 93-590, Lodz University of Technology, Poland

[1]bartlomiej.stasiak@p.lodz.pl

This study was devoted to the analysis of EEG signals collected over sensorimotor cortex. The aim was to recognize hand motor activity of a user, either imagined or real, and to select the most effective approach yielding sufficiently reliable classification results that would be useful in real-life applications. This task is considered within an important and actively explored research area of BCI (brain-computer interface) with many potential applications e.g. in neurorehabilitation of post-stroke patients.

In our approach, pre-processing of the EEG signal included band-pass filtering (4Hz – 35Hz) and computation of CAR (Common Average Reference). Three methods of EEG signal analysis and feature extraction were used and compared: based on a raw EEG signal spectrogram, based on CSP (Common Spatial Pattern) [1] and on PARAFAC (Parallel Factor Analysis) [2]. Finally, the obtained features were used for classification with an MLP classifier (Multi-Layer Perceptron). Ten EEG channels (C3, C1, CP3, C5, FC3, C4, C6, CP4, C2, FC4) were used as the signal source. For our experiments a dataset containing EEG signal recordings of 52 subjects performing either motor or motor imagery hand movements was used [3]. Each subject performed 100 or 120 trials for left/right hand motor imagery movement (7-8 seconds per trial). The number of trials involving real motor activity (non-imaginary), available in the database, was significantly lower. For both data types (imaginary/real movement) and for each of the three classification methods, the dataset was split into three parts: train (60%) validation (20%) and test (20%).
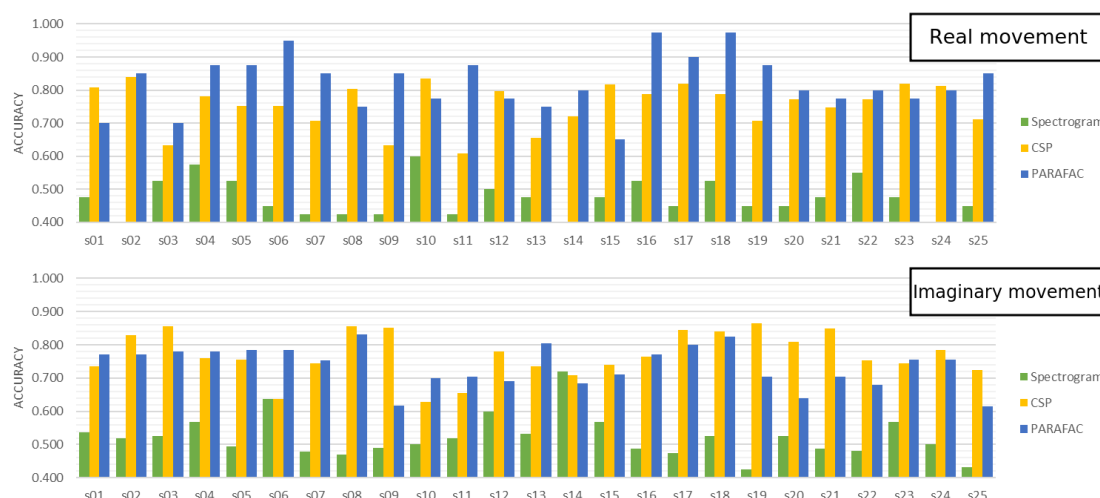
The classification results obtained for the first 25 subjects are presented above. The first conclusion is that the raw spectrogram was definitely inferior than two other, more sophisticated methods. Interestingly, CSP often performed better than PARAFAC in imaginary movement recognition, while PARAFAC was significantly more useful in the case of real movements, exceeding 95% for some subjects. The reason for this observation may be related to the number of trials available and to the fact that CSP is basically a *supervised method* which directly aims at maximization of differences in variance between the output signals it produces. Having more data in the imaginary movement dataset probably created better conditions for CSP training and yielded better results with respect to PARAFAC. This may lead to formulation of some practical clues regarding the choice of the preferred EEG feature extraction method in future works.

References:

[1] G. Pfurtscheller, C. Guger and H. Ramoser, *EEG-based brain-computer interface using subject-specific spatial filters*, Engineering applications of bio-inspired artificial neural networks, LNCS, 1999, Vol. 1607/1999, pp. 248-254;

[2] R. Rosipal, Z. Rošťáková and L. J. Trejo, *Tensor decomposition of human narrowband oscillatory brain activity in frequency, space and time*, Biological Psychology, 2022, Vol. 169;

[3] H. Cho, M. Ahn, S. Ahn and M. Kwon, *EEG datasets for motor imagery brain computer interface* GigaScience, 2017, Vol. 6 (7);

A new approach to identifying an individual's quantitative color vision sensitivity

Szymon Antonowicz[1], Julia Miziołek[1], Zuzanna Ratajczyk[1], Sandra Zmysłowska[1], Joanna Szkudlarek[2]
[1] Lodz University of Technology, [2] Central Institute for Labour Protection-National Research Institute
joszk@ciop.lodz.pl

People with color vision dysfunction face many problems when choosing a career path or performing daily activities. Currently available tests used to diagnose the accuracy of color vision simply categorize the test participants as either people with normal color vision or those with color vision dysfunction. There is no efficient tool for quantitative assessment of the level of color vision loss for people with partial color vision deficits caused by non-genetic defects. As a result, people with only partial color vision loss may experience professional exclusion and lack of development opportunities [1]. There is a need to develop a sufficiently sensitive tool/test to assess color vision, which will quantitatively enable the assessment of the individual level of color vision. Based on such an approach, it will be possible to determine a standardized scale in relation to color vision sensitivity.

Studies have shown that color vision is an individual trait that can be quantitatively assessed. An investigation was conducted to identify levels of color vision using two publicly available color vision tests. The first one involved matching color elements of varying saturation, brightness, and color combination, enabling the determination of color vision sensitivity and their recognition. The second indicated the boundary of color vision in the range of red-green (R-G) and yellow-blue (Y-B) color channels.

The study was conducted on a group of 38 volunteers aged 18-66 years. The results indicate that among the surveyed population, 11% of people have a reduced level of color vision. Based on the results obtained, a five-level color vision sensitivity scale was developed. The presented research is preliminary in nature, serving to determine the assumptions for the construction of a research position for effective (quantitative and qualitative) assessment of color vision ability.

The development of a sufficiently sensitive tool for assessing color vision will improve the quality of life for people with a mild deficit and their inclusion in professional activities. On the other hand, for people with correct color vision, the proposed assessment system will mean a more accurate diagnosis. The obtained results will allow for future collaboration with medical examiners from the Institute of Occupational Medicine and for the determination of appropriate legal regulations in this regard.

References:
[1] Rodriguez-Carmona, M., O'Neill-Biba, M., & Barbur, J. L. (2012). Assessing the severity of color vision loss with implications for aviation and other occupational environments. *Aviation, space, and environmental medicine*, *83*(1), 19-29.

Evaluation of the Influence of Fabrication Techniques on the Photocatalytic Activity of TiO2 Thin Films

Zofia Błaszczyk, Dominika Kowalska, Rukudzo Chihota

Politechnika Łódzka, Instytut Inżynierii Materiałowej, ul. Stefanowskiego 1/15 90-924 Łódź

E-mail: 236029@edu.p.lodz.pl

This article focuses on investigating the photocatalytic activity of TiO2 thin films fabricated using different methods. The growing interest in utilizing the photocatalytic properties of TiO2 in the fields of biomedicine and materials engineering has prompted this study. TiO2 coatings exhibit potential for eradicating pathogenic microorganisms, degrading biological pollutants, and promoting tissue regeneration. Therefore, in order to fully understand these promising applications comprehensively, it is imperative to evaluate the influence of commonly employed production methods on the resulting TiO2 film's photocatalytic performance.

Titanium samples were employed as substrates for depositing TiO2 thin films using three distinct techniques: the sol-gel method, low-voltage electrolytic method, and high-voltage electrolytic method. To characterize the fundamental properties of the fabricated films, preliminary assessments were conducted, including surface morphology analysis using scanning electron microscopy and optical microscopy, roughness analysis, and thickness measurements. The photocatalytic effect was assessed by monitoring changes in the contact angle of the TiO2 films following exposure to UV light.

The results revealed that coatings produced via the sol-gel method exhibited the highest hydrophilicity, indicating the most promising photocatalytic properties. The high-voltage electrolytic method yielded porous coatings with pronounced hydrophilicity, in contrast to the low-voltage electrolytic method which produced relatively smooth, thin coatings with significantly lower hydrophilicity, thus demonstrating less promising photocatalytic activity.

Based on the obtained findings, it is evident that the photocatalytic activity of TiO2 films is contingent upon the employed production method and its associated parameters. This aspect is crucial in selecting an appropriate method for specific applications, such as employing TiO2 as a self-cleaning agent where high hydrophilicity and a high photocatalytic activity rate are imperative.

References:
[1] K. G. Relationship between photocatalytic activity, hydrophilicity and self-cleaning effect of TiO2/SiO2 films, Surface & Coatings Technology, 2005, no. 191, str. 155 – 160
[2] M. J. Photoactive titanium dioxide thin films deposited by reactive gas impulse magnetron sputtering (GIMS), 2016, no. 3, str. 53-59

YOLO AI method for lesion detections in PET/CT exams

Pawel Bzowski[1,2][0000−0002−0689−1006] and Damian Borys[1,2][0000−0003−0229−2601]

[1] Department of Systems Biology and Engineering, Silesian University of Technology,
ul. Akademicka 16, 44-100 Gliwice, Poland
[2] Maria Sklodowska-Curie National Research Institute of Oncology (MSCNRIO),
Gliwice branch, ul. Wybrzeze AK 15, 44-100 Gliwice, Poland

pawel.bzowski@io.gliwice.pl

Developments in technology and medicine have led to the generation of large amounts of imaging data in ever shorter periods of time. In addition, modern equipment allows precise and accurate detection of even the smallest changes in medical images. The enormity of the data has made the waiting time for the doctor to analyze it longer. The use of artificial intelligence methods that allow searching for pathological changes in the patient's body is becoming helpful here.

The aim of the study was to teach the YOLO neural network to detect the physiological distribution of the 18F-FDG radiolabel for PET imaging, and then remove the signal from the PET image to visualize pathological changes

The network software RoboFlow was used for the work. Two collections were used in the work. The first learning set consisted of 15 real PET-CT studies. MIP projections from 11 different angles were created from each PET series. The physiological uptake of organs such as the brain, heart, left kidney, right kidney and urinary bladder was then marked on the
resulting 165 images. The learned network was tested on 20 images. Finally, the effects of the network's automatic performance were compared with manual evaluation

Areas selected by artificial intelligence were compared with those determined by humans. Assuming that the human had delineated the basic organs well, the quality of the artificial intelligence-based system's delineation was checked. The number of times the algorithm correctly selected a structure was calculated, confidence threshold of more than 40% was taken into account. The urinary bladder was correctly detected at 70%, the brain at 55%, the left kidney at 35%, the heart at 30%, and the right kidney at only 10%. Conclusion The results obtained confirm the usefulness in detecting organs based on physiological uptake of the radioisotope. It gives the possibility to remove the physiological signal from the image, so that only the signal that may indicate pathological uptake remains. This makes it possible to create an algorithm that will assist physicians during the analysis of PET scans or, in the future, allow automatic analysis of the scans

References:

[1] Joseph Redmon, Santosh Kumar Divvala, Ross B. Girshick, Ali Farhadi. You only look once: Unified, real-time object detection. CoRR, abs/1506.02640, 2015.

[2] Masashi Kawakami, Hiroyuki Sugimori, Kenji Hirata, Chietsugu Katoh. Evaluation of automatic detection of abnormal uptake by deep learning and combination technique in FDG-PET images. Journal of Nuclear Medicine, 61(supplement 1):3007–3007, 2020.

[3] Saeedeh Afshari, Aicha Bentaieb, Ghassan Hamarneh. Automatic localization of normal active organs in 3d pet scans. Computerized Medical Imaging and Graphics, 70, 09 2018.

Reconstruction of the cephalometric image based on magnetic resonance imaging

Piotr Cenda[1], Adam Cieślak[1], Elżbieta Pociask[1], Rafał Obuchowicz[2], Adam Piórkowski[1]
AGH University of Science and Technology,
Mickiewicza 30 Av., 30-059 Kraków, Poland
Jagiellonian University Medical College,
Kopernika 19, 31-501 Kraków, Poland
cenda@student.agh.edu.pl

Cephalometric images are the basic examination in orthodontic treatment, allowing to diagnose malocclusion and plan orthodontic treatment. Unfortunately, such tests, especially when performed in childhood, increase the risk of complications. Numerous scientific papers in reputable journals [1,2] indicate a significant correlation between the performance of tests with ionizing radiation in children under 10 years of age with the occurrence of meningiomas in the future (almost five-fold increase in risk). This problem has raised the question of whether it is possible to obtain a similar reconstruction from MRI.

First, two image series obtained from T1-weighted and T2-weighted magnetic resonance sequences underwent geometric transformation for spatial alignment. Next, bone and soft tissue segmentation was conducted using specific morphological operations and sequence correlation. The resulting segmented masks were then interpolated and projected onto the chosen plane, generating a unified image.

Fig.1. Sample MRI images for different patients: generated (a) and the original (b) [3].

The developed methodology aims to reconstruct a cephalometric-like image, replacing harmful ionizing radiation methods like cephalometry. Despite air segmentation limitations causing distortions in the output, the method resembles cephalometric imaging, excluding crucial areas like cervical vertebrae and dentition used in dental treatment. By increasing the sections in MRI sequences, accuracy and legibility would improve, reducing the impact of interpolation on image integrity. The method primarily describes human cerebral, craniofacial, and cervical vertebrae structures, serving as an initial screening and diagnostic test for cephalometric images. Clear sinus imaging can also aid in identifying sinusitis or other pathologies. Despite its limitations, the algorithm can guide whether further diagnostic steps are necessary.

References:
[1] Claus, E. B., Calvocoressi, L., Bondy, M. L., Schildkraut, J. M., Wiemels, J. L., Wrensch, M.. Dental x-rays and risk of meningioma: Dental X-Rays and Risk of Meningioma. *Cancer*, 2012, 118, pp. 4530–4537.
[2] Hwang, S.-Y., Choi, E.-S., Kim, Y.-S., Gim, B.-E., Ha, M., & Kim, H.-Y. Health effects from exposure to dental diagnostic X-ray. Environmental Health and Toxicology, 2018, 33(4), e2018017.
[3] Cenda, P., Obuchowicz, R., Piórkowski, A. Construction of a Cephalometric Image Based on Magnetic Resonance Imaging Data. In *International Conference on Information Technologies in Biomedicine, 2022*, pp. 143-154.

Variation of electromyography patterns during gait in healthy children

Kristina Daunoraviciene[1], Jurgita Ziziene[1], Jolanta Pauk[2]

[1]Vilnius Gediminas Technical University, Department of Biomechanical Engineering, Plytines g. 25, Vilnius, Lithuania
[2]Bialystok University of Technology, Biomedical Engineering Institute, Wiejska 45C, 15-351 Bialystok, Poland, j.pauk@pb.edu.pl

Electromyography (EMG) patterns can vary based on individual factors such as age, sex, and physical development. Here are some common variations: activation of lower limb muscles, timing of muscle activation, muscle activity level, and muscle co-contraction. The aim of this paper is to present the variation of electromyography patterns during gait in healthy children. The study involved 17 healthy kids aged 4–11 years Five muscles per leg were selected for examination, biceps femoris (BF), rectus femoris (RF), semitendinosus (SE), lateral gastrocnemius (LG), and medial gastrocnemius (MG), 10 EMG wireless sensors (Delsys Trigno) were attached to the skin. A total of 171 trials were further processed. The experimental protocol was approved by the regional ethical review board (No. 2020/9-1256-738). The EMG data collected were pre-processed in the following order: filtered with a high-frequency 4th order zero-phase Butterworth filter with a 50 Hz cut-off frequency; filtered with a zero-lag low-frequency 2nd order Butterworth filter with a 6 Hz cut-off frequency; cropped from heel contact to heel contact to strides; transformed using the Teager-Kaiser Energy Operator (TKEO); subjected to full-wave rectification; and smoothed. The EMG curves were normalized to 100%. Statistical analysis was perfomed by using Shapiro-Wilk test. The variation of electromyography patterns during gait in healthy children was presented in Fig.1.
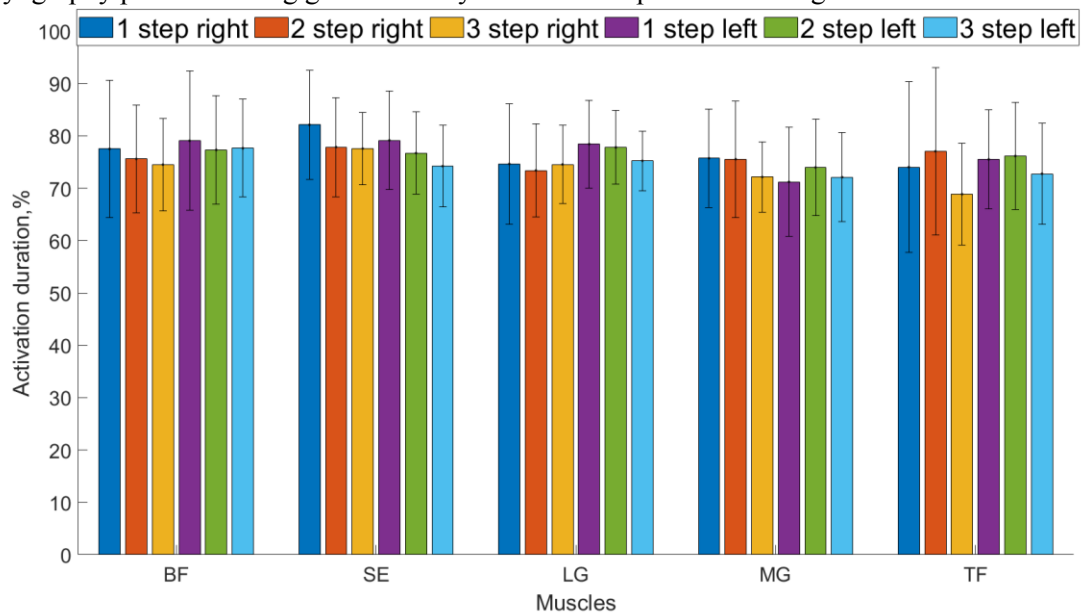
Figure 1. Variation of electromyography patterns during gait in healthy children: comparison of three steps on both sides right and left. Activation duration represented as mean± SD of muscles in % of stride.

Detailed analysis showed that activation duration in first stride significantly *(p<0.05)* longer in LG, SE and BF muscles in comparing with MG muscle and in SE muscle in comparing with TF muscle. But activation duration in third stride is significantly shorter in MG and TF muscles in comparing with BF and SE muscles. Muscle activation may start at the beginning of one stride and end in another, and secondary muscle activation may also occur. Knowing the variation of EMG patterns during gait in healthy children can provide valuable insights into the development and function of the neuromuscular system during gait, and can inform clinical interventions and research studies related to gait analysis and rehabilitation.

References:
[1] Daunoraviciene K., Ziziene J., Pauk J., Juskeniene G., Raistenskis J. EMG based analysis of gait symmetry in healthy children. Sensors, 2021, 21, 17, 5983; https://doi.org/10.3390/s21175983.
[2] Kim J., Chung C.Y., Park M.S., Choi I H. Differences in muscle activity during gait between children with and without flatfeet. Journal of Electromyography and Kinesiology, 2010, 20, 4, 667-672. doi: 10.1016/j.jelekin.2009.10.010.

Effect of non-thermal atmospheric plasma treatment to accelerate diabetic wound healing

Sara Fathollah[1,2,*], Piotr Sawosz[1], Shahriar Mirpour[3], Ahmad Reza Dehpour[4], Mahmood Ghoranneviss[2], Parvin Mansouri[5]

1. Institution Nałęcz Institute of Biocybernetics and Biomedical Engineering, Polish Academy of Sciences, Ks. Trojdena 4, 02-109 Warsaw, Poland.
2. Plasma Physics Research Center, Science and Research branch of Islamic Azad University, Tehran, Iran.
3. Department of Applied physics, Eindhoven university of Technology, Eindhoven, The Netherlands.
4. Experimental Medicine Research Center, Tehran University of Medical Science, Tehran, Iran.
5. Skin and Stem Cell Research Center, Tehran University of Medical Sciences, Tehran, Iran.
*Corresponding Author Email: sfathollah@ibib.waw.pl

Aims: The purpose of this study is to evaluate the effect of non-thermal plasma on diabetics wound healing. Wound healing is a common concern among diabetic patients, who experience complications due to neuropathy, vascular disease, and foot deformities [1-2]. The use of a plasma jet to ionize helium gas can generate ions and free radicals, leading to sterilization and chemical processes that aid in wound healing and tissue repair [3-4].

Materials and Methods: A plasma jet was used to generate helium plasma at a frequency of 6 kHz and 8 kV. The study included three groups of male rats, each containing five rats. After each rat's weight reached 300 ± 25 grams, 60 mg/kg of intravenous Streptozotocin (STZ) was injected to induce diabetes. After four days of injection, the rats were anesthetized and excisional wounds were inflicted, with the wound area measuring approximately 2 ± 0.1 cm. The helium plasma was then exposed to one of the experimental groups for 10 minutes, while another group was treated with helium gas, and the control group received no treatment under dressing. The plasma exposure, the size of the incision cross-sectional area, blood glucose levels, and tissue pathology were evaluated and compared among the groups for 30 days.

Results: After just one session of plasma treatment, the wounds in the experimental group had healed completely compared to the control and helium gas samples. Histological analyses revealed the formation of an epidermal layer, neovascularization, and cell proliferation. The plasma treatment also resulted in the release of TGF-β1 cytokine from cells in the tissue medium.

Conclusion: This study demonstrates the potential of atmospheric pressure plasma as an effective treatment for diabetic wounds which requires improvement in microcirculation, oxygen, and nutrients supply to the tissue. In continuation of these experiments, we aim to investigate the blood flow variation during wound healing process using an optical technique of the diffuse correlation spectroscopy and assess the possible influences of cold plasma treatment on this procedure.

References:
[1] Balakumar P, Maung-U K, Jagadeesh G. Prevalence and prevention of cardiovascular disease and diabetes mellitus. *Pharmacological research*. 2016 Nov 1;113:600-9.
[2] Armstrong DG, Boulton AJ, Bus SA. Diabetic foot ulcers and their recurrence. *New England Journal of Medicine*. 2017 Jun 15;376(24):2367-75.
[3] Jung JM, Yoon HK, Jung CJ, Jo SY, Hwang SG, Lee HJ, Lee WJ, Chang SE, Won CH. Cold plasma treatment promotes full-thickness healing of skin wounds in murine models. *The International Journal of Lower Extremity Wounds*. 2023 Mar;22(1):77-84.
[4] Xu GM, Shi XM, Cai JF, Chen SL, Li P, Yao CW, Chang ZS, Zhang GJ. Dual effects of atmospheric pressure plasma jet on skin wound healing of mice. *Wound Repair and Regeneration*. 2015 Nov 12;23(6):878-84.

Optimization of the optode configuration in subtraction-based time-domain Near Infrared Spectroscopy

Elham Fazliazar, Aleh Sudakou, Anna Gerega, and Adam Liebert

Institute of biocybernetics and biomedical engineering (IBIB, PAN), Trojdena 4 st., 02-109 Warsaw, Poland

efazli@ibib.waw.pl

Aims: Near Infrared Spectroscopy (NIRS) is a noninvasive optical method with an application for the assessment of tissue oxygenation. A serious obstacle for this method is the contamination of signals originated in brain cortex by the signal originated in the extracerebral layer. Time-domain-NIRS (td-NIRS) which is based on the injection of ultra-short laser pulses into tissue, can reduce this problem by increasing the sensitivity to the deeper layer. As the order of statistical moments of the distribution of time of flight of photons (DTOF) from source to detector measured by td-NIRS increases and/or the source-detector separation (ρ) increases, the maximal sensitivity moves towards deeper layers. Unfortunately, this also results in a decrease in the contrast to noise ratio (CNR). Subtraction-based methods were introduced to provide more suppression of the contamination of extracerebral layer in td-NIRS. Recently, a dual subtraction method was introduced, which exploits the advantages of using an average of two single subtractions [1]. Decreasing the distance between two detectors (Fig. 1.a) causes the maximal sensitivity to shift towards the deeper layers, but also causes the CNR to decrease. This trade-off between the depth selectivity, which is a ratio of sensitivity in the deep layer compared to the superficial layer, and the CNR is a topic that has not yet been quantitatively analyzed in subtraction-based methods. In the present work, we study this trade-off for single distance and dual subtraction methods with a variety of optode arrangements with the use of Monte Carlo (MC) simulations.

Methods: We ran MC simulations to generate DTOFs before and after selective changing the absorption coefficients in a 2-layered medium, representing the deep and superficial layers of tissue. We repeated simulations for single-distance scenario at different source-detector separations; ρ ranging from 10 to 35 mm with 5 mm intervals and for double-subtraction scenario with various combinations of ρ as the ρ_{far} and ρ_{near} (fig.1a). The depth selectivity and CNR were calculated for all the considered scenarios. The product of depth selectivity and CNR [2] was calculated for the zeroth (N), first (<t>) and second centralized (v) statistical moments of the DTOF to compare the overall performance of different optode configurations.

Results: The performance of the measurements at different ρ for the single distance subtraction method and
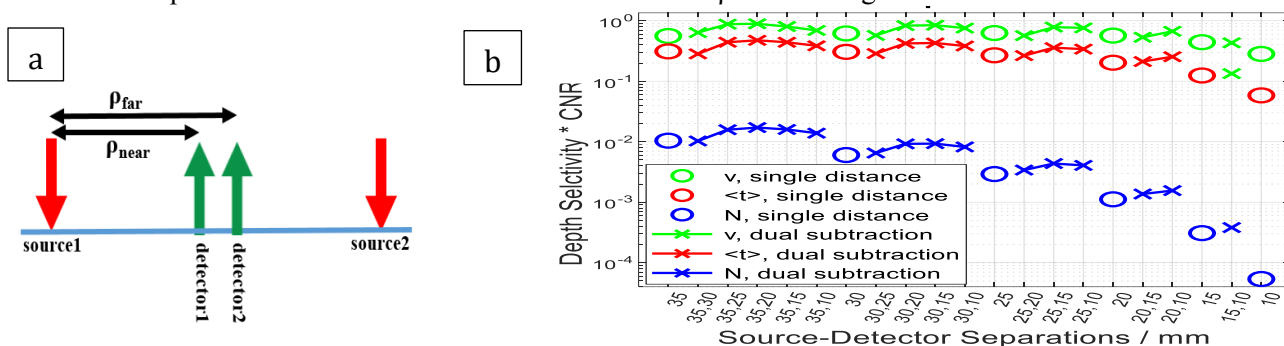
Figure 1: a) Optode configuration for dual subtraction method. b) Analysis of performance of statistical moments for different optode configurations in single distance and dual subtraction scenarios.

different ρ_{far}, ρ_{near} for the dual subtraction method was compared in fig. 1b. .

Conclusion: The results showed that the overall performance of the measurement is correlated with the order of statistical moments in both single distance scenario, in agreement with [2], and in dual subtraction scenario. Measurements with ρ_{far}-ρ_{near} >10mm in dual subtraction method features a higher overall performance in comparison to the single distance method and ρ_{far}-$\rho_{near} \approx$10-15mm is the optimal configuration. Therefore, by optimizing the configuration of optodes in subtraction-based methods, it is possible to reach the deepest possible sensitivity while maintaining an adequate level of CNR.

References:

[1] P. Sawosz and A. Liebert, Method to improve the depth sensitivity of diffuse reflectance measurements to absorption changes in optically turbid medium. *Biomedical optics express*, 2019. **10**(10): p. 5031-5041.

[2] A. Sudakou, et al., Performance of measurands in time-domain optical brain imaging: depth selectivity versus contrast-to-noise ratio. *Biomedical Optics Express*, 2020. **11**(8): p. 4348-4365.

Using digital planimetry for wound surface area measurement: improved calibration procedure

Piotr Foltyński, Piotr Ładyżyński

Nalecz Institute of Biocybernetics and Biomedical Engineering PAS, 4 Trojdena Str., 02-109 Warszawa, Poland

pfoltynski@ibib.waw.pl

Introduction. Wound surface area monitoring is important because the change in wound area over time can be used to predict healing success and to assess the effectiveness of the therapy [1]. It is also used in testing new drugs or therapies where the rate of wound decrease is a crucial outcome parameter. Digital planimetry is a popular two-dimensional method for wound surface area measurement based on the digital photograph of a wound. In this method, the number of pixels belonging to wound N_w has to be transformed into a surface area A expressed in units of area, and for that purpose, a scale calibration coefficient k must be found. Thus, there are two fields of exploration, as N_w and k have to be found, and there are many methods to find these two parameters. From the point of view of area measurement errors, it can be found that those methods differ because (a) there is natural skin curvature, (b) usually the optical axis of the camera is not perpendicular to the wound plane, and (c) there are differences in the way in which the scale calibration coefficient is achieved. The aim of the current research was to develop a new calibration procedure for calculating the mean calibration coefficient with the use of two calibration markers [2]. This new procedure was used in the web-based AutoPlanimator service (APS), which is devoted to automatic wound area measurement with an artificial intelligence method for wound and calibration marker localization at the picture. [3].

Methods. Forty wound models as paper printouts with red wound shapes were used. Each printout was attached to the lateral side of two cylinders with diameters of 62 and 94 mm. Then, the area of this artificial wound was measured with the APS, the Planimator app (PA) developed earlier in our laboratory, and 2 commercial devices: Silhouette Mobile device (SMD) and Visitrak device (VD). The reference area of each wound shape was determined by scanning the printout and counting the pixels belonging to the wound shape. Using a reference value of the wound area, it was possible to calculate the relative error (RE) for each measurement taken by each device. The comparison of those errors enabled us to determine whether the used methods differ in terms of accuracy.

Results. The medians of REs were 2.3%, 2.6%, 2.2% and 1.3% for the VD, the SMD, the PA, and the APS, respectively. The Kruskal–Wallis test revealed significant differences in the REs for the APS vs the VD (p=0.0012), SMD (p=0.0006), and the PA (p=0.0196). The REs for the VD, SMD, and PA were not significantly different, with a p value equal to 1.00 for each pair of methods.

Conclusion. The wound area measurement on a curved surface was the most accurate by the AutoPlanimator service, in which the new procedure of adaptive calibration for automatic wound area measurement is used.

References:
[1]. Hingorani A, LaMuraglia GM, Henke P, Meissner MH, Loretz L, Zinszer KM et al. The management of diabetic foot: A clinical practice guideline by the Society for Vascular Surgery in collaboration with the American Podiatric Medical Association and the Society for Vascular Medicine. *J Vasc Surg*, 2016; 63(2 Suppl):3S-21S. doi: 10.1016/j.jvs.2015.10.003.

[2]. Foltynski P, Ladyzynski P. Digital Planimetry With a New Adaptive Calibration Procedure Results in Accurate and Precise Wound Area Measurement at Curved Surfaces. *J Diabetes Sci Technol,* 2022; 16:128–36. https://doi.org/10.1177/1932296820959346.

[3]. Foltynski P and Ladyzynski P. Internet service for wound area measurement using digital planimetry with adaptive calibration and image segmentation with deep convolutional neural networks. *Biocybernetics Biomed Eng*, 2023; 43:17-29. https://doi.org/10.1016/j.bbe.2022.11.004.

From monomers to lovers: understanding the aggregation and interaction of peptides

Marlena Gąsior-Głogowska[1*], Natalia Szulc[1,2], Monika Szefczyk[3], Małgorzata Trzpis[3], Karina Twardak[1], Marta Kopaczyńska[1], Witold Dyrka[1]

[1]Department of Biomedical Engineering, Faculty of Fundamental Problems of Technology, Wrocław University of Science and Technology, Wrocław, Poland
[2]Wrocław University of Environmental and Life Sciences, Department of Physics and Biophysics, Wrocław, Poland
[3]Department of Bioorganic Chemistry, Faculty of Chemistry, Wrocław University of Science and Technology, Wroclaw University of Science and Technology, Wrocław, Poland
[*]e-mail: marlena.gasior-glogowska@pwr.edu.pl

Amyloids are peptides and proteins that, due to misfolding, are able to form long, unbranched, highly ordered fibrils. The unique cross-β-structure of amyloid fibrils is responsible for the high thermodynamic stability of amyloid aggregates, the insolubility of water, and the proteolytic resistance. Amyloids are capable of not only self-aggregation but also inducing the aggregation of other native globular or intrinsically disordered proteins. Although most of the known amyloids are associated with a wide range of human diseases, a growing number of functional amyloids has been discovered [1]. They are involved in biofilm formation, as well as the innate immune system of multicellular organisms. In fungi, bacteria and archaea, amyloid signaling motifs are used by Nod-like receptors (NLR) to activate effector proteins in controlling immune responses. In this process, upon activation, a motif located at the N-terminus of the NLR initiates the oligomerization of a similar motif located at the C-terminus of the effector protein [2]. Understanding this conserved evolutionary signaling mechanism may help treat various infectious and inflammatory diseases, as well as drug design.

Two triplets of C-terminal and N-terminal sequences of fungal and bacterial amyloid signaling motifs predicted by a new machine learning grammatical model [3] were synthesized on the solid support, purified using the preparative HPLC method (>95% purity) and lyophilized. Their amyloidogenic abilities were studied using a wide gamma of techniques, i.e. CD, ATR-FTIR, µIR, FT-Raman, ThT assays, and AFM imaging. All experimental studies were conducted under different experimental conditions (pH, temperature, buffer, type of solvent, and presence of ions) to identify the key factors that affect the physical stability of formed fibrils. Special attention was paid to the heteroaggregation of signaling pairs.

On the basis of the spectroscopic data, we concluded that all studied sequences adopted beta-solenoid conformations reported before for the HET-s and PrPSc prion motifs, but their aggregation properties were sensitive to external factors. The secondary structure and morphology of the amyloid fibrils also contingent on the initial particle size. We showed that the assembly pathways that started from the monomer phase did not lead to fibril formation in all cases, while in the presence of seeds fibrilization occurred. Particularly, the presence of ions could accelerate this process and stabilized formed structures. Moreover, the C-terminal sequences seemed to need a trigger in the form of a N-terminal sequence. These in vitro findings indicate that cross-interactions of amyloidogenic peptides are sufficient to explain the NLR signaling observed in vivo.

References:
[1] Otzen D, Riek R. Functional Amyloids. Cold Spring Harb Perspect Biol. 2019 Dec 2;11(12):a033860. doi: 10.1101/cshperspect.a033860.
[2] Dyrka W, Coustou V, Daskalov A, Lends A, Bardin T, Berbon M, Kauffmann B, Blancard C, Salin B, Loquet A, Saupe SJ. Identification of NLR-associated Amyloid Signaling Motifs in Bacterial Genomes. J Mol Biol. 2020 Nov 20;432(23):6005-6027
[3]Dyrka W, Gąsior-Głogowska M, Szefczyk M, Szulc N. Searching for universal model of amyloid signaling motifs using probabilistic context-free grammars. BMC Bioinformatics. 2021 Apr 29;22(1):222. doi: 10.1186/s12859-021-04139-y.

Title: The design and development of a bioink for interface tissue engineering using rheological analysis

Rency Geevarghese[a], Daniele Parisi [c], Malgorzata Wlodarczyk-Biegun [a,b], *

[a] Biotechnology Center, The Silesian University of Technology, B. Krzywoustego 8, 44-100 Gliwice, Poland.
[b] Zernike Institute for Advanced Materials, University of Groningen, Nijenborgh 4, 9747 AG Groningen, the Netherlands.
[c] Dep. Chemical Engineering, Product Technology group, University of Groningen, Nijenborgh.

Introduction and Aim: The emergence of bio-fabrication techniques like 3D bio-printing (3DBP) have widened the possibility for regeneration of tissue with high precision, shape versatility and patient specific designs. Bioink is a printable formulation comprising of biomaterials, cells and biochemical cues used in 3DBP with ability to mimic the physiological 3D microenvironment. Although several polymeric bioinks are available for tissue regeneration applications, the optimisation of an ideal bioink is challenging, time consuming and demands multi-disciplinary knowledge. This difficulty could be resolved by a systematic approach using rheology that serves as an effective tool, enabling a correlation between bioink, printability aspects, and the mechanical property of the printed scaffolds. The current work focuses on design and development of a well-printable bioink based on biopolymers commonly used in TE, such as sodium alginate (Alg), carboxy-methyl cellulose (CMC) and methacrylated gelatin (GelMA). Bioink compounds are mixed at different ratios and link between rheology and 3D-printing is studied with aim of detecting the optimized conditions for printability, shape fidelity and stability of 3D-printed specimen.

Methods: Ink composed of 4%Alg-(4,8,10 & 12)%CMC was prepared in PBS to obtain optimal formulation of 4%Alg-10%CMC followed by addition of different concentrations of GelMA to 4%Alg-10%CMC obtain 4% Alg-10%CMC-GelMA (4,8 &12)% (w/v). Rheological experiments were performed including flow sweep, amplitude sweep, frequency sweep, thixotropic test, time sweep under UV-curing and temperature ramp followed by printing. For experiments involving UV curing 0.25% (w/v) photoiniator (Lithium phenyl trimethylbenzoyl phosphinate) was added to formula. Printing with included fibroblasts was performed to assess cell viability in the optimized formulation.

Results: The rheological testing of different combinations of Alg-CMC conc. revealed that the addition of CMC increased the G', G'' and η*(Fig 1 A) and better printing of 4%Alg-10%CMC (Fig 1. C) over 4%Alg-8%CMC (Fig 1. D) was associated with these rheological properties. Incorporation of GelMA (4,8 and 12)% to 4%Alg-10%CMC led to an increase in G', G'', η* (Fig 1. G and H), and all the solutions were well-printable. 4%Alg-10%CMC-12%GelMA (with highest GelMA content) showed best printability defined as the possibility of obtaining the thinnest printed strands (Fig 1. D, E and F). Alg improves the viscosity and shear-thinning property of the formulation, CMC serve as a thickening agent, and photocrosslinked GelMA support the cell attachment and growth. We concluded that GelMA can moderately influence printability with additional influence expected to improve cell performance.

Fig 1. (A) Frequency sweep and printability test of (B) 4%Alg-8%CMC and © 4%Alg-10%CMC depicting good printability for 10%Alg-10%CMC. Printability of (D) 4%A-10%CMC-4%GelMA, (E) 4%A-10%CMC-8%GelMA, (F) 4%A-10%CMC-12%GelMA. (G,H) Frequency sweep of 4%A-10%CMC-GelMA conc. proving 4%A-10%CMC-12%GelMA to be the best printable bioink owing to high modulus, viscosity and thinnest fiber deposition in comparison to other formulations.

Conclusions: Characterization of rheological properties of the tested materials gave a strong indication of the shape fidelity, stability and printability, and is a powerful tool in the development of optimal printable materials. The printed constructs are intended to be used in the interface tissue engineering such as musculoskeletal interfaces.

Reference: (1) J Groll, et al, A Review, (2019) *Biofabrication* Vol 11.; (2) Qingbo Wang, et al, (2021) Front. Chem. Eng. (3)W. Peng, et al., Acta Biomater. 57 (2017) 26–46. (4) A.A. Aldana, et al., Bioprinting. 21 (2021) e00105.

Cerebral perfusion assessment by multiwavelength time-resolved NIRS: clinical validation

Anna Gerega[1], Piotr Sawosz[1], Michał Juszynski[2], Grzegorz Madycki[2], Adam Liebert[1]
[1]Nalecz Institute of Biocybernetics and Biomedical Engineering PAS, Warsaw, Poland
[2]Department of Vascular Surgery and Angiology, Centre of Postgraduate Medical Education, Warsaw, Poland
agerega@ibib.waw.pl

Recently, there are variety of techniques for brain imaging, however near-infrared spectroscopy (NIRS) has the advantage of being able to assess cerebral perfusion and oxygenation at the bedside [1]. Moreover, the effective bedside method to assess brain hemodynamic parameters easy applicable in clinical conditions and which exclude the contamination of the extracerebral layers on the measured signal is still missing. Cerebral blood flow can be evaluated by combining NIRS with optical contrast agent Indocyanine green (ICG) which has high absorption in the NIR range [2]. Following intravenous injection of an ICG bolus, its transit through intra- and extracerebral tissue compartments can be evaluated by analysis of collected distributions of times of flight of photons (DTOF). In the present work, the usefulness of the wavelength- and time-resolved NIRS technique in combination with ICG-bolus tracking for brain perfusion monitoring was evaluated in clinical conditions.

The measurement setup is based on time-correlated single photon counting electronics and picosecond supercontinuum laser source [3]. We used 680-880 nm spectral region and the optical signal after penetrating the tissue was detected at 16 spectral channels. The optodes were positioned on a skin of patient's forehead. The NIRS measurements with the ICG injections were carried out on patients with carotid artery stenosis in order to assess the cerebral perfusion in normal conditions and after total cessation of extracerebral blood flow during endarterectomy. Data analysis involve assessment of optical properties of the layered head structure from on-skin measurements based on statistical moments of DTOFs calculated for 16 wavelengths and its sensitivity factors [3].

The changes of ICG concentration ΔC_{ICG} was calculated separately for extra- and intracerebral layers in tree cases: 1) in condition of reduced cerebral perfusion due to the carotid stenosis before any clamping, 2) after external carotid artery clamping while maintaining the brain cortex perfusion (reduced due to the atherosclerotic plaques), and 3) after removing of atherosclerosis plaques and declamping of the internal (ICA) and external (ECA) carotid arteries (Figure 1). It can be seen that ICG inflow exactly follows the condition of the perfusion: in the reduced intracerebral perfusion condition (case 1) the atypical narrow (related to a smaller blood volume) delayed peak appeared in the brain cortex simultaneously with the strong ICG inflow into the extracerebral layer. After the total cessation of the extracerebral layer perfusion (case 2) only delayed ICG bolus can be observed without any trace in the extracerebral tissue. After the surgery, ICG inflows into the both compartment as expected in normal perfusion condition (case 3): broad peak (increased blood volume comparing with case 1) related to the intracerebral ICG inflow appeared firstly in the brain cortex and after few seconds in the extracerebral tissue [4].
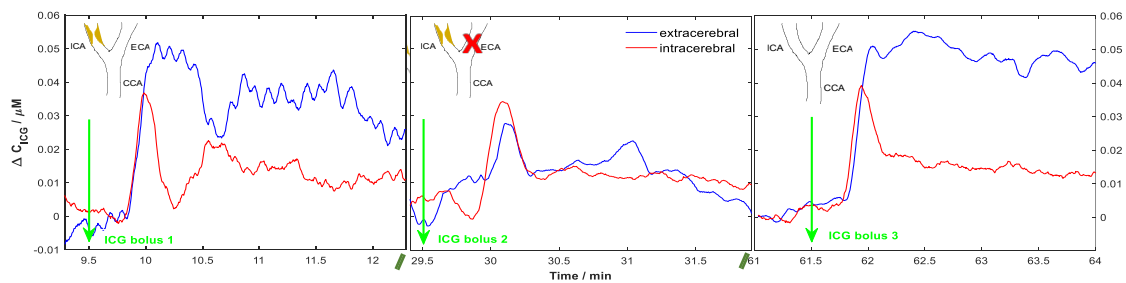
Figure 1: Changes of the ICG concentration ΔC_{ICG} which reflect the inflow of the optical contrast agent ICG into extra- and intracerebral layers separately, calculated during endarterectomy before (left panel), during (middle) and after internal artery clamping (right panel). ICA – internal cerebral artery, ECA – external cerebral artery, CCA- common cerebral artery.

Results of the measurements show that application of the proposed method based on monitoring of multiwavelength diffuse reflectance and injection of the optical contrast agent bolus may allow us to derive depth-resolved kinetics of the ICG, thus, allowing the selective assessment of the blood flow in the brain cortex.

1. H. Obrig and A. Villringer, *J Cereb Blood Flow Metab*, 2003, 23(1), 1-18.
2. A. Liebert *et al.*, *Appl Opt,* 2004, 43(15), 3037-3047.
3. A. Gerega *et al.*, *Biomed Opt Express,* 2018, 9(7), 2974-2993.
4. M. Kohl-Bareis *et al.*, J. Biomed. Opt. **7**, 464-470 (2002).

Construction of the model of biologically active function block of improved BAL

<u>Małgorzata Jakubowska</u>, Monika Wiśniewska, Agnieszka Wencel, Dorota G. Pijanowska, Krzysztof D. Pluta

Laboratory of Tissue Engineering, Department of Hybrid and Analytical Microsystems, Nalecz Institute of Biocybernetics and Biomedical Engineering Polish Academy of Sciences, Ks. Trojdena 4 st., 02-109 Warsaw

Email: mjakubowska@ibib.waw.pl

Aims

Liver diseases are one of the most frequent causes of death worldwide. Taking into account liver's complexity, there are no effective medical solutions for acute or chronic liver failure. Currently, liver transplantation (LT) is the only cure for its failure. Unfortunately donor shortage is a great limitation to this therapy. One of the most promising alternatives for LT are bioartificial livers (BALs). These hybrid devices constitute a bridging therapy for patients waiting for LT or until liver regeneration. The most advanced system is ELAD, which came to the third phase of clinical trials, but did not live up to expectations. ELAD utilizes as the biological component C3A cells derived from human hepatocellular carcinoma (HCC). These cells are characterized by non-functional urea cycle resulted from the lack of expression of arginase 1 (*ARG1*) and ornithine transcarbamylase (*OTC*) genes. In fact, this could be a reason for failure of clinical trials for ELAD system as detoxification of ammonia is an essential liver function. Here we show the construction of the model of the biologically active function block, based on genetically modified HCC cell lines, that can be applied in an improved BAL.

Methods

In order to restore urea cycle we conducted genetic modification of C3A cells using lentiviral vectors. We proposed two different approaches – two transgenes, h*ARG1* and h*OTC*, were carried on by the same lentiviral vector or by two different vectors. After establishment of the new cell lines we compared them with their parental C3A cells in dynamic culture conditions. These conditions were ensured by flow system constructed in our laboratory, based on polysulfone hollow fiber bioreactors. At the end of the experiment cell viability was determined using trypan blue exclusion method. Additionally, glucose consumption (colorimetric method) and albumin production (ELISA test) in collected media samples were measured. Corresponding stationary culture controls were performed.

Results

Results showed that in dynamic culture both genetically modified cell lines were characterized by higher albumin secretion and increased glucose consumption than their unmodified counterpart. In case of cell viability, the determination of this parameter was partially successful, because we were not able to detach all cells from capillary membranes. However, cells after successful trypsinization were mostly viable, without significant differences between analyzed cell lines. Comparison of dynamic cultures with stationary controls indicated that flow conditions ensured better environment for hepatic cells growth and performance (for example albumin synthesis).

Conclusion

Genetically modified HCC cells outperformed their unmodified counterparts. Therefore, they can be used as a better source of cells in biologically active function block of BAL. Next, we will test the dynamic culture with feeder layer cells – genetically modified fibroblasts overexpressing specific liver-related growth factors.

SmartBackpack - wearable system for monitoring posture and backpack load distribution

Ludwik Janowski, Angelika Kauc, Sylwia Michalska, Zofia Sikorska, Aleksandra Królak.
Institute of Electronics, Lodz University of Technology,
Al. Politechniki 10, 93-590 Łódź, Poland
aleksandra.krolak@p.lodz.pl

Nowadays back pain is a common health problem. Very often it is a result of carrying heavy bags or backpack and uneven distribution of the load. It is an important issue especially in case of school children, as improper posture and carrying too heavy backpacks may have negative long-term effects on their body. The suggested load weight limit for school children is 10% to 15% of the child's body weight, while in case of physically fit adults the maximum backpack weight should not exceed 30% of the body weight [1]. A promising approach to monitor the carried load and the posture is to use wearable devices mounted in the backpack, based on microcontrollers. The systems presented in the literature use various sensors, including load cells, RFID tags, as well as accelerometers and force sensitive resistors [2,3].

Our project is an intelligent backpack equipped with two force sensitive resistors (FSR) placed on the backpack shoulders and one FSR at the bottom of the backpack. The FSRs are sensors that measure the force and pressure exerted on the backpack during usage. Our solution involves collecting data from these sensors for backpack load analysis and to ensure optimal carrying comfort for the user. By using FSRs on the backpack shoulders, we can accurately monitor the forces acting on the user's back. An additional sensor at the bottom of the backpack provides information about overall pressure on the backpack. All this data is collected using Arduino NANO 33 IoT and processed in real-time by algorithms implemented in Arduino Cloud. The system notifies about incorrect force distribution using a Buzzer. The mobile application developed can work on Android and iOS systems thanks to the IoT Remote App. Proposed solution utilizes collected data to notify the user about weight distribution on the shoulders and the overall weight of the backpack, enabling the user to correct the posture when necessary. Using the built-in wireless communication system (BT), the backpack can transmit information about its status and parameters to the user's smartphone or other external devices in real-time. With the added GPS system in our prototype, it is possible to track its location at any given time.

Tests of the prototype were performed with a group of 4 volunteers. All situations of improper backpack carrying were detected correctly. The intelligent backpack can find applications in various fields such as tourism, sports, parental control, or medical care. It can assist users in avoiding back strains, providing greater comfort, and reducing the risk of injuries.

Conclusions drawn from research conducted using the prototype of the intelligent backpack have shown that our solution allows for effective optimization of backloads and improved carrying comfort. The intelligent backpack can be a valuable tool for individuals who regularly carry heavy luggage, as well as for those with poor physical fitness or back-related health issues. It can also benefit school children to prevent injuries such as scoliosis or kyphosis, which are often caused by the weight and improper carrying of backpacks.

References:
[1] M. Benocci, M. Bächlin, E. Farella, D. Roggen, L. Benini and G. Tröstery: Wearable assistant for load monitoring: recognition of on—body load placement from gait alterations, 2010 4th International Conference on Pervasive Computing Technologies for Healthcare, Munich, Germany, 2010, pp. 1-8, doi: 10.4108/ICST.PERVASIVEHEALTH2010.8894.
[2] A. Baihaqi, w. Djatmiko, M. Yusro: Development of smart and safe-bags for children based on microcontroller, Journal of Physics: Conference Series, 2019, vol. 1402, 044017, doi:10.1088/1742-6596/1402/4/044017
[3] H. Y. Hung, G. Millaway, S. Mustafa, H. Peng, A. Geiger, J. Raiti: Detection and Low-Latency Notification of Improper Backpack Posture using Deep Learning. 2022 IEEE Global Humanitarian Technology Conference (GHTC), 2022, pp. 433-436, doi: 10.1109/GHTC55712.2022.9910981

Stability of reference genes in stress-induced cells.

Daria Kałużyńska[1,2], Olga Kocikowska[1,3], Roman Jaksik[1], Anna Lalik[1,2]
[1]Department of Systems Biology and Engineering, Silesian University of Technology,
Akademicka 16, 44-100 Gliwice, Poland
[2]Biotechnology Center, Krzywoustego 8
44-100 Gliwice
[3]Department of Physiology, Faculty of Medical Sciences, Silesian University of Medicine,
Medyków 18, 40-055 Katowice
Roman.Jaksik@polsl.pl

Gene expression is studied at both the mRNA and protein levels. Research on gene expression regulation is a crucial element of research, e.g., signaling pathways or cell cycle study. Changes in expression are caused by the impact of the system factors, causing disturbance of cell homeostasis, e.g. siRNA, ionizing radiation, or drugs. Changes in expression are tested using various techniques. The results of the techniques are analyzed by comparing the tested protein/transcript with the so-called references – a stable molecules, which are not influenced by factors regulating the studied genes [1]. There are many references in the literature, but they are not universal. Furthermore, reference genes are typically selected based on the analysis of expression differences between a large number of cell types, however, they might not be the best choice in experiments which aim at characterizing responses to stress factors. Commonly used methods like geNorm [2] and NormFinder [3], that assess expression level stability, are expected to be used with data obtained in a single experiment performed using various cell lines only.

In this project, we developed a new tool to evaluate the stability of reference genes in experiments that test the influence of physical or chemical treatments on cells. We used it on a large dataset comprising of over 300 human RNA samples, extracted from irradiated and non-irradiated cells at various time points, and studied using RNA-seq or oligonucleotide microarrays.

Genes identified to be highly stable after irradiation in different cell lines were further selected for validation on mRNA and protein levels using RT-qPCR and Western Blot techniques, respectively. The tests were performed using HCT116, MCF7 and HCT116 p53-/-, with a radiation dose of 4 Gy. In addition, for proteins, total protein analysis using Ponceau S and Revert Protein Stain was used. TP53, which is known to be strongly expressed in the presence of DNA double-strand breaks, was used as a negative control in all experiments. We found that the B2M, TPB, and RPL41 genes have the most stable expression levels, regardless of radiation dose, cell line and time after treatment.

Our study provides not only information on the stability of genes in radiation-treated cells but also a methodology that can be used to assess gene expression stability in experiments that test the influence of other treatment factors on gene expression levels.

References:
[1] Pérez-Pérez R, López JA, García-Santos E, Camafeita E, Gomez-Serrano M, Ortega-Delgado FJ, Ricart W, Fernández-Real JM, Peral B. Uncovering suitable reference proteins for expression studies in human adipose tissue with relevance to obesity. *PLoS One*. 2012 Jan 17;7(1):e30326.
[2] Vandesompele, J., et al., Accurate normalization of real-time quantitative RT-PCR data by geometric averaging of multiple internal control genes. *Genome Biol,* 2002. 3(7): p. RESEARCH0034.
[3] Andersen, C.L., J.L. Jensen, and T.F. Orntoft, Normalization of real-time quantitative reverse transcription-PCR data: a model-based variance estimation approach to identify genes suited for normalization, applied to bladder and colon cancer data sets. *Cancer Res*, 2004. 64(15): p. 5245-50.

Influence of selected electrolytes on morphology and chemical structure of obtained calcium phosphate coatings on Ti$_6$Al$_7$Nb by electrochemical method

Klaudia Lauk[1], Witold Kaczorowski[1], Barbara Burnat[2], Jacek Grabarczyk[1], Bartłomiej Januszewicz[1]

[1] Institute of Material Science and Engineering, Faculty of Mechanical Engineering, Lodz University of Technology, 1/15 Stefanowskiego St, 90-537 Lodz, Poland; e-mail klaudia.lauk@dokt.p.lodz.pl

[2] Department of Inorganic and Analytical Chemistry, Faculty of Chemistry, University of Lodz, 12 Tamka St., 91-403 Lodz, Poland

klaudia.lauk@dokt.p.lodz.pl

Titanium alloys are widely used biomaterials in implantology due to their good mechanical strength, corrosion resistance and biocompatibility. These alloys are classified as bioinert materials, which is related to their inability to properly stimulate the proliferation of osteoblasts and bone cells, and thus a common post-operative complication is implant loosening. In addition, titanium alloys, such like Ti$_6$Al$_4$V or Ti$_6$Al$_7$Nb, contain elements such as vanadium or aluminium, which can lead to allergic reactions or the release of ions of these elements into the surrounding tissues [1]. To minimize post-implantation complications or to give bioactive properties to implants, surface modification of the substrate can be used, e.g. by applying calcium-phosphate coatings (CaP coatings). CaP coating can be applied using a variety of techniques, including plasma spraying, sol-gel or by electrochemical deposition. The electrochemical method can be an alternative to other methods due to the low cost of the process, customisable parameters and volumetric surface modification. The problem in using the electrochemical method commercially is the selection of a suitable electrolyte and process parameters to produce a homogeneous and continuous hydroxyapatite coating [2]. Hydroxyapatite is the most desirable of the other calcium phosphate coatings, due to the fact that it has the most similar structure structurally and chemically to that found in the inorganic structure of bone. Nowadays, most researchers rely on the analysis of the effect of applying one salt pair in solution, while more extensive research is carried out in different ranges of current and time values [3].

In this work, the focus is on the influence of different solutions, having ions involved in the formation of calcium phosphate coatings, on the surface morphology and chemical structure of the deposited coatings. The deposition processes of CaPs coatings were carried out using an electrochemical method with three different salt pairs for the electrolytes: Ca(NO$_3$)$_2$·4H$_2$O and (NH$_4$)$_2$HPO$_4$, Ca(NO$_3$)$_2$·4H$_2$O and NH$_4$H$_2$PO$_4$, Ca(NO$_3$)$_2$·4H$_2$O and KH$_2$PO$_4$. The study used a two-electrode potentiostatic mode at a direct constant voltage of -6V for 2h, where the modified substrate and cathode was titanium alloy Ti$_6$Al$_7$Nb, while the anode was a platinum sheet. Identification of the coatings was performed using SEM, EDS, Raman spectroscopy and X-ray diffraction.

From the analysis of the SEM images, it can be seen that when the electrolyte with (NH$_4$)$_2$HPO$_4$ is used, the most cracked coating structure and partially occurring powders are observed, while when NH$_4$H$_2$PO$_4$ is used, the coating is more continuous. The EDS study confirms the presence of elements such as calcium and phosphorus in each case; in addition, the elemental ratio Ca/P=1.67 is preserved, which corresponds to the presence of hydroxyapatite. The spectra obtained by Raman spectroscopy confirm the appearance of a single-phase hydroxyapatite coating from each electrolyte. XRD studies show that the most homogeneous hydroxyapatite coating was deposited when an electrolyte with a NH$_4$H$_2$PO$_4$ component was used.

These studies and observations confirmed that, using the electrochemical method in potentiostatic mode and using each electrolyte, it is possible to deposit a hydroxyapatite coating. However, to obtain a homogeneous and continuous coating, the most optimal electrolyte is a variant that includes NH$_4$H$_2$PO$_4$.

References:
[1] Beig, B.; Liaqat, U.; Niazi, M.F.K.; Douna, I.; Zahoor, M.; Niazi, M.B.K. Current Challenges and Innovative Developments in Hydroxyapatite-Based Coatings on Metallic Materials for Bone Implantation: A Review. *Coatings* 2020, 10, 1249
[2] Safavi, M.S.; Walsh, F.C.; Surmeneva, M.A.; Surmenev, R.A.; Khalil-Allafi, J. Electrodeposited Hydroxyapatite-Based Biocoatings: Recent Progress and Future Challenges. *Coatings* 2021, 11, 110
[3] Drevet, R.; Benhayoune, H. Electrodeposition of Calcium Phosphate Coatings on Metallic Substrates for Bone Implant Applications: A Review. Coatings 2022, 12, 539

Near infrared spectroscopy: sensitivity factors for absorption and scattering

<u>Adam Liebert</u>, Stanisław Wojtkiewicz, Roman Maniewski

Nalecz Institute of Biocybernetics and Biomedical Engineering, Polish Academy of Sciences

Abstract

Near-infrared spectroscopy (NIRS) is an optoelectronic technique used to assess the hemodynamic properties and oxygenation of living tissue. It involves emitting light in the near-infrared wavelength region and detecting the diffusely remitted light from tissue at a nearby spot a few centimeters away from the source.

Measurements in NIRS are typically conducted at multiple wavelengths to monitor changes in light attenuation, which can be attributed to variations in the concentration of hemoglobin, a highly absorbing chromophore in tissue, and a carrier of oxygen. By utilizing the distinct spectral properties of oxygenated and deoxygenated hemoglobin, changes or absolute concentrations of oxyhemoglobin, deoxyhemoglobin, and regional oxygen tissue saturation can be determined.

The time-resolved NIRS technique utilizes short, picosecond light pulses at the source, enabling the recording of distributions of photon time of flight (DTOF) at the photodetector. This technique allows the differentiation of optical signals originating from photons traveling through different path lengths within the investigated tissue.

Traditional NIRS-based measurement techniques assume that only the absorbing properties of tissue change during an experiment, establishing a direct relationship between changes in absorption and chromophore concentration. Changes in the scattering properties of living tissue can affect NIRS signals, resulting in crosstalk between scattering and absorption.

In this presentation, we will show a more comprehensive relationship between changes in optical signals measured on the tissue surface and changes in its optical properties. We will present analytic formulas linking changes in measured signals with alterations in the absorption and scattering properties of the investigated medium. Additionally, we will demonstrate that these formulas enable the derivation of changes in absorption and reduced scattering coefficients from changes in statistical moments of DTOFs. We will also explore the sensitivities of measurements of changes in these moments to variations in absorption and reduced scattering coefficients, as well as different combinations of sensitivities, potentially allowing for the non-direct derivation of the optical properties of a medium.

Brain electrical activity measures of embodied cognition - comprehension of action verbs in figurative context

Karina Maciejewska[*,1,2], Tomasz Nowak[3]
[1]Institute of Biomedical Engineering, Faculty of Science and Technology, University of Silesia in Katowice, 75 Pulku Piechoty Street 1a, 41-500, Chorzow, Poland
[2]Campus Bio-Medico University of Rome, Via Álvaro del Portillo, 21 - 00128 Rome, Italy
[3]Faculty of Humanities, University of Silesia in Katowice, pl. Sejmu Slaskiego 1, 40-032, Katowice, Poland
[*]Corresponding author: karina.maciejewska@us.edu.pl

A better knowledge of how the human brain interacts with the surrounding world is important not only to understand neuronal processes responsible for these interactions but also to develop devices that can better simulate human perception and actions. A promising approach is embodied cognition, according to which the cognitive processes are grounded in the body's interactions with the environment via sensorimotor processing [1]. Understanding the embodied language grounding is of special importance. The embodied model involved in the language processing of action words has been widely debated, also in the view of agency and sensorimotor integration. It is especially interesting to recognize how the human brain understands non-literal context. Thanks to the state-of-the-art tools of biomedical engineering we can study neurophysiological signals which give a deeper insight into cognitive processes. The aim of this work was to study brain electrical activity measured by EEG signal in response to action verbs related to the upper limb, in the Polish language, in different contexts.

32-channel EEG was recorded from 34 young, healthy participants. ERPs elicited by short sentences with an action verb "to throw" were compared between 4 conditions: (1) where the verb was used literally, (2) where the verb was used figuratively, (3) where the verb was used as an unfamiliar (unknown) figure of speech, and (4) with a mental verb as a control. Signal preprocessing and analyses were performed using EEGLAB, ERPLAB, and Fieldtrip MATLAB toolboxes. Statistical analysis was performed using the nonparametric cluster-based permutation test with Monte Carlo correction for the MCP and 2000 permutations.

The stimuli elicited a dominant anterior P2 component, seen as a positive waveform around 200-250 ms after stimulus onset, maximal over the midline central area, which was the highest in the figurative condition and the lowest in the mental condition, followed by anterior negativity (anterior N2), and a parietal positivity. Statistical analysis of the averaged ERPs revealed two effects: a figurative effect, and an unknown effect. The figurative effect was observed as a difference between figurative and mental conditions, with two significant clusters (P=0.085 and P=0.0155, cluster corrected), which corresponded to a spatiotemporal cluster around 250 to 350 ms, and a spatiotemporal cluster around 450 to 600 ms, respectively, both maximal over the right frontocentral area. The unknown effect was observed as a difference between unknown and mental condition, with a significant cluster (P=0.0215, cluster corrected), which corresponded to a spatiotemporal cluster around 300 to 400 ms, maximal over the right frontocentral area.

The most apparent result is the figurative effect. The unknown condition is similar to the figurative condition, but more positive than the mental one. From these results, it seems the non-literal effect has two components: an earlier one, that correspond to a higher amplitude of the P2-N2 complex in the figurative and unknown conditions (i.e. more positive P2 and less negative N2 compared to mental), and a later one, less negative ERP, in figurative context only. Our results suggest a specific way in which the human brain processes action verbs in a non-literal context and that the neurophysiological marker may be observed as early as the P2 component. Studying neuronal correlates of human language comprehension by means of EEG signal, especially in the paradigm of embodied cognition, allows us to better understand the interaction and communication of the embodied brain with the surrounding world. This in turn, is crucial in a human-robot interaction (HRI) research field for designing and developing more ecologically valid biomedical engineering solutions, e.g. to build more accurate embodied language models for robotics (e.g. [2]), in neuroprosthetics, and brain-machine interfaces for patients with sensorimotor and cognitive disorders, which better adapt to the dynamic environment and better simulate the interaction of the human brain and body with the world.

References:
[1] M. Wilson (2002) Six views of embodied cognition. Psychon Bull Rev. 9(4), pp. 625-36
[2] D. Dries et al. (2023) PaLM-E: An Embodied Multimodal Language Model, arXiv:2303.03378

Hemodynamic changes measured using time domain diffuse correlation spectroscopy during Valsalva maneuver on healthy subjects

Neda Mogharari[a], Stanisław Wojtkiewicz[a], Adam Liebert[a], Michał Kacprzak[a]

[a] Nalecz Institute of Biocybernetics and Biomedical Engineering, Polish Academy of Sciences, Poland

nmogharari@ibib.waw.pl

Cerebral blood flow (CBF) is a physiologically relevant parameter that is not routinely measured in clinics because of the lack of a reliable and easy to apply bedside technology. However, management of CBF is essential in neurosurgery and neurology [1]. Time-domain diffuse correlation spectroscopy (TD-DCS) is an optical method to evaluate CBF. In this technique the autocorrelation function is computed for a given time gates within the measured distribution time of flight of photons (DTOF) and the depth resolution is achieved by the selected time gate. It's supposed photons in earlier and later time gate carry information from superficial layer and deep layer respectively [2]. So, the gate start time and gate width are considered as important parameters in time gating strategy.

The most common lasers which are used in TD-DCS have low coherency. Moreover, the number of photons in later times of flight is low, which leads to noisy date. Our td-DCS system equipped with Vis-IR laser generates a large emission spectrum bandwidth which leads to the short coherence length and lose more photon correlation in later time of DTOF. We found the gates around DTOF peak have highest coherence parameter (β) with lower standard deviation amplitude in β and Brownian diffuse sufficient (αD_B) which refers to dynamics of scatterers. So the time gates around DTOF peak were considered for gate positioning. Here, it has been suggested that the gate width is a parameter depending on broadness of instrument response function (IRF) and DTOF and can be calculated by difference between Variance (V) of DTOF and IRF. $\sqrt{V}$ (expressed in ns) before the DTOF peak is defined as the early gate and $\sqrt{V}$ ns after the DTOF peak as the late gate and has been calculated by statistical moments method [3].

$$V = m_2 - m_1{}^2 \qquad (1)$$

Where m_1 and m_2 are the first and the second moments.

In this study first we optimized the system using a two layer phantom with different dynamics of scatterers in bottom layer and validated the gate positioning and gate width at various source detector separations (SDS). Then we assessed the system ability to monitor blood flow changes during Valsalva maneuver (a validated quantifying autonomic function tests) at each SDS on 4 healthy subjects. Increase SDS leads to shift the DTOF peak to later time gate, broadening the DTOF and as a result larger variance and wider gate width. So in longer SDS, the probability of detecting photons with later time of flight coming from deep layer is increased.

According to the literature [4], the hemodynamics response during Valsalva maneuver includes four phases of blood flow changes. We associate the natural difference in the muscle depth location and skin fat layer in different subjects affect the detected signals and as a results blood flow changes measured by TD-DCS [5]. D.J. Davies, et al., [6] reported lower response of skin perfusion during Valsalva manure after applying skin pressure. So, Valsalva manure is a strong stimulation which affects both BFI changes in superficial and deep layer. According to our results 4 phases of blood flow changes mostly was observed in longer SDSs which photons with later time of flight coming from deep layer were detected. Moreover the proximity of the early and late time gates might be the reason that there is no significant difference in the hemodaynamics response of early and late gate. Summarizing, we show results of the preliminary tests leading to a depth-resolved perfusion measurement.

References:

[1] Shapiro, B et al. "Large Intensity Fluctuations for Wave Propagation in Random Media" *Physical Review Letters* 57, no. 17 (10/27/ 1986): 2168-71

[2] Sutin, J et al. "Time-Domain Diffuse Correlation Spectroscopy." *Optica* 3 9 (2016): 1006-13.

[3] Liebert, A. et al. "Evaluation of optical properties of highly scattering media by moments of distributions of times of flight of photons," *Appl. Opt.* 42, 5785-5792 (2003)

[4] Novak, P. "Quantitative autonomic testing," J. *Visualized Exp.* (53), e2502 (2011).

[5] Yang, Y. et al. "Influence of a fat layer on the near infrared spectra of human muscle: quantitative analysis based on two-layered Monte Carlo simulations and phantom experiments," Opt. Express 13, 1570-1579 (2005)

[6] Davies, D.J., et al., The Valsalva maneuver: an indispensable physiological tool to differentiate intra versus extracranial near-infrared signal. Biomed Opt Express, 2020. 11(4): p. 1712-1724.

Visible and Near-Infrared Image Processing for Improving Portrait Illumination Effect

Robert Olbrycht

Lodz University of Technology, Institute of Electronics, Al. Politechniki 10, 93-590, Łódź, Poland
robert.olbrycht@p.lodz.pl

The research presented in this work was inspired by the paper [1], where authors combined facial images taken in visible (VIS) and near-infrared (NIR) spectral ranges to obtain the effect of skin smoothing. This is possible, because NIR radiation is not strongly absorbed by melanin and hemoglobin. It leads to smoother rendering of skin tones, however delivered as a grayscale image. By means of bilateral filtering, this image may be used to fuse its detail layer with base layer of the visible luminance. There are also other applications of combining VIS and NIR images, such as haze removal or shadow detection [2]. The motivation for the author to perform the presented research was the need for investigation, if combining VIS and NIR images can be used for improving portrait illumination effect, as this can be beneficial for the biomedical purposes. Currently, many solutions for simulating lighting set-ups are present, however relying on VIS image only.

The solution proposed by the author relies on using the NIR channel as the source of image data for adding illumination effect to the VIS image. It can make portrait images looking more natural. This processing approach can be implemented e.g. with the aid of free GIMP software. It is necessary to have one layer with VIS image and the second one with NIR image. Then, the blending mode of the NIR layer needs to be set to "screen". It inverts the values of each of the visible pixels in the two layers of the image, multiplies them together, divides by 255 and inverts this value again, according to the formula (1) [3]. It results in usually brighter image, and this brightness is proportional to the brightness of the NIR layer. It means that, as shown in fig. 1(b-e), the strength of brightening can be regulated by changing the black point input level for the NIR layer, what results in zeroing pixel values not greater than a desired level.

$$E = 255 - \frac{(255-M) \times (255-I)}{255} \tag{1}$$

The example of the proposed processing is realized with the VIS and NIR portrait images taken from [2]. For better visualization of the desired effect, the contrast of NIR portrait taken from [2] is increased – fig. 1(f).

| (a) [1,2] | (b) | (c) | (d) | (e) | (f) [2] |
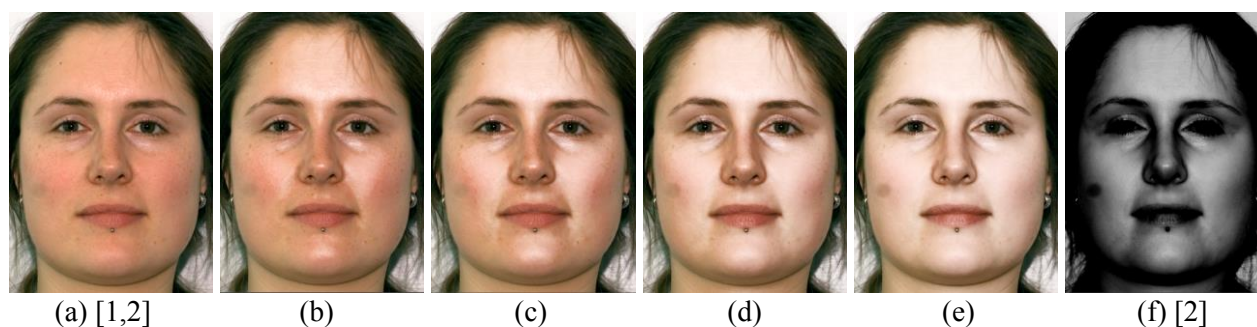
Fig. 1. (a) Exemplary portrait image before processing taken from [1,2] and with processing using the proposed approach with (b) the highest to (e) the lowest black point input level setting, that affects the NIR image (f) taken from [2], here shown and used with increased contrast.

Obtained results demonstrate that the proposed approach can provide results similar to the ones, that could be obtained using additional, physical illumination set-up for taking human skin photographs.

References:
[1] Fredembach, C., Barbuscia, N., & Süsstrunk, S., Combining visible and near-infrared images for realistic skin smoothing. International Conference on Communications in Computing, 2009.
[2] Süsstrunk, S., Fredembach, C. 8.1: Invited Paper: Enhancing the Visible with the Invisible: Exploiting Near Infrared to Advance Computational Photography and Computer Vision. SID Symposium Digest of Technical Papers, 2010, 41: 90-93. https://doi.org/10.1889/1.3500628
[3] GNU Image Manipulation Program User Manual – available online: https://docs.gimp.org/2.10/en/

Combined antimicrobial photodynamic therapy: a new approach for modern treatment

Aleksandra Pietrowska [1], Agnieszka Ulatowska-Jarża [1], Iwona Hołowacz [1], Anna Matczuk [2], Alina Wieliczko [3], Igor Buzalewicz [1]

[1] Department of Biomedical Engineering, Faculty of Fundamental Problems of Technology, Wroclaw University of Science and Technology, Poland
[2] Department of Pathology, Division of Microbiology, Faculty of Veterinary Medicine, Wrocław University of Environmental and Life Sciences, Poland
[3] Department of Epizootiology and Veterinary Administration with Clinic of Infectious Diseases, Wrocław University of Environmental and Life Sciences, Poland

aleksandra.pietrowska@pwr.edu.pl

Currently, the presence of antibiotic-resistant bacteria and the infections caused by them is a huge threat to public health. There are a lot of strategies used to kill bacteria cells, but they are limited by possibility of developing resistance. Antimicrobial photodynamic therapy (aPDT) emerges as a promising alternative for the prevention of infections due to the inability of bacteria to become resistant to aPDT inactivation processes. A combined therapy becomes the most common strategy in modern treatment [1]. Particularly noteworthy is the use of efflux pump inhibitors (EPIs) in combined photodynamic therapy, which may contribute to an increase in the accumulation of the photosensitizer (PS) inside the cells and, consequently, to a more effective therapy.

The main objective of our study was to demonstrate the increase in PS accumulation within bacteria single-cells by using the functionalized combination of PS and EPI. The examination was carried out on *Escherichia coli* bacteria (ATCC 25922) belonging to Gram-negative bacteria using anionic Chlorin e6 (Ce6) and cationic Pheophorbide a (Pheo). Pheo exhibits a lower accumulation within the cell than Ce6, but, being the EPI it can be used in combination with anionic Ce6 to improve Ce6 accumulation within the bacteria cell and consequently also to perform a more effective aPDT. The accumulation of PSs was investigated by digital holotomography (DHT) and fluorescence confocal microscopy. The technique DHT provides a three-dimensional distribution of refractive index (RI) enabling visualization of the internal structure of biological materials. This allows for non-invasive imaging of living cells without their fixation, damage or chemical modification. Observation of the spatial distribution of the refractive index provides information about the changes that occur as a result of the bacterial cell division, growth, accumulation of substances inside the cells or photoinactivation caused by aPDT.

Based on the reconstructed 3D-RI tomograms by DHT and proposed algorithm for processing to obtain RI value of cells, it was possible to determine the dry mass density of cells. The efficiency of aPDT was equal to 29.45% for Ce6 + Pheo, 13.77% for Ce6, and 16.15% for Pheo. The obtained results suggest that the use of functionalized PS mixtures can contribute to an increase in the efficiency of bacterial cell penetration and can create new perspectives for more efficient aPDT in the case of Gram-negative bacteria species, which was confirmed based on *E.coli* examination [2].

The results obtained in this in vitro study show that the use of the functionalized combination of two substances, in which one of them acts as an EPI, enables an increase in the efficiency of the *E.coli* cells penetration by PS. The results suggest that when a functionalized combination of PSs was used, the efficacy of the photodynamic effect was significantly higher than when each of the PSs was used alone. Furthermore, the use of the functional combination of substances can contribute to a more efficient photoinactivation of Gram-negative bacteria cells, which have a lower permeability to single anionic and neutral PSs compared to those of Gram-positive bacteria cells.

References:
[1] Youf, R et al. Antimicrobial Photodynamic Therapy: Latest Developments with a Focus on Combinatory Strategies. *Pharmaceutics,* 2021, vol. 13, no. 1995, pp. 1-56
[2] Pietrowska, A. et al. The Enhancement of Antimicrobial Photodynamic Therapy of Escherichia Coli by a Functionalized Combination of Photosensitizers: In Vitro Examination of Single Cells by Quantitative Phase Imaging. *International Journal of Molecular Sciences*. 2022, vol. 23, no. 6137, pp. 1-17

Investigating factors affecting functional amyloid aggregation

Oliwia Polańska[1]*, Marlena Gąsior-Głogowska[1], Monika Szefczyk[2], Natalia Szulc[1], Andrzej Żak[3],
Witold Dyrka[1], Małgorzata Kotulska[1]
Wroclaw University of Science and Technology, Wybrzeże Wyspiańskiego 27, 50-370 Wrocław, Poland:
[1]Department of Biomedical Engineering, Faculty of Fundamental Problems of Technology
[2]Department of Bioorganic Chemistry, Faculty of Chemistry
[3]Institute of Advanced Materials, Faculty of Chemistry
*e-mail: oliwia.polanska@pwr.edu.pl

Aims: Amyloid fibers, which are formed by misfolded proteins, are associated with different diseases such as Alzheimer's disease. However, there are also functional amyloids, which are used by different organisms for physiological processes. A characteristic feature of all amyloids is the presence of a *β-cross* structure. As a result, they have high mechanical strength and stability through resistance to denaturing agents and proteolytic enzymes, which prevents their degradation. Due to these properties, amyloids have become objects of research as new biomaterials e.g.: scaffolds for tissue regeneration, antimicrobial agents, biosensors, hydrogels, and nanodevices [1]. The purpose of this study was to characterize amyloid peptides, including investigating the temperature stability of the formed fibers and determining factors affecting aggregation, such as peptide concentration, solution pH and the type of surface on which the samples were tested.

Methods: Two amyloid-forming motifs of PUASM, which likely act as an interface between NLRs and ATP nucleosidases, were predicted by a novel machine-learning grammatical model [2]. The peptides were synthesized on solid support, purified using preparative HPLC in water/acetonitrile eluent system to obtain >95% purity, and eventually lyophilized. Recent studies have confirmed their amyloidogenic properties [3]. The samples were tested in several solvents, such as NaCl solution or a 3.3% mixture of DMSO with PBS at different pH values. The peptides were characterized with the use of the ThT assay and FTIR spectroscopy. The first technique allows the monitoring of aggregation kinetics under different experimental conditions. With FTIR, it is possible to determine the secondary structure of the peptides and observe their conformational changes.

Results: The ThT assay showed that an increase in pH and peptide concentration lead to accelerated aggregation. Interestingly, the experiment yielded two different results when two 96-well plates with different surfaces (standard and low-binding) were used. On the low-binding plate, peptides aggregated more slowly or did not aggregate. FTIR spectroscopic studies showed that both peptides exhibited intense absorption, around 1630 cm^{-1}, corresponding to the *β-cross* amyloid architecture. In addition, strong bands between 1692 and 1651 cm^{-1} were also noticed, indicating the presence of turns and loops. Moreover, the studied peptides were found to be thermally unstable, and an increase in temperature caused a change in their conformation. N-terminus peptide aggregated faster and formed more stable aggregates, while C-terminus peptide aggregated more slowly and was more sensitive to external factors.

Conclusion: The experiments showed that the aggregation process can potentially be controlled by various factors, such as pH, peptide concentration or the type of surface on which the experiments are performed. In our case, an increase in concentration and pH promoted fibrillization of the studied PUASM peptides. As functional amyloids, they are more sentive to enviromental factors than pathological ones.

References:
[1] A. K. Thakur, et al., ToxPoint: A Need for Regulatory Thinking for Amyloid-Based Biomaterials, *Toxicological Sciences*, 2021, vol. 179, no. 1, pp. 1–2.
[2] J. W. Wojciechowski et al., Exploring a diverse world of effector domains and amyloid signaling motifs in fungal NLR proteins, *PLoS Comput Biol*, 2022, vol. 18, no. 12, e1010787.
[3] O. Polańska, et al., Aggregation properties of peptides mediating interaction between NLRs and ATP nucleosidases, *#RSCPoster Twitter Conference*, 2023.

Optimization of ornithine determination by the optical method in a microfluidic system with an enzymatic microreactor

E. Remiszewska[a], M. Grzeczkowicz[a], K. Malecha[b], D.G. Pijanowska[a],

[a] Nalecz Institute of Biocybernetics and Biomedical Engineering, Polish Academy of Sciences,
Ks. Trojdena 4, 02-109 Warsaw, Poland
email:eremiszewska@ibib.waw.pl

[b] Faculty of Microsystem Electronics and Fotonics, Wrocław University of Science and Technology

*Wybrzeże Wyspiańskiego 27, 50-370 Wrocław, Polan*d

Determination of ornithine - an amino acid, gives the insight into the cellular urea cycle. The urea cycle disorders are associated with inherited metabolic diseases in which high levels of ornithine and ammonia, glutamine, citrulline are observed, are characterized by significant mortality and morbidity in infants and children. Several techniques for determination of ornithine have been reported in the literature. These technique were mainly chromatography with optical detection [1, 2], less commonly voltamperometric methods are used [3, 4].

The aim of the research was to develop a flow-through enzymatic microreactor for the microfluidic system with optical detection of ornithine in small volume samples. The enzyme - lysine oxidase (LyOx) is immobilized on the surface of the microreactor. The biofunctionalization was performed with use of aminopropyltriethoxysilane and bi-functional agent - glutaraldehyde. The conditions of the oxidation reaction of ornithine (L-Orn) catalysed by the LyOx in the alkaline environment and colour reaction were optimized. Products of the enzymatic reaction are 2-keto-5-aminovaleric acid (KV) and hydrogen peroxide (H_2O_2) (Fig.1). In the second reaction, ammonium ions (NH_4^+) reacting with NaSal and NaClO, and in the presence of SNP a colour product – indophenol salt with a maximum of absorbance at 700 nm is produced.
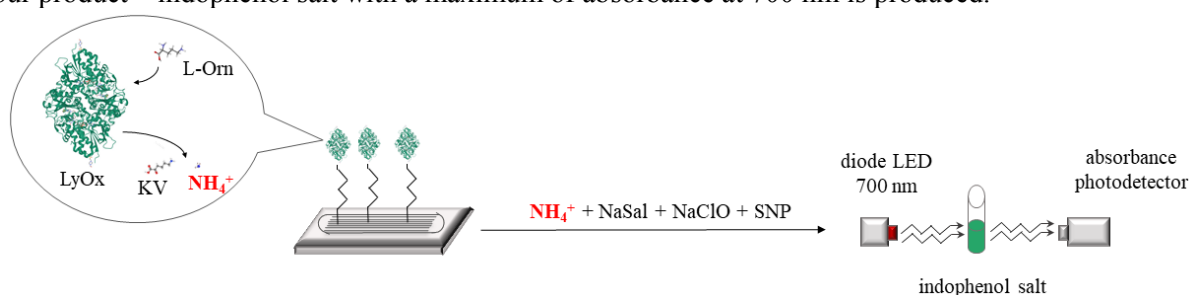
Fig.1. Scheme of reaction of oxidation of ornithine catalysed by the LyOx in an alkaline environment, (KV - 2-keto-5-aminovaleric acid, NaSal - sodium salicylate, NaClO - sodium hypochlorite, SNP - sodium nitroprusside).

The concentration of reagents were optimized earlier [5], but it was necessary to adjust temperature for the reaction. Three temperatures of 25°C, 30°C and 37°C were tested and the results are shown in Fig. 2.a. The optimum temperature turned out to be the highest of the tested ones. Linear range for ornithine determination using absorbance measurements for the microfluidic system was 0.06 – 1 mM (Fig.2.b). The sensitivity of this method was 0.258 ABS/mM. The developed method enables monitoring of low concentration of the analyte in biological samples, reducing the measurements time and costs.
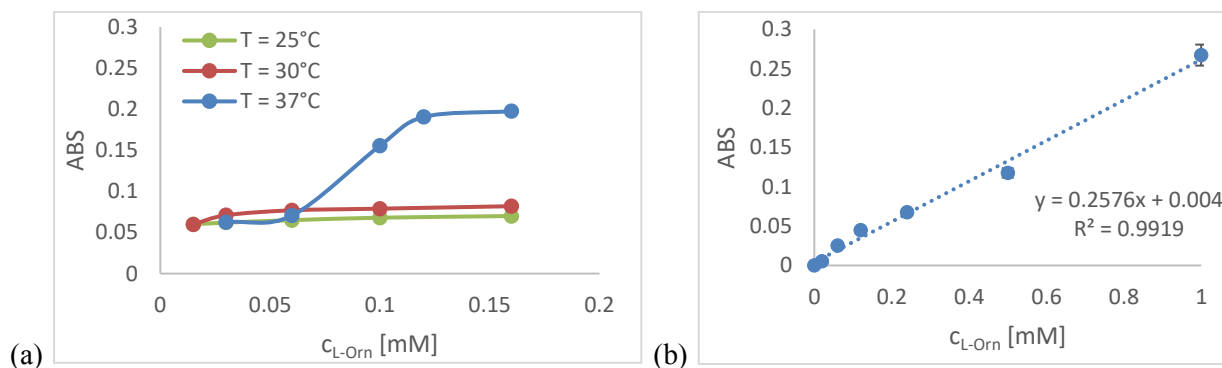
Fig.2. Calibration curves for ornithine obtained (a) under stationary conditions at different temperatures (spectrophotometer Synergy HT, BioTek) and (b) in the microfluidic system with the enzymatic microreactor.

Ref.: [1] D. Trisrivirat, et al., J Biol Chem, 295 (2020) 11246-61. [2] K.H.A. Sowdani, et al., Int J Sci and Res, 3 (2014) 1920-5. [3] N. Sato, et al., Anal Chim Acta, 456 (2002) 219-26. [4] A. Guerrieri, et al., Anal Chim Acta, 795 (2013) 52-9. [5] E. Remiszewska, et al., Sens. Actuators B: Chem, 285 (2019) 375-84.

Electrochemical determination of azathioprine based on selective drug-DNA interactions

Anna Sołdatowska[1], Marcin Urbanowicz[1], Magdalena Urbanowicz[2], Kamila Sadowska[1], Dorota Pijanowska[1]

[1]Nalecz Institute of Biocybernetics and Biomedical Engineering Polish Academy of Sciences

Ks. Trojdena 4 st. Warsaw, Poland

[2]Falsified Medicines and Medical Devices Department, National Medicines Institute

Chełmska 30/34 st. Warsaw, Poland

email: asoldatowska@ibib.waw.pl

Therapeutic drug monitoring (TDM) is a practice in clinical pharmacology that involves measuring drug concentrations in a patient's blood or other biological fluids to optimize drug therapy. It is used for drugs that have a narrow therapeutic index, meaning there is a small range between the drug's effective and toxic doses [1]. An example of such medications is thiopurines, which are commonly used to treat inflammatory bowel disease (IBD), autoimmune diseases, and some types of cancer. Due to a number of potential adverse effects, patients taking thiopurines should be monitored closely, but at the moment, there is a lack of analytical tools enabling physicians to quickly and simply optimize their therapy [2].

The main goal of this research is the development of an electrochemical biosensor with selectivity for one of the thiopurines, namely azathioprine (AZA). To achieve this goal, initial investigations were performed to evaluate the electrochemical behaviour AZA on miniaturized graphite electrodes. Furthermore, the interactions between the azathioprine and DNA, which could serve as a potential bioreceptor, were explored using techniques such as UV–Vis spectroscopy and high-performance liquid chromatography (HPLC). The results obtained from the interaction studies were confirmed electrochemically using an electrode modified with a selected DNA sequence.

Electrochemical studies confirmed the activity of AZA and showed that it undergoes a reduction reaction. The measurement environment and analytical parameters of the biosensor, i.e. linear response range, sensitivity and limit of detection (LOD), were determined (Table 1). The conducted interaction studies of azathioprine with a total of 20 DNA strands identified couple sequences as a potential bioreceptors. Finally, miniaturized graphite electrodes were modified with the selected DNA sequences to confirm the results obtained from the interaction studies.

Table 1. Summary of results obtained from electrochemical investigations.

	AZA
pH	7.4
Linear range (μM)	5 – 100
Sensitivity (μA/μM)	0.330
LOD (μM)	2.66

There are many literature reports on various approaches for the determination of azathioprine. However, a significant gap remains in the development of an electrochemical measurement system that utilizes a bioreceptor ensuring the selectivity needed for analysing samples of complex matrices. In this context, these preliminary studies present a vital step forward. They not only establish the groundwork for the development of a DNA-based biosensor capable of selectively detecting AZA but also provide valuable insights into the nature of the interactions involved. By addressing this research gap, these studies offer promising prospects for advancing the field and addressing the challenges associated with thiopurine determination in complex sample matrices.

References:

[1] Kang J.-S.; Lee M.-H.; Overview of Therapeutic Drug Monitoring, *The Korean Journal of Internal Medicine*, 2009, vol. 24, no. 1, pp. 1-10

[2] Luber R.P.; Honap S.; Cunningham G.; Irving P. M.; Can We Predict the Toxicity and Response to Thiopurines in Inflammatory Bowel Diseases, *Frontiers in Medicine*, 2019, vol. 6

Determination of oxygen saturation in two layers with TD-NIRS using a single DTOF versus changes in moments of DTOFs

Aleh Sudakou[a,*], Heidrun Wabnitz[b], Stanisław Wojtkiewicz[a], and Adam Liebert[a]

[a] Nalecz Institute of Biocybernetics and Biomedical Engineering Polish Academy of Sciences, Trojdena 4, 02-109 Warsaw, Poland
[b] Physikalisch-Technische Bundesanstalt (PTB), Abbestraße 2-12, 10587 Berlin, Germany

*asudakou@ibib.waw.pl

Aims: Near-infrared spectroscopy (NIRS) is a well-established method for measuring tissue oxygen saturation (StO_2), which is useful for clinical applications. Determining StO_2 values for different layers within layered tissues, such as the brain and scalp, is needed but remains challenging. Recently we presented an improved method that allows more accurately determining StO_2 in two layers based on changes in moments of the distribution of times of flight of photons (DTOFs). One limitation of the method is the need to know the baseline optical properties of two layers and the thickness of the superficial layer. In the current study, we implement a method that is based on a single DTOF for determining the StO_2 in two layers, which is known as the multi-layered curve-fitting method and which determines the absolute optical properties (i.e. also the baseline optical properties). We present a comparison of the two methods, based on changes in moments versus a single DTOF. We test both methods using data measured on our recently presented two-layered blood-lipid phantom that allows changing StO_2 in two compartments separately.

Methods: The method based on moments utilizes changes in statistical moments of DTOFs, an analytical solution of the diffusion equation, and the Levenberg–Marquardt algorithm (LMA) to determine changes in absorption ($\Delta\mu_a$) in two layers. The absolute μ_a can be obtained by adding the baseline μ_a to the determined $\Delta\mu_a$. The multi-layered curve-fitting method utilizes a DTOF and an analytical solution of the diffusion equation to determine absolute optical properties (μ_a and/or the reduced scattering μ'_s) in multiple layers. The concentrations of oxy- (HbO_2) and deoxyhemoglobin (Hb), and hence StO_2, can be obtained using the determined μ_a values at multiple wavelengths and the known molar extinction coefficients of HbO_2 and Hb.

We describe and test the capabilities of the two methods, comparing their theoretical uncertainties and their robustness. Experimentally, we test and compare the capabilities of the two methods for determining optical properties and StO_2 in two layers, using multi-wavelength time-domain NIRS measurements on a two-layered blood-lipid phantom. The phantom has two liquid layers that correspond to superficial (variable thickness) and deep layers mimicking scalp and brain, which were separated by a thin (0.050 mm) Mylar foil. Each layer contained water, SMOFlipid, and human blood, which we deoxygenated using yeast and oxygenated by bubbling oxygen from a tank. We deoxygenated the blood in the deep layer twice, then in the superficial layer once, and finally in the deep layer three more times (six deoxygenation cycles in total). The experiment was repeated three times, each time with a different superficial layer thickness (12, 15, and 17 mm). We measured simultaneously on the two-layered medium and on the deep layer for reference.

Results: Analyzing measurements on the deep layer (using a homogeneous model), showed that StO_2 in the deep layer followed the expected desaturation trends (from 100 to 0%) for all deoxygenation cycles in all experiments. Analyzing measurements on the two-layered medium, when using a homogeneous model, the determined StO_2 was strongly influenced by the superficial layer, which demonstrated the need for a two-layered model. The method based on moments accurately determined StO_2 in both layers, using the knowledge of the baseline optical properties of both layers. The multi-layered curve-fitting method is able to accurately retrieve StO_2 of both layers for theoretical data, but not always for the measured data because of multiple sources of noise. Determining many parameters (μ_a and μ'_s in multiple layers) is challenging because of the limited amount of information contained in a DTOF.

Conclusion:
The multi-layered curve-fitting method allows obtaining baseline optical properties of two layers, although with limited robustness. A combination of both methods (based on moments and DTOFs) could allow the more accurate determination of StO_2 in two layers, including for *in-vivo* measurements, overcoming the contamination from the superficial layer for measurements of the deep layer.

Evaluation of the effect of titanium dioxide coatings produced by different methods on eukaryotic cellproliferation

Klaudia Szafarz, Maryna Silchenko, Paweł Petelewicz, Michał Kozłowski, Marian Cłapa, Dorota Bociąga

Department of Biomedical Engineering and Functional Materials, Faculty of Mechanical Engineering, Lodz University of Technology, 1/15 Stefanowskiego Street, 90-537 Lodz, Poland.

Email: pawelpetelewicz@edu.p.lodz.pl

Abstract

Titanium dioxide (TiO_2) is currently one of the most extensively researched metal oxides worldwide for its potential applications in biomedicine. This article presents the relationship between eukaryotic cell proliferation and titanium dioxide coatings produced by different methods on Ti6Al4V alloy substrates. TiO_2 coatings exhibit varying properties depending on their fabrication methods and selected parameters. The motivation behind this research was to determine the cell proliferation capability on TiO_2 coatings for tissue engineering and biomedicine applications [1][2].

Studies were conducted coatings on fabricated on Ti6Al4V titanium alloy samples using the sol-gel method, high-voltage electroanalytical method and low-voltage electroanalytical method with variable fabrication parameters. As a result of this work, coatings with different roughness and surface development were obtained. The following characterization tests were conducted to assess the coating properties: roughness measurement using a profilometer, wettability examination using a goniometer and sessile drop method, coating thickness measurement using an ellipsometer, surface morphology analysis using an optical microscope and scanning electron microscope. In the biological investigation, direct testing (LIVE/DEAD) and indirect testing (MTT) were performed to evaluate cytotoxicity and cell proliferation capacity.

The biological evaluation test results revealed information regarding titanium dioxide coatings potential biomedical application depending on their fabrication method. The obtained MTT test results indicate that thecoatings fabricated through high-voltage and low-voltage electroanalytical methods exhibit similar values to the control sample (Ti6Al4V), indicating non-toxicity towards cells. Additionally, it was observed that coatings produced using the sol-gel method are on the verge of biocompatibility. Correlations between fabrication parameters and coating properties were also observed.

Keywords: titanium dioxide (TiO_2), anodization method, sol-gel method, eukaryotic cell proliferation.

Literatura:

[1] K.O., C.C., C. H. & partners. Effect of Multi-nano-titania Film on Proliferation and Differentiation of Mouse Fibroblast Cell on Titanium, *Journal of The Electrochemical Society*, 2008, vol. 155, no. 6, st155-172

[2] M. P. , P.B. , A.C. & partners. Analysis of cytotoxicity and genotoxicity in a short-term dependent manner induced by a new titanium dioxide nanoparticle in murine fibroblast cells: Toxicology Mechanisms and Methods, *Taylor & Francis Group*, 2021, vol. 32, no. 3, tr. 213-223,

Multiscale Vesselness Approach for Precise Radii Estimation in MRA

Piotr M. Szczypiński

Institute of Electronics, Lodz University of Technology, Lodz, Poland
piotr.szczypinski@p.lodz.pl

This study introduces a novel method for estimating blood vessel radii by utilizing multiscale vesselness functions [1]. Angiographic images commonly employ multiscale vesselness techniques to enhance blood vessels and reduce noise. The resulting image is corrected and binarized, enabling the construction of a 3D vector model of the blood vessel tree [2]. However, the accuracy of the model and the estimated radii may be limited by the image voxel spacing. To address this limitation, the proposed method takes advantage of the vesselness functions obtained during the enhancement process, eliminating the need for additional computations.
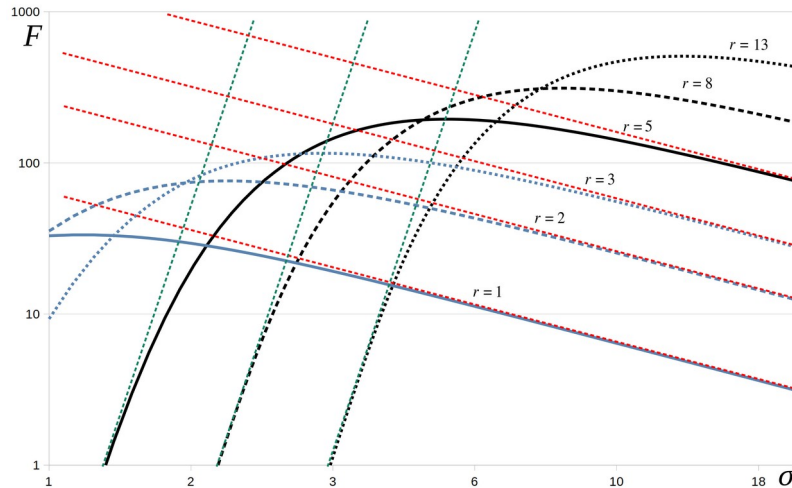
Fig. 1. The vesselness computed at centerlines of cylindrical structures of various radii r as a function of the standard deviation of Gaussian smoothing window.

$$f(\sigma;A,r)=\left(\frac{\left(\frac{\sigma}{\omega r}\right)^2}{1+\left(\frac{\sigma}{\omega r}\right)^2}\right)^{\eta}\frac{\omega\kappa A r}{\sqrt{1+\kappa^2\left(\frac{\sigma}{\omega r}-\frac{\omega r}{\sigma}\right)^2}} \qquad (1)$$

The relationship between the vesselness function, computed along the centerline of the blood vessel, and its radius was determined through experimental analysis (Fig. 1). It was discovered that this relationship can be effectively approximated by the function (1) with $\kappa = 17.29$, $\omega = 0.034$ and $\eta = 432$. By fitting the function to actual data, the parameter r serves as an estimator for the radius of the blood vessel.

This approach improves estimation speed while maintaining sub-voxel accuracy. The method is validated by comparing it with two state-of-the-art ray-casting-based approaches: one involving image binarization and the other fitting the complementary error function [2] to a brightness profile. Quantitative evaluation utilizes artificially generated images of tubes with known geometries, while qualitative assessment involves analyzing a real magnetic resonance angiogram. The results demonstrate the high accuracy and practicality of the proposed method. The algorithm has been implemented, and the source code is freely available to support further research endeavors.

References:
[1] Sato, Y., Nakajima, S., Atsumi, H., Koller, T., Gerig, G., Yoshida, S., Kikinis, R.: 3D multi-scale line filter for segmentation and visualization of curvilinear structures in medical images. In: Troccaz, J., Grimson, E., Mösges, R. (eds.) CVRMed MRCAS'97. pp. 213–222. Berlin, Heidelberg (1997)
[2] Materka, A., Kociński, M., Blumenfeld, J., Klepaczko, A., Deistung, A., Serres, B., Reichenbach, J.R.: Automated modeling of tubular blood vessels in 3D MR angiography images. In: 2015 9th International Symposium on Image and Signal Processing and Analysis (ISPA). pp. 54–59 (2015)

Real-time 3D ultrasound volume reconstruction supported with PlusToolkit libraries

Ewelina Świątek-Najwer, Martyna Kiełbasa

Department of Mechanics, Materials and Biomedical Engineering, Faculty of Mechanical Engineering,
Wrocław University of Science and Technology, Łukasiewicza 5, 50-371 Wrocław
ewelina.swiatek-najwer@pwr.edu.pl

Aims

The aim of this work was to evaluate the efficiency of real-time volume reconstruction by a navigated probe applying PlusToolkit libraries in comparison to the Computed Tomography (CT). Reported in the PlusToolkit software calibration error value [1] is not a conclusive characteristic, since it considers only 3D imaging technique accuracy with no relation to the volume reconstruction algorithm itself.

Methods

The Ultrasound EchoBlaster 128 System by Telemed (Lithuania) and Polaris Spectra Optical Tracking System by Northern Digital Inc. (Canada) were communicated with the Plus (Public software Library for UltraSound), an open-source BSD-style license software package [1]. Plus software enables recording data, temporal and spatial calibration of an ultrasound probe (fCal) as well as processing and streaming data (PlusServer). The software can also transmit the data to the 3D Slicer application for further analysis and multiple exports options. In our study the probe was equipped with a frame with passive optical tracking markers and calibrated both temporarily and spatially using a PerkLab designed "fCal 2.0" phantom made of polylactide by FDM method. The system was tested on a femur phantom with an angular shaft deformation. A 3d ultrasound model was achieved in the real time volume reconstruction mode applying linear interpolation algorithm available in Plus package and exported to a STL file in 3D Slicer. The obtained ultrasound 3d model was compared to the CT-based model. The CT dataset (with a pixel size 0.18 mm and slice thickness 0.9 mm, 1080 images with 768x768 pixels) was thresholded using Materialise Mimics Innovation Suite and a 3d model was exported to a STL file. The CT and ultrasound-based surface models were aligned in MeshLab by the Iterative Closest Point (ICP) registration method.
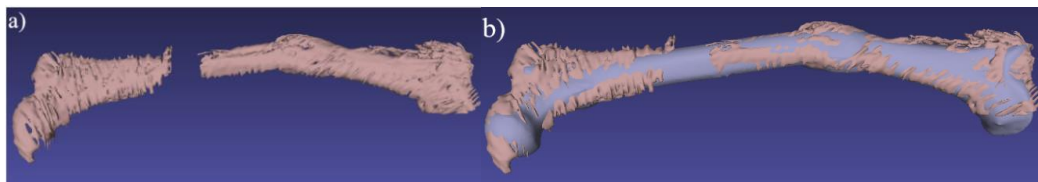
Fig. 1. a) Result of ultrasound-based volume reconstruction, b) aligned CT and 3D ultrasound-based volume

Results

The calibration error of the ultrasound probe was relatively low (0.34 mm) in comparison to reported by PerkLab [1]. A mean error of CT and ultrasound-based model ICP alignment was 0.85 mm. Four linear distances on ultrasound-based model were measured 10 times and mean values were compared to corresponding distances measured on CT-model. The results were as following (A - width of deformation region) 42.44 mm ± 0.34 mm (0.81%), (B - length of deformation region) 67.72 mm ± 0.54 mm (0.79%), (C - medial condyle to the top of femur head) 435,72 mm ± 6,14 mm (1,43%), (D - diameter of femur head) 38,89 mm ± 0,63 mm (1,60%). Another compliance metric such as Hausdorff distance could not be applied because of lacking regions of phantom scanning (caused by location of reference frame).

Conclusion

Our study confirms the compatibility of ultrasound based real-time volume reconstruction to CT-based model. The relative distance errors were small, between 0.8 and 1.6%, proving that the low calibration error led to satisfying volume reconstruction results. The tool can facilitate the 3D bone measurements [2][3].

References:

[1] Lasso A., Heffter T., Rankin A., Pinter C., Ungi T., Fichtinger G., *PLUS: Open-source toolkit for ultrasound-guided intervention systems*, IEEE Trans Biomed Eng. 2014 Oct; vol. 61, no. 1, pp. 0:2527-37.

[2]K. Krysztoforski, P. Krowicki, E. Świątek-Najwer, R. Będziński, P. Keppler, *Noninvasive ultrasonic measuring system for bone geometry examination*, International Journal of Medical Robotics and Computer Assisted Surgery, 2011, vol. 7, no 1, pp.85–95.

[3] E. Świątek-Najwer, K. Krysztoforski, S. Ł. Dragan, R. Będziński, *The investigation of the lower limb geometry using 3D sonography and magnetic resonance*, Measurement, 2012, vol. 45, no 4, pp. 702–710.

Effect of Dendrimer Interlayers on Enzyme Immobilization in Electrochemical Sensing

Marcin Urbanowicz, Kamila Sadowska, Agnieszka Paziewska-Nowak Anna Sołdatowska, Marek Dawgul, Dorota G. Pijanowska

Nalecz Institute of Biocybernetics and Biomedical Engineering Polish Academy of Sciences, Ks. Trojdena 4, 02-109 Warsaw, Poland

murbanowicz@ibib.waw.pl

Biosensor performance depends on the properties of the immobilized bioreceptor. The effectiveness of electrochemical sensors is dependent on the quantity and availability of bioreceptor molecules that are immobilized onto the electrode's surface [1]. An optimal distance between the electrode and bioreceptor is necessary for efficient electron transfer and analytical signals in amperometric biosensors. Linear linkers, commonly used for immobilization, limit the thickness and organization of the biosensor matrix. On the other hand, dendrimers can be used as intermediate layers, providing a thicker layer for immobilization and keeping the necessary distance between the electrode and bioreceptor [2].

The aim of this research was to propose a novel approach to design bioactive layers for electrochemical biosensors using the surface plasmon resonance (SPR) method to optimize enzyme loading on the gold sensing surface. The dendrimer interlayer (poly(amidoamine) dendrimers, PAMAM) was shown to increase the

amount of biomolecules bonded to the surface, with the best electrochemical performance achieved using a system based on PAMAM 4G. The developed procedure was used to manufacture electrochemical biosensors for glutamate, which demonstrated higher sensitivity for dendrimer-based biosensors compared to those with linear linkers. This research suggests the possibility of increasing the sensor response without electrochemical enrichment components. The study also highlights the potential of the SPR technique in designing new biosensors based on enzymatic bioreceptors.
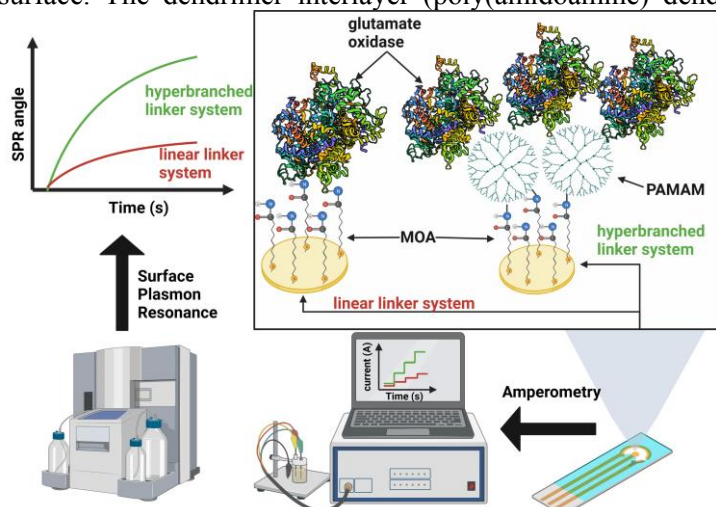
Electrochemical studies have confirmed that biosensors based on dendrimer architecture show better metrology performance than those based on linear linkers. In particular, in the case of the CV method for the glutamate biosensor based on the MOA-PAMAM 4G-GlutOx system, the sensitivity was 118.47 ± 1.64 μA/(mM·cm^2) and the limit of detection (LOD) = 1.9 mM, while for the biosensor based on linear linkers, such as the MOA-GlutOx system, the sensitivity was 46.85 ± 1.63 μA/(mM·cm^2) and the LOD = 7.2 mM. Moreover, for MOA-PAMAM 4G-GlutOx, in the case of the chronoamperometric method, the determined sensitivity was 3.36 ± 0.08 nA/μM, and LOD = 1.52 μM [3].

Despite the fact that dendrimers have been utilized in biosensors for several years, there has been a lack of systematic research on the impact of electrochemically nonenriched dendrimers on the performance of electrochemical biosensors. Distinguishing between the effects of dendrimers and other materials on the sensor's response is crucial because it enables a better understanding of the processes occurring at the electrode surface. Our research has established that, depending on the type of linker, we can control the surface loading of the bioreceptor, which has a direct influence on the metrological parameters of the biosensor. This research serves as an initial investigation into developing a series of glutamate biosensors which have the potential to be utilized in clinical analysis.

References:

[1] B. Eggins, Chemical Sensors and Biosensors, John Wiley & Sons Ltd, 2007.
[2] J. Satija, V.V.R. Sai, S. Mukherji, J. Mater. Chem. 21 2011, vol. 21, pp. 14367–14386
[3]. M. Urbanowicz, K. Sadowska, B. Lemieszek, A. Paziewska-Nowak, A. Sołdatowska, M. Dawgul, D.G. Pijanowska, Bioelectrochemistry, 2023, 152, 108407.

Examination of the effect of various C3A liver cells culturing conditions on the level of expression of selected genes - RT-qPCR analysis

Agnieszka Wencel, Monika Joanna Wisniewska, Malgorzata Jakubowska, Dorota Genowefa Pijanowska, Krzysztof Dariusz Pluta
Nalecz Institute of Biocybernetics and Biomedical Engineering Polish Academy of Sciences
Ks. Trojdena 4 st.
02-109 Warsaw
awencel@ibib.waw.pl

Rapid dedifferentiation of human isolated hepatocytes *ex vivo*, the liver parenchymal cells which are the gold standard in studies on liver metabolism and diseases, constitute the problem that still requires a solution [1]. Among others, hepatocyte growth factor (HGF) has been considered as a potential addition to liver cell culture because it is involved in various physiological processes: it increases cell proliferation, neovascularization, angiogenesis, activates neighbouring cells and reduces apoptosis, inflammation, and fibrosis [2]. Recently, we have examined the effect of various culture conditions, e.g. presence of HGF alone and in combination with collagen, coculture with fibroblasts and genetically modified fibroblasts overproducing HGF or with dried fibroblast growth substrate (drHSF), on human hepatocellular carcinoma (HCC) C3A cells - model of hepatocytes, in order to find an optimal support for liver cell culture [3]. To better understand the effect of these different culture conditions on liver cells, our research had to be extended with RT-qPCR analysis.

The analysis of the expression of selected liver-related genes: *CPS1, CYP3A4, ALB, HNF1A, HNF4A, GLUL CYP2E1, PXR* on transcript level, in different culture conditions, was performed using the RT-qPCR. In addition, the secretion of albumin, the most important protein synthetised by hepatocytes, and the ability of HCC cells to produce urea, were measured.

The addition of HGF to the culture medium resulted in increased expression of the *CYP3A4* and *HNF1A* genes. The increase of *CYP3A4* expression was also observed in the culture carried on dried fibroblasts and in coculture with fibroblasts (HSF). Coculture with HSF also increased *CYP2E1* and *PXR* gene expression. There were no differences in the expression of the examined genes in the C3A culture carried on collagen in combination with HGF supplementation. Similar tendency in expression of these genes was observed in the C3A culture on collagen alone, only a decrease in the expression of the CPS1 and PXR genes was observed compared to the control. Summing up the RT-qPCR analysis, it can be concluded that the best results, among tested culture methods, were achieved with the medium supplemented with HGF or with the coculture of HCC cells with HSF. An interesting observation is that despite the lower expression of the *ALB* gene encoding albumin, a significant increase in the protein production, as determined in the conditioned medium by ELISA, was noted in several culture versions. Increased albumin synthesis was observed when HGF was added to the medium and when C3A cells were cocultured with HSF and on drHSF substrate. On the other hand, there was no significant effect of culture conditions on urea production.

Based on our RT-qPCR results, the conclusion can be drawn that the addition of HGF to the culture or coculture with HSF could support the culture of hepatic cells, improve their metabolic capacity and slow down the process of dedifferentiation connected with the loss of their liver-specific features such as a decrease of activity of cytochrome P450 or a rapid lowering of albumin secretion.

References:
[1] Lőrincz T. et al. The Performance of HepG2 and HepaRG Systems through the Glass of Acetaminophen-Induced Toxicity. *Life*, 2021, vol. 11 no.8 pp. 856
[2] Gunawardena T.N.A et al. Conditioned media derived from mesenchymal stem cell cultures: The next generation for regenerative medicine, *J Tissue Eng Regen Med.*, 2019; vol. 13: pp. 569-586
[3] Wencel A. et al. Effects of genetically modified human skin fibroblasts, stably overexpressing hepatocyte growth factor, on hepatic functions of cocultured C3A cells, *Biotechnol Bioeng*, 2021, vol. 118, no. 1, pp. 72–81

Virtual platform for medical data and modern diagnostics
"MDB-MEDICAL DATA BANK"

Slawomir Wiak [I], Lukasz Szymanski [*I], Dariusz Trzmielak [II], Beata Kolesinska [III], Katarzyna Wojtera [I]

[I] Institute of Mechatronics and Information Systems, B. Stefanowskiego 22 Street, 90-537 Lodz, Poland
[II] Institute of the Polish Mother's Memorial Hospital, Rzgowska 281/289 Street, 93-338 Lodz, Poland
[III] Institute of Organic Chemistry, Zeromskiego 116 Street, 90-924 Lodz, Poland
[*] lukasz.szymanski@p.lodz.pl

The MDB[1] platform integrates and makes available in digital form unique medical data acquired by the "Polish Mother's Memorial Health Center" Institute in Lodz and the Lodz University of Technology. The main purpose of the MDB virtual platform is to collect, store and share medical data that has been digitized in good quality, anonymized, described with metadata, organized and grouped by tissue and diagnosis. The anonymized image data includes, according to standards, a description of the examinations and the medical diagnosis of each specimen, including those not affected by disease.

The virtual medical data platform (MDB) provides the ability to view and download data without creating an account. The open database via API provides access to resources relevant to scientific entities, doctors, companies in the pharmaceutical and insurance industries, researchers. The created tool facilitates the use of the database for the above-mentioned audiences by searching for a dedicated group of resources and the possibility to download them in open DICOM and XML formats.

The MDB[2] application's functionalities are aimed at accessing medical resources with the option to download source images with descriptions, and the ability to view good quality medical images through the website with the option to scale and move around the thumbnail of the specimen, and display the original description and diagnosis of the specialist (Figure 1).

(a)   (b)
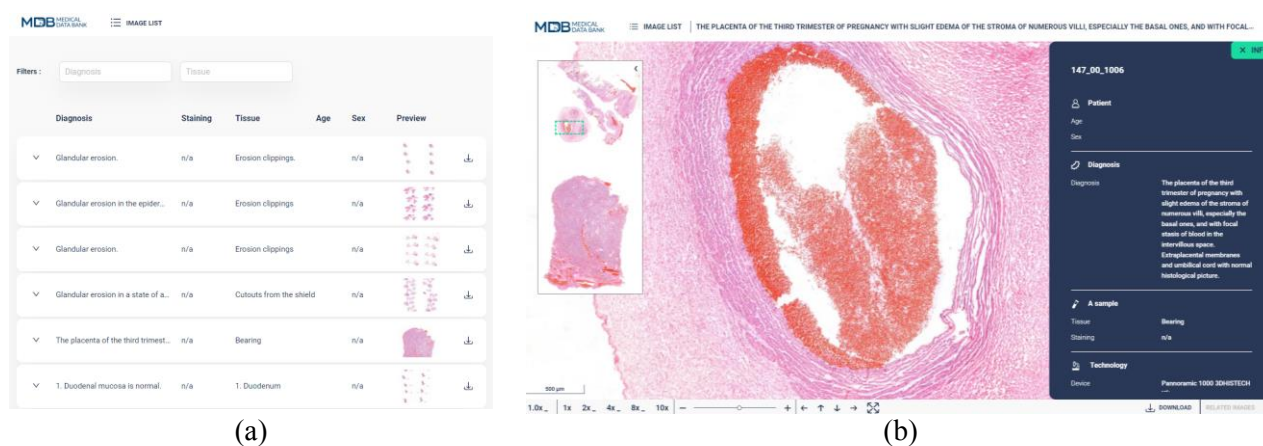
Figure 1. MDB platform, (a) access to resources stored in the database with the ability to search by diagnosis and tissue, (b) image viewing capabilities with diagnosis.

MDB is an open-access digital database of unique medical data on histopathology makes images available for biometric analysis, didactic work, doctors' self-education, statistics and as a unique source of popular-scientific information for the public. The resources made available will serve the development of oncological diagnostics, through further research on disease entities. The MDB platform is a response to the diagnosed problem of impeded access to attractive and unique digital medical data, which in its current dispersed, non-integrated, analogue form, significantly delays the emergence of innovations and new technologies necessary for medical progress, slows down research and scientific work, competence improvement and education of medical specialists and scientific staff.

---

[2] https://app.mdb.p.lodz.pl/

Evaluation of the impact of hydrogel composition solvent on the material properties, viability and proliferation of cells contained in 3D printouts

Adrianna Wierzbicka[1*], Mateusz Bartniak[1], Anna Sobczyk-Guzenda[1], Jacek Grabarczyk[1], Dorota Bociąga[1]

[1] Faculty of Mechanical Engineering, Institute of Materials Science and Engineering,
Lodz University of Technology, 90-537 Lodz, Poland
*e-mail: adrianna.wierzbicka@dokt.p.lodz.pl

Hydrogel materials have been used in a wide range of medical applications for more than 60 years. As biomaterials, they are distinguished by the high water content, plasticity and relatively low stiffness, which makes them similar to the natural tissues and can provide favorable environment for 3D cell culture. The large-scale development of 3D printing capabilities is creating increasingly promising solutions for tissue engineering and personalized medicine. The materials commonly used to produce bioinks for 3D printing are compositions based on sodium alginate and gelatin [1][2]. In addition to the properly selected composition of hydrogel bioinks, the type of solvent used for the preparation of polymer solutions becomes also important. The solvent has a significant impact on the mechanical properties and crosslinking time of the hydrogel, which directly affects the parameters of the 3D bioprinting processes [3][4]. Currently, the commonly used solvents for polymer compositions based on sodium alginate and gelatin are physiological saline, deionized water, PBS or HEPES buffer and a variety of cell culture media. However, the use of culture medium as a solvent leads to a significant improvement of the viability and proliferation of the cells contained in the material [4][5].

The research focuses on evaluating the influence of a culture medium dedicated to individual cell lines as a solvent of polymeric solutions on the rheological properties and printability of the developed compositions, physicochemical and mechanical properties of hydrogel materials. In addition, it was also evaluated the viability, proliferation and ability to spread of cells contained in the 3D printouts during their incubation for up to five weeks. The study included comparative analysis of immortalized fibroblast cells line NIH/3T3 and human adipose derived stem cells (ADSC). Research was carried out with the use of compositions based on 2 % (w/v) sodium alginate and 9% (w/v) gelatin prepared in media dedicated to the particular cell lines, i.e. DMEM and ADSC-BM.

The results indicate that the use of different types of culture media for the preparation of polymer solutions leads to obtain hydrogel materials with different properties. Both compositions are characterized by good 3D printability. Polymer solutions prepared in a medium dedicated to fibroblast cells are characterized by a slightly lower viscosity. DMEM-based hydrogel materials also feature slightly lower Young's modulus values. The analysis of the viability and proliferation of cells contained in the 3D printouts indicates that fibroblast cells are characterized by their ability to proliferate and spread homogeneously inside the material to form cellular network structures. ADSC cells during individual incubation periods are characterized by high viability, but they do not show the ability to proliferate. Their morphology after a 5-week culture in the printouts remains spheroidal. This phenomenon may be correlated with the slightly higher stiffness of the polymer matrix prepared in ADSC-BM culture medium, which may limit the proliferative capacity of the cells. Consequently, it is necessary to optimize the hydrogel composition used to encapsulate the stem cells to enable them the proliferation, spreading and form cellular network structures in the polymer matrix.

References:
[1] Łabowska M. B., Cierluk K., Jankowska A. M., Kulbacka J., Detyna J., Michalak I. A review on the adaption of alginate-gelatin hydrogels for 3D cultures and bioprinting. *Materials (Basel)*. 2021, 14(4):858.
[2] Wierzbicka A., Bartniak M., Rosińska K., Bociąga D. Optimization of the preparation process stages of the bioink compositions based on sodium alginate and gelatin to improve the viability of biological material contained in hydrogel 3D printouts. *Engineering of Biomaterials*. 2022;(165):7-16.
[3] Freeman F. E., Kelly D. J. Tuning alginate bioink stiffness and composition for controlled growth factor delivery and to spatially direct msc fate within bioprinted tissues. *Sci Rep*. 2017, 7(1):17042.
[4] Rosińska K., Bartniak M., Wierzbicka A., Sobczyk-Guzenda A., Bociąga D. Solvent types used for the preparation of hydrogels determine their mechanical properties and influence cell viability through gelatine and calcium ions release. *J Biomed Mater Res B Appl Biomater*. 2023, 111(2):314-330.
[5] Wang T., Sun W., Liu X., Wang C., Fu S., Tong Z. Promoted cell proliferation and mechanical relaxation of nanocomposite hydrogels prepared in cell culture medium. *React. Funct. Polym*. 2013, 73(5):683-689.

Cellular characterization of dedifferentiated human hepatocytes

Monika J. Wiśniewska[1], Małgorzata Jakubowska[1], Agnieszka Wencel[1],
Dorota G. Pijanowska[1], Krzysztof D. Pluta[1]

(1) Nałęcz Institute of Biocybernetics and Biomedical Engineering Polish Academy of Sciences, Ks. Trojdena 4, 02-109 Warsaw, Poland
mwisniewska@ibib.waw.pl

Aims
Nowadays organ transplantation is the only effective treatment for patients with liver failure. However, the main problem of this technique is donor shortage. Alternative therapies which can extend patients' life till transplantation or liver regeneration are still being sought. One of the most promising solutions currently being elaborated are hybrid devices called Bioartificial Liver (BAL). The best source of cells for these hybrid systems would be human isolated hepatocytes, but it is difficult to obtain large amounts of good quality biological material since human hepatocytes *ex vivo* do not proliferate and quickly lose their specific for differentiated cells features.

Method
One of our tasks is to elaborate an efficient isolation method for human hepatocytes. The new method is quick and gentle and enables the isolation of the whole spectrum of liver cells. It is based on mechanical defragmentation and enzymatic digestion of liver tissue. Using a special culture medium dedicated to hepatocytes we obtained dedifferentiated fibroblasts-like cells which are capable of dividing yet still are producing markers characteristic for differentiated hepatocytes. These new cells, called Liver Derived Fibroblasts (LDF), are designated to be used for seeding our self-manufactured hollow fiber flow bioreactors. This culture module constitutes our model of the novel biologically active function block (BAFB) of improved BAL.

Results
LDF were successfully cultured in both stationary and dynamic conditions. Preliminary results obtained from flow cytometry, immunocytochemistry, and ELISA tests showed that our new dividing cells could still produce characteristic for hepatocytes proteins, even if dedifferentiated. Moreover, we could also observe urea production by the LDF.

Conclusions
We concluded that our newly established cells, derived from isolated human hepatocytes, can be a suitable biological material for the use in our model of BAFB of BAL.

The use of trend change indicators to visualize differences between cohorts in postural stability tasks

Piotr Wodarski[1], Jacek Jurkojć[2], Elke Warmerdam[3], Clint Hansen[4], Robbin Romijnders[5], Markus A. Hobert[6], Walter Maetzler[7], Krzysztof Cygoń[8], Marek Gzik[9]

[1,2,9]Silesian University of Technology, Faculty of Biomedical Engineering,
Department of Biomechatronics, Gliwice, Poland
[3,4,5,6,7]Department of Neurology, Kiel University, 24105 Kiel, Germany
[3]Division of Surgery, Saarland University, 66421 Homburg, Germany
[8]Skyfi Sp. z o.o., Gliwice, Polska
Corresponding Author: Piotr Wodarski, piotr.wodarski@polsl.pl

Introduction: Disturbances in body balance and stability are key symptoms of neurodegenerative diseases, indicating functional and anatomical system degeneration [1]. Assessing the clinical condition of patients and early detection of these diseases, as well as fall prevention, can be aided by postural stability measurements. However, current methods exhibit low sensitivity, making it challenging to differentiate between specific diseases and disease stages. This research aimed to explore the potential of utilizing trend change analysis techniques to evaluate signals recorded during postural stability measurements [2] in order to differentiate between groups as well as between on and off state in individuals with Parkinson's disease.

Methods: A total of 142 participants were involved, including 41 young people (YO), 61 elderly people (Old), 12 people with Parkinson's disease in OFF state (PDoff), and 28 people with Parkinson's disease in ON state (PDon). All participants underwent a postural stability test, standing with their eyes open for 10 seconds, while wearing three accelerometers (Noraxon USA Inc., myoMOTION, Scottsdale, AZ, USA) on their head, sternum, and pelvis. Signals were low-pass filtered using an IIR LPF filter with a cutoff frequency of 7 Hz. The adopted algorithm for detecting changes in stock market trends facilitated identifying moments of trend changes in the measured signal. Subsequently, the number of these changes is the Trend Change Index (TCI), the difference in signal value between successive trend changes (dS), and the time between these changes (dT) were calculated. Statistical analysis was conducted using JASP (Version 0.17.2).

Results: Significant differences were observed for TCI and dT values between the PDoff group and the other groups. Additionally, the relationship between dT and dS was analyzed and presented in the form of ellipses. Each ellipse's center represents the average value of these quantities, with the individual axes representing standard deviations. The obtained results facilitated clear differentiation between the PDoff and PDon groups. Furthermore, it was observed that the best differentiation was achieved at the pelvic level among the three sensor locations analyzed.
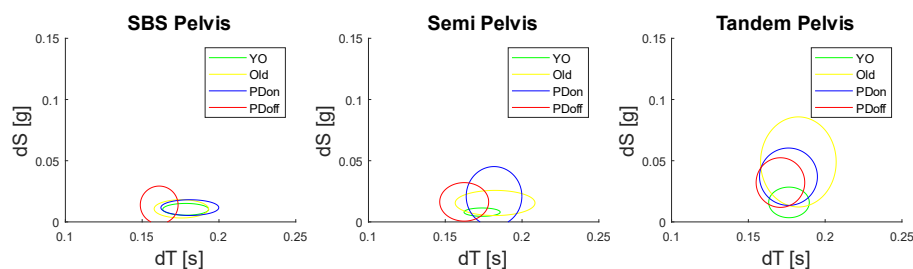
Figure 1 Relationship between dS and dT parameters for all the analyzed groups

Discussion: The results of this study demonstrate the potential of utilizing stock market analysis techniques to evaluate signals recorded during postural stability studies for differentiating between subject groups as well as individuals with Parkinson's disease in on and off state. The analysis focused on measurements of postural stability using accelerometer highlighting that the pelvis has the highest potential to effectively differentiate between subject groups.

References:
[1] Błaszczyk J.W., Czerwosz L.: Postural stability in the process of aging, Gerontol. Pol. 2005;13(1):25–36.
[2] Wodarski P., Chmura M., Gruszka G., Romanek J,. Jurkojć J.: The stock market indexes in research on human balance, Acta of Bioengineering and Biomechanics, 2022, 24(2):163-176,

Lock-in NIRS technique to improve contrast to noise ratio in functional brain studies

Stanislaw Wojtkiewicz, Karolina Bejm and Adam Liebert

Nalecz Institute of Biocybernetics and Biomedical Engineering, Warsaw, Trojdena 4, 02-109, Poland

swojtkiewicz@ibib.waw.pl

The accurate localization of carried information in functional near infrared spectroscopy (fNIRS) imaging remains a significant challenge due to the diffuse nature of light transport in tissues. To enhance the resolution of fNIRS imaging, a high-density diffuse optical tomography (HD-DOT) approach can be considered [1]. It employs a large number of overlapping source-detector pairs with varying spatial separations. Here, we introduce a method to focus the fNIRS sensitivity region within the brain tissue by utilizing the biological variability in signals originating from the grey matter. By employing two symmetrical and 90-degree rotated source-detector pairs, we can create a common volume of sensitivity that is shifted towards the brain. This spatial sensitivity profile enables the amplification of brain activation signals while canceling out noise and sensitivity near the superficial tissue.

The spatial sensitivity profiles of both pairs generate a common volume of sensitivity. However, if analyzed according to the up-to-date knowledge, the sensitivity region for both pairs sums up as shown in Fig. 1a. The proposed method involves product of both sensitivities (the Hadamard product) which is non-zero only within the intersecting volumes of sensitivity as in Fig. 1b. This feature fits well the HD-DOT approach. A lock-in amplification (wide-band homodyne detection) is applied to both optical signals within a sliding time window. A lock-in approach requires a reference (e.g. a single frequency) signal to extract data at the reference signal frequency. Here, we propose to use a multifrequency (biological variability) signal as a reference, i.e. signal from one of the arms (as in Fig. 1) is the lock-in reference. This amplification technique enhances the components originating from the common sensitivity volume (frequency components present in both signals/arms at the same time). The resulting locked-in signal, can be utilized for further analysis, such as the HD-DOT reconstruction or modified Beer-Lambert law.
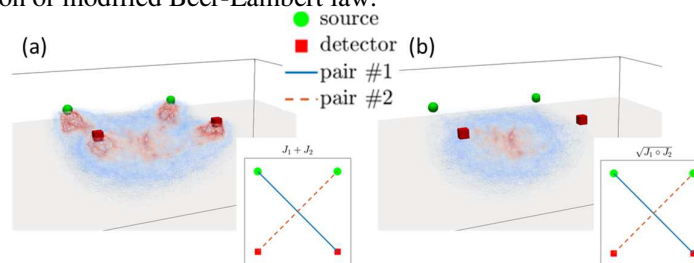
Fig. 1. Spatial distributions of sensitivity of measurements for two, 90-degree shifted source-detector pairs. Both sources and detectors are placed on a slab surface. Panel (a) classical approach (superimposed two 'banana-shaped' distributions), panel (b) the proposed method (common volume of two 'banana-shaped' distributions). A significant reduction in superficial sensitivity is observed in panel (b).

In-vivo experiments were carried out on healthy volunteers under visual stimulation conditions with the protocol as in [2]. The measurements involved arranging sources and detectors according to the geometry as shown in [3]. The measurements setup utilized an in-house developed system capable of simultaneously detecting data from multiple source-detector pairs and wavelengths. The lock-in procedure was implemented with varying sliding window sizes, including durations greater and smaller than the visual stimulation period. The in-vivo results demonstrated the effectiveness of the proposed lock-in filtering method. Results for the worst case with noisy signals and a weak visual stimulation response, still show the visual cortex hemodynamic response from the locked-in signal. The proposed lock-in solution provides real-time brain activation signals with high signal-to-noise ratio, even in the presence of movement artifacts. Please refer to [3] for examples of in-vivo results or measured data to download.

The lock-in filtering of fNIRS signals offers several advantages, including the preservation of frequency components present in both interfering signals, suppression of instrumental and biological noise, and removal of movement artifacts. The lock-in procedure does not introduce a time shift or alter the signal phase, making it suitable for real-time NIRS monitors, e.g. for brain computer interfaces or intensive care units monitoring.

[1] K. M. Bergonzi et al., "Lightweight sCMOS-based high-density diffuse optical tomography," Neurophotonics 5, 035006 (2018).

[2] K. Bejm et al., "Influence of contrast-reversing frequency on the amplitude and spatial distribution of visual cortex hemodynamic responses," Biomedical optics express 10, 6296-6312 (2019).

[3] Stanislaw Wojtkiewicz et al., "Lock-in functional near-infrared spectroscopy for measurement of the haemodynamic brain response," Biomed. Opt. Express 13, 1869-1887 (2022)

Study of the UR10e cobot's potential to use in neurological therapy

Wojciech Wolański[1], Robert Michnik[1], Sławomir Suchoń[1], Michał Burkacki[1], Miłosz Chrzan[1], Hanna Zadoń[1], Piotr Szaflik[1], Justyna Szefler-Dera[2], Dagmara Wasiuk-Zowada[2], Marek Gzik[1]

1. Department of Biomechatronics, Faculty of Biomedical Engineering, Silesian University of Technology
2. Department of Physiotherapy, School of Health Sciences in Katowice, Medical University of Silesia
Miłosz.Chrzan@polsl.pl

It has been determined that there is a need to simplify, enhance, and most importantly increase the accessibility of rehabilitation due to the rising number of patients and an aging population[1]. Therapy with the use of a robot is intended to help mobilize the nervous system through repetitive time summation, which is part of the process of neuroplasticity [2,3]. Research was done in the current study to determine if it would be feasible to modify an industrial robot to help with the rehabilitation process. The study used 10 repetitions of the PNF exercise in 4 measurement series. A physiotherapist helped with the first two series, and the Cobot UR10e helped with the next two. The Noraxon Ultium Motion system's inertial sensors (IMU) were used to evaluate the movement of the lower limbs. Hip and knee flexion and abduction angles, ankle dorsiflexion angle, knee flexion and rotation angles, and motion cycle were all examined in the study.

Table 1. Average values of min, max and RoM for individual movements in the joints

		Test 1 physiotherapist		Test 2 physiotherapist		Test 1 cobot		Test 2 cobot	
		mean	std	mean	std	mean	std	mean	std
Hip flexion [°]	max	121.43	2.97	117.71	3.92	103.46	0.35	106.70	0.65
	min	15.90	1.21	6.30	2.44	5.58	0.26	9.95	0.23
	RoM	105.53	3.49	111.42	5.88	97.88	0.32	96.75	0.82
Hip abduction [°]	max	24.64	1.12	19.68	2.75	1.77	0.68	1.87	1.71
	min	-22.66	1.94	-23.87	1.77	-29.85	0.56	-30.29	2.25
	RoM	47.3	2.51	43.54	1.77	31.62	0.98	32.16	0.88
Knee flexion [°]	max	116.09	3.28	117.63	4.84	95.11	1.22	90.50	1.26
	min	30.40	3.17	20.13	3.53	13.28	2.27	2.50	1.03
	RoM	85.69	4.84	97.5	4.66	81.84	2.07	88.00	1.93
Knee rotation [°]	max	17.23	3.25	21.05	3.56	28.05	0.32	31.06	0.68
	min	-19.20	3.11	-19.25	2.76	-13.55	1.19	-13.00	0.53
	RoM	36.44	3.41	40.3	5.66	41.6	1.34	44.06	0.67
Ankle dorsiflexion [°]	max	-10.18	3.94	-4.26	4.70	-47.62	0.63	-46.92	0.14
	min	-36.25	4.55	-32.87	4.98	-61.45	1.83	-54.28	1.33
	RoM	26.07	6.35	28.61	5.2	13.82	2.36	7.37	1.34
Cycle time [s]		5.268	0.15	4.78	0.06	22.22	0.06	22.21	0.04

Physiotherapeutic motions are carried out by the robot with higher accuracy and reliability. By adapting the orthosis to the limb for improved comfort, it is possible to modify the robot's pace so that it reflects the physiotherapist's rate of movement. Physiotherapists utilize motions that are less repetitious and have a limited range with each repetition, which may be the source of weariness. The ankle joint cannot be correctly reproduced by the robot due to the way the limb is attached; thus, an extra device or accessory may be required to more effectively manage this joint. The robot can accurately duplicate movement in the hip and knee joints.

References:
[1] Gassert, R.; Dietz, V. Rehabilitation Robots for the Treatment of Sensorimotor Deficits: A Neurophysiological Perspective. J. Neuroeng. Rehabil. 2018, 15, doi:10.1186/S12984-018-0383-X.
[2] Hu, X.; Suresh, N.L.; Rymer, W.Z. Estimating the Time Course of Population Excitatory Postsynaptic Potentials in Motoneurons of Spastic Stroke Survivors. J. Neurophysiol. 2015, 113, 1952, doi:10.1152/JN.00946.2014.
[3] JC, C.; FZ, S. Progress in Sensorimotor Rehabilitative Physical Therapy Programs for Stroke Patients. World J. Clin. cases 2014, 2, 316, doi:10.12998/WJCC.V2.I8.316.

Attribute Selection and Action Rules for Secondary Stroke Prediction

Małgorzata Zdrodowska, Agnieszka Dardzińska-Głębocka

Institute of Biomedical Engineering/Institute of Mechanical Engineering, Faculty of Mechanical Engineering, Bialystok University of Technology, ul. Wiejska 45C, 15-351 Bialystok, Poland
m.zdrodowska@pb.edu.pl

Stroke ranks as the third most prevalent factor leading to mortality and holds the top position in causing enduring disabilities among adults globally. Consequently, forecasting and diagnosing strokes assume immense significance [1]. In this regard, data mining methods prove invaluable by facilitating the identification of connections between specific patient traits. By extracting vital information from medical systems, these techniques equip us with the requisite knowledge to anticipate and address diverse ailments [2]. The aim of this study is to select attributes that affect the occurrence of secondary stroke and to extract decision rules and action rules that show the relationship between individual patient characteristics and secondary stroke.

The study involved the analysis of data from 369 patients who experienced ischemic strokes and received treatment at the Department of Neurology in the University Clinical Hospital in Bialystok. Each patient's profile consisted of 40 characteristics, including, among others: baseline information, test outcomes, comorbidities, and administered treatments. The initial phase of the study focused on feature selection and examining its effect on the precision of categorizing patients into various groups. Three approaches were used to reduce features: Correlation-Based Feature Selection, Information Gain-Based Feature Selection, and the Chi-Square test. The next step of the study involved constructing models that included all attributes, as well as attributes extracted through 10 feature selection (ischemic-heart-disease, statin, ACEI-ARB, cholesterol-calculus, LDL-cholesterol, narrowing-arteries, old-anticoagulants, triglycerides, CA-blocker). Then we applied classification techniques to assess whether feature selection yielded the expected results. For classification, we selected methods that facilitated the simple construction of decision rules: J48, JRip, PART, CART and Random Tree. To evaluate we used the ACC (overall accuracy) measure. The final stages of the study involved formulating classification rules and extracting action rules.

The classification results are shown in Table 1. We can see that a 75% reduction in attributes achieved very similar results, with CART and Random Tree classifiers even achieving 7% higher accuracy. As mentioned earlier, the selected classifier algorithms allowed us to extract classification rules. Classification rules were compared for the model containing all features and the model after feature extraction. In

Table 1. Comparison of model accuracy

algorithm/model	Model 1 (40 attributes)	Model 2 (10 attributes)	Difference
J48 (C4.5)	73,17%	72,08%	-1,09%
Jrip	74,52%	71,54%	-2,98%
PART	68,02%	75,33%	7,31%
CART	74,79%	72,89%	-1,90%
Random Tree	64,22%	71,54%	7,32%

most cases, the rules overlapped, demonstrating the benefits of feature selection. The final stage of the study was to extract action rules that would allow specific patients to be reclassified from one group to another. Below are few selected action rules: [ischemic heart disease, no] ∧ [total cholesterol, 0] ∧ [CA-blocker, yes→no] ⟹ [class, secondary stroke → one stroke], [ischemic heart disease, no] ∧ [total cholesterol, 1] ∧ [carotid artery stenosis, yes] ∧ [statin, yes→no] ⟹ [class, secondary stroke → one stroke], [ischemic heart disease, yes] ∧ [statin, no] ∧ [glucose, 0→1] ⟹ [class, secondary stroke → one stroke].

In conclusion, we can say that the results obtained in this study confirmed the benefits of attribute selection, as the accuracy rates of each algorithm applied to the data after attribute reduction were similar to those with the raw data. Decision rules and action rules can also prove useful in the work of physicians, which can direct them to those patient attributes where even a minimal change will be of great benefit to the patient.

References:
[1] Sacco R.L et al., An updated definition of stroke for the 21st century: a statement for healthcare professionals from the American Heart Association/American Stroke Association, *Stroke*, 2023, vol. 44, pp. 2064-2089
[2] Yoo I., Alafaireet P., Marinov M, Data mining in healtcare and biomedicine, A survey of the literature, *Journal of the Medical Systems*, 2012, vol. 35, no. 4, pp. 2431–2448

A new control algorithm of pneumatic power-controlled independent lung ventilation

Krzysztof Zieliński, Szymon Kruszewski, Anna Stecka, Maciej Kozarski, Marek Darowski

Nalecz Institute of Biocybernetics and Biomedical Engineering, Polish Academy of Sciences, Ks. Trojdena 4, 02109 Warsaw, Poland

e-mail: kzielinski@ibib.waw.pl

Aims: In the case of respiratory failure and asymmetrical lung pathologies the Independent Lung Ventilation (ILV) can be used. Usually ILV is applied by two ventilators. However one ventilator can be used but with a special pneumatic divider. This study aimed to develop a new pneumatic power-based ventilation algorithm for the divider, enabling cooperation with the ventilator working on the Biphasic Positive Airway Pressure (BiPAP) mode.

Methods: A Ventil is a splitter developed in IBBE PAS specially for ILV. It was used in this study. A new electronic control module, based on microprocessor architecture was developed and implemented in this system. Electrical signals from pressure (HSC series, Honeywell, New Jersey) and flow (SpiroQuant H, Envitec, Germany) sensors in Ventil's outlets were acquired as inputs for the control algorithm. The ventilatory power was calculated as a product of pressure and flow. The output of the algorithm was an electrical signal for the stepper motor's controller to drive Ventil's dividing head. The Ventil together with the ventilator (Evita V600, Draeger, Germany) was connected to 2 artificial lungs (ALs) (Smart Lung 2000, IMT Analytics, Switzerland). The simulations were performed for different parameters set in the ventilator (BiPAP pressures, respiratory rate, inspiratory to expiratory ratio etc.) and Ventil (pneumatic power division ratio) along with various resistive and compliant properties of the ALs. The results were analyzed in terms of peak inspiratory pressures (PIPs), peak inspiratory flows (PIFs) as well as pressure and flow profiles and the system's stability.

Results: The preliminary simulation results show stable work of the whole system ventilator – Ventil – artificial lungs. The Ventil device was able to split ventilatory power delivered to the ALs according to set division ratio. Power-controlled ventilation prevents exceed PIPs and PIFs, thus reduces the risk of the ventilator-induced lung injury, in comparison to the flow-controlled splitting algorithm in Ventil.

Conclusions: The new pneumatic power-based control algorithm might improve ILV performance by Ventil in comparison to its default flow-control algorithm, by preventing volu- and baro-trauma in ventilated lungs. The work was supported by the National Science Centre, Poland (Grant No 2021/43/D/ST7/01912).

Chapter II

Applications of Deep Learning in Biomedical Image Analysis

Session organizers:

Prof. Józef Korbicz, University of Zielona Góra
Prof. Marek Kowal, University of Zielona Góra

T regulatory Lymphocyte Nuclei Segmentation in DAB - Stained Breast Cancer Biopsy Digital Images Using Deep Learning Algorithms

Shrief Abdelazeez[1], Lukasz Roszkowiak[1], Krzysztof Siemion[1,2], Carlos Lopez[3,4], Marylene Lejeune[3,4], Anna Korzynska[1]

[1] Laboratory of Analysis and Processing of Microscopic Image, Nałęcz Institute of Biocybernetics and Biomedical Engineering Polish Academy of Sciences, Ks. Trojdena 4, 02-109 Warsaw, Poland
sabdelazeez@ibib.waw.pl
[2] Medical Pathomorphology Department, Medical University of Bialystok, Bialystok, Poland
[3] Department of Pathology, Oncological Pathology and Bioinformatics Research Group, Hospital de Tortosa Verge de la Cinta, ICS, IISPV, C/Esplanetes no 14, 43500 Tortosa, Spain
[4] Universitat Rovira I Virgili(URV) – Campus Terres de 1'Ebre, Avinguda Remolins no 13-15, 43500 Tortosa, Spain

The breast cancer patient's immune response to the tumor in its microenvironment is important in stating the patient's prognosis and proposing personalized treatment. The immunohistochemical staining of tissue samples is performed to examine the response and to visualize different types of lymphocytes using various cell markers. Accurate detection and localization of FOXP3 protein, crucial for studying Treg lymphocytes' distribution and their impact on the immune response and tumor growth, remains a challenge despite previous attempts using traditional machine learning methods. This paper presents the results of a review of deep learning models and their validation for the task of FOXP3-positive nuclei segmentation. The dataset used in this investigation is described in [1] and obtained from the Molecular Biology and Research Section and the Pathology Department of Hospital de Tortosa Verge de la Cinta, IISPV, URV (Tortosa, Spain). Image normalization and resizing were used as a preprocessing step before training. Due to the limited size of the dataset, image augmentation was applied. Different segmentation models (U-Net, Link-Net, SegFormer) were trained on the data using various backbone architectures as pre-trained encoder blocks. This included basic architecture, MobileNet-v2, VGG16, Inception-V3, Inception-ResNet-V2, ResNet50, and DenseNet201. For SegFormer, different size Mix Transformer (MiT) encoders (MiT-B0, MiT-B1, MiT-B2, and MiT-B3) were investigated and trained. Two cross-validation (CV) techniques were employed: hold-out CV on augmented data and k-fold CV on raw data. The final results presented in the Table 1 indicate that the SegFormer model consistently outperformed other models in terms of the Dice's coefficient metric. Regardless of the encoder size used, the SegFormer model achieved an average Dice's coefficient of 0.99.

Table 1 Loss and Dice Coefficient for best models

Models	Hold-out CV						5-fold CV			
	U-Net	MobileNet-LinkNet	MiT-B0	MiT-B1	MiT-B2	MiT-B3	U-Net	VGG16-LinkNet	MiT-B2	MiT-B3
Loss	0.002	0.0072	0.0174	0.0139	0.015	0.0108	0.01 ± 0.015	0.004 ± 0.0006	0.05 ± 0.032	0.031 ± 0.014
Dice's Coeff.	0.965	0.975	**0.997**	**0.998**	**0.998**	**0.998**	0.981 ± 0.011	0.9744 ± 0.0104	**0.99757 ± 0.00024**	**0.99763 ± 0.00013**

The McNemar test was conducted to determine if there were statistically significant differences in performance between model pairs. In K-fold CV, the pairs VGG16-LinkNet and U-Net showed similar performance with no significant difference. However, for the remaining pairs, there were statistically significant differences in performance.

References:
[1]   L. Roszkowiak *et al.*, "System for quantitative evaluation of DAB&H-stained breast cancer biopsy digital images (CHISEL)," *Sci. Rep.*, vol. 11, no. 1, pp. 1–14, 2021, 10.1038/s41598-021-88611-y.

Classification of breast cancer histopathological images using a vision transformer

Marek Kowal, Mikołaj Kaczmarek and Józef Korbicz
Faculty of Computer, Electrical and Control Engineering,
University of Zielona Góra, Poland, Licealna 9, 65-417
M.Kowal@issi.uz.zgora.pl

The aim of this study was to verify the effectiveness of a Vision Transformer (ViT) neural network in the classification of breast cancer (benign/malignant) based on histopathological images from the BreakHis collection. The neural network classifier was built based on the ViT-Base architecture [1]. It receives an input image with a size of 224x224 RGB pixels, which is then divided into 16x16 patches flattened to 768-element vectors (tokens). The result is a 196-element token sequence. The first layer maps tokens to patch embeddings (latent vectors) using linear projection. We prepend an additional [class] token embedding to the sequence to adapt the transformer architecture to the classification task. The vector representing [class] embedding is the same size as other patch embeddings but is tuned during training. The model must understand the internal structure of the input image, therefore, it needs to know the order of the patches in the sequence. To achieve this, each patch embedding is augmented with a corresponding learnable positional embedding vector. The sequence prepared in this way is fed to the transformer encoder, which consists of 12 self-attention blocks. Each of these blocks includes a multi-head self-attention layer, a feed-forward dense layer, and two normalizing layers. Finally, a latent vector corresponding to the [class] token is generated on the output of the transformer encoder. It is fed to dense layers to achieve class probabilities.

The research was carried out with the help of 1820 images (1232 malignant, 588 benign) representing 82 patients (58 malignant, 24 benign) [2]. Images have been normalized and resized from 700x460 to 224x224 pixels. The collection was split into two subsets with a ratio of 80:20, maintaining the balance of benign to malignant cases and ensuring that images from a given patient could only be in one of the subsets. The dataset containing 80% of the images was used for training and validation, and the other dataset (20%) was used for testing. Training and validation were repeated 5 times using stratified 5-fold cross validation. Due to the few training images, it was impossible to train the ViT model from scratch. Therefore we used the ViT-Base model pre-trained on ImageNet-21k (a collection of 14 million images of 21k classes). Then the top dense layers of the ViT-Base model were replaced, and the whole model was fine-tuned using the histopathological images. The fine-tuning was done using the ADAM optimization algorithm with batch size 40, learning rate set to 0.000001, and weight decay equal to 0.001. The values of learning rate and weight decay were determined using the grid search approach. Early Stopping was used to prevent overfitting.

Table 1 Classification metrics for training, validation, and test subsets.

Dataset		Accuracy	Precision	Recall	Specificity	F1 Score	AUC
Train	mean	0,981	0,992	0,969	0,993	0,980	0,998
	std	0,019	0,005	0,034	0,005	0,020	0,002
Validation	mean	0,871	0,895	0,842	0,900	0,867	0,924
	std	0,051	0,055	0,063	0,056	0,053	0,070
Test	value	0,847	0,855	0,837	0,858	0,846	0,870

Table 1 presents the values of classification metrics. The training and validation subsets are described by mean and standard deviation for 5-fold cross-validation. Metrics for the test subset were obtained using a hold-out approach. We can observe that the ViT model received an accuracy of 84.7% for the test subset. If we compare this result with some reports which show that CNNs can reach an accuracy of 95%, then it doesn't seem like much. Nevertheless, if we limit the studies to those that strictly followed the experimental protocol proposed by Spanhol et al. [2], then the accuracy of the ViT model is comparable to the accuracy of CNNs [3]. When analyzing the detailed classification results, we noticed that images belonging to some patients are responsible for a very large number of misclassifications. We see this as an opportunity to improve classification accuracy through, for example, active learning or boosting.

References:
[1] Dosovitskiy A. et al., An Image is Worth 16x16 Words: Transformers for Image Recognition at Scale, *Proc. 9th Int. Conf. Learning Representations*, ICLR 2021, Austria, May 3-7, pp. 1-21, 2021
[2] Spanhol A. et. al., A Dataset for Breast Cancer Histopathological Image Classification, *IEEE Trans Biom Eng*, vol. 63, no. 7, pp. 1455–1462, 2016.
[3] Mahesh G. et. al. . Residual learning based CNN for breast cancer histopathological image classification. *Int. J. Imaging Systems and Technology*, vol. 30, no. 3, pp. 621–635, 2020.

Detection of MYC translocations in DLBCL by analysis HE stained tissue slides

Zaneta Swiderska-Chadaj[1], Tomasz Markiewicz[1,2], Szczepan Cierniak[2], Stephan Dooper[3], Geert Litjens[3], Slawomir Pakula[4], Konnie Hebeda[3]

[1] Warsaw University of Technology, Faculty of Electrical Engineering, Warsaw, Poland
[2] Military Institute of Medicine, Warsaw, Poland
[3] Radboudumc, Department of Pathology, Nijmegen, The Netherlands
[4] National Research Institute of Oncology, Gliwice, Poland
zaneta.swiderska@pw.edu.pl

Introduction and Objectives

Machine learning and computer vision advancements have transformed the field of pathology by enabling whole-slide imaging (WSI) of histopathological specimens. The microscopic examination of histopathological specimens serves as the foundation for cancer classification. One of the most common types of non-Hodgkin's lymphoma is diffuse large B cell lymphoma (DLBCL). MYC translocation has been identified as an important prognostic biomarker in 5-12% of DLBCL cases. When treated with standard chemotherapy regimens, patients with MYC-translocation-positive DLBCL have a worse prognosis. Fluorescence In Situ Hybridization (FISH) is the gold standard for detecting MYC+, BCL2, and BCL6, but it is very expensive and not widely available. As a result, we concentrated on the possibility of predicting the occurrence of translocations using histopathological data analysis. The motivation for pursuing the presented research topic is the dynamic development of methods based on deep neural networks and their enormous potential, which enables the development of new methods of analyzing medical images and, thus, the possibility of improving medical diagnostics and assisting patients who are hampered by the limitations of current methods. Our preliminary research [1,2] demonstrated that deep neural networks could automatically classify MYC+ specimens.

Methods and Results

A multicenter cohort of 408 histopathological specimens from medical centers in the Netherlands was used in the study and split into training, validation, and test sets. Each specimen was scanned and saved as a whole slide image (the size of a single WSI is 2-4 GB). We proposed and investigated neural image compression, CLAM, and streaming methods to analyze a whole image in a single step, without dividing WSIs into patches. CLAM is a clustering-constrained-attention multiple-instance learning method, that is using attention-based learning to identify subregions of high diagnosis. Next, we compare the results to those obtained using the patch-based method described in [2]. The method's performance was assessed on a test set using receiver-operating characteristic (ROC) analysis. Table 1 shows the area under the ROC curve.

Table 1. Achieved results.

	Patch based method [2]	CLAM	StreamingClam
AUC	0.834	0.659	0.7351

We can see that the whole-slide strategy achieves lower results than the patch-based method [2]. However, the possibility of a presentation attention map provides better exploitability. We intend to improve on the results obtained by developing new methods.

Conclusion

Our findings indicate a promising area under the ROC curve. Based solely on an H&E-stained tissue slide, the algorithm could identify MYC+ DLBCL specimens. Our findings suggest that clinical application of the algorithm could enable very quick and low-cost prescreening, directing the use of genetic tests for MYC rearrangement. However, the results show that there is still room for improvement. Prospective validation on larger datasets and improving the interpretability of algorithm decisions are the next steps. Detecting morphological features as a marker for specific genetic abnormalities is a promising avenue for assisting DLBCL diagnosis and oncology in general.

References:
[1] Swiderska-Chadaj Z., et al. Predicting MYC translocation in HE specimens of diffuse large B-cell lymphoma through deep learning. Medical Imaging 2020: Digital Pathology.2020;11320:132010
[2] Swiderska-Chadaj, Z., et al. Artificial intelligence to detect MYC translocation in slides of diffuse large B-cell lymphoma. Virchows Arch 479, 617–621 (2021)
[3] Tellez D, et al. "Neural image compression for gigapixel histopathology image analysis." IEEE transactions on pattern analysis and machine intelligence 43.2 (2019): 567-578.

Chapter III

Biomaterials and Implants

Session organizer:

Prof. Bogdan Walkowiak, Lodz University of Technology

Conductive hydrogel-based electrode for neural stimulation

Karolina Cysewska*, Sylwia Pawłowska

Laboratory of Functional Materials, Faculty of Electronics, Telecommunications and Informatics, and Advance Materials Centre, Gdańsk University of Technology, ul. Narutowicza 11/12, 80-233 Gdańsk, Poland

*karolina.cysewska@pg.edu.pl

Currently, one thousand million people suffer from neurological issues, such as epilepsy, Alzheimer's and Parkinson's diseases, migraines, sclerosis, or neural infections. In most cases, restoration of the neural path can be done by the introduction of electrodes within the neural tissue. Because signal transmission in the nervous system depends on the electrical carrier (ions) and chemical carrier (neurotransmitters), monitoring/stimulating the nervous system by the electrode can be obtained through the electrical and chemical interface [1]. Most electrodes available on the market today are based on pure metals or their composites such as platinum (Pt), gold (Au), or iridium (Ir). Because of their inertness, limited reactivity, and relatively high resistance to corrosion, they have become the materials of the first choice [2]. However, the metallic electrodes are characterized by unfeatured surface morphology and are around four orders of magnitude stiffer than neural tissue (Young modulus: 140 GPa) which significantly lower the electrode lifetime. Thus very important is to develop more a flexible, but still with good electrical interface parameters interface material.

In this work, the procedure for the fabrication of conductive hydrogel coating on the platinum commercial electrodes was developed. The coating was composed of pure hydrogel connected electrochemically with the conducting polymer poly(3,4-ethylenedioxythiophene) doped with polystyrene sulfonate (PEDOT:PSS). In the first step, hydrogel was synthesized via a one-step UV-VIS polymerization procedure directly on platinum electrode. The synthesis proceeded in the presence of N-isopropylacrylamide, use as the main monomer (NIPAAm), N,N-methylene bisacrylamide (BIS-Aam) as a cross-linker dissolved in deionized water (90 % wt.), and photoinitiator used to trigger the hydrogel polymerization reaction upon UV irradiation. In the second step, PEDOT:PSS was incorporated into the hydrogel by different electropolymerization routes. The concentration of the chemicals, time and type of the deposition route were optimized in order to obtain the most desirable electrical interface parameters (impedance, potential window, double-layer capacitance, charge storage capacitance, charge injection limit, stability) of the electrodes measured in the simulated body fluid at the body temperature. The electrochemical performance of hydrogel-PEDOT:PSS, pure hydrogel and pure PEDOT:PSS modified platinum electrodes was compared and discussed.

The studies showed that it is possible to fabricate hydrogel-based PEDOT:PSS by electrochemical route with the electrical interface parameters at the level of the pure PEDOT:PSS electrode. Moreover, the hydrogel form of the PEDOT partially inhibited the overoxidation of the coating, which in turn led to higher electrical stability during the stimulation.

The results obtained in the work are very promising for further fabrication of the neural electrode. First of all, the soft interface of the electrode is very desirable to obtain for many medical applications: in addition to the fact that such an electrode shows greater stability during the stimulation, it also significantly increases the overall biocompatibility. Secondly, the conductive polymer was introduced into the hydrogel by electrodeposition, which allowed easy controlling of the synthesis parameters, and in turn, achieved a very reproducible process. The latter is not the case for the chemical polymerization route, which is usually done in the literature.

References:
[1] Y. Cho, H. Shin, J. Park, S. Lee, Advanced Neural Interface toward Bioelectronic Medicine Enabled by Micro-Patterned Shape Memory Polymer, Micromachines 12 (2021) 720.
[2] H. Wunderlich, K.L. Kozielski, Next generation material interfaces for neural engineering, Current Opinion in Biotechnology 72 (2021) 29.

Assessment of hot deformation behaviour of Spark Plasma sintered Magnesium -based composites for temporary orthopaedic application

Anshu Dubey[1,2], Satish Jaiswal[2], Nitish Raja[2], Debrupa Lahiri[2], Vignesh Kumaravel[1]

[1]International Centre for Research on Innovative Biobased Materials (ICRI-BioM)—International Research Agenda, Lodz University of Technology, Lodz 90-924, Poland.
[2]Biomaterials and Multiscale Mechanics Laboratory, Department of Metallurgical and Materials Engineering, Indian Institute of Technology Roorkee, Uttarakhand, India 247667
*Corresponding Authors - anshu.dubey@p.lodz.pl and vignesh.kumaravel@p.lodz.pl

Abstract

Various conventional metallic materials, such as titanium alloys, cobalt-chromium alloys, and stainless steel, have been used for temporary orthopaedic applications due to their excellent mechanical properties and biocompatibility[1]. However, the high elastic modulus and non-degradable nature of these materials cause major limitations, such as the stress-shielding effect and the requirement of a second surgery to remove the implants after bone healing. Biodegradable material such as magnesium (Mg) could suffice the requirement of temporary load-bearing implants. Mg is biodegradable in physiological environments and has approximately similar elastic modulus, facilitating overcoming the stress shielding effect and second surgery[2]. However, the high degradation rate in the physiological environment and brittle nature of Mg alloys cause early implant failure during actual service in the body. The fabrication of Mg-based composites using osteoconductive hydroxyapatite (HA) bioceramics as reinforcement can minimize the degradation rate of the implants. But adding HA to pure Mg with 3 wt% zinc (Zn) makes the implants more brittle and shows poor ductility at room temperature due to their intrinsic properties, which can deform at elevated temperatures. The optimum hot deformation of Mg-3Zn/HA composites will improve the corrosion behaviour and their mechanical and microstructural properties. Mg-3Zn alloy with 15 wt. % HA composites were fabricated through the spark plasma sintering route followed by the hot deformation processing. The high-temperature deformation behaviour was scrutinized using compression tests in the Gleeble 3800 with temperature ranges of 300 - 400⁰, and strain rates of 0.001-1s^{-1}. 3D processing map of power dissipation with true stress-strain diagrams and instability maps and the microstructural observations were analyzed for both composites. Through constitutive equations, the activation energy obtained for both the composites is 153 and 199 Kj/mol. The hot deformation of SPS-fabricated Mg-HA composites has shown enormous potential for load-bearing temporary orthopaedic implants.

Keywords: magnesium, hydroxyapatite, spark plasma sintering, hot deformation, orthopedics

Reference:

[1]   Kumaravel V, Nair KM, Mathew S, Bartlett J, Kennedy JE, Manning HG, et al. Antimicrobial TiO2 nanocomposite coatings for surfaces, dental and orthopaedic implants. Chem Eng J 2021. https://doi.org/10.1016/j.cej.2021.129071.
[2]   Dubey A, Jaiswal S, Garg A, Jain V, Lahiri D. Synthesis and evaluation of magnesium/co-precipitated hydroxyapatite based composite for biomedical application. J Mech Behav Biomed Mater 2021. https://doi.org/10.1016/j.jmbbm.2021.104460.

The cytotoxic *Staphylococcus aureus* PSMα3 inhibits the aggregation of human insulin *in vitro*

Aleksandra Kalitnik[1], Monika Szefczyk[2], Marlena Gąsior-Głogowska[1], Joanna Olesiak-Bańska[3], Małgorzata Kotulska[1]

[1]Department of Biomedical Engineering, Faculty of Fundamental Problems of Technology, [2]Department of Bioorganic Chemistry, Faculty of Chemistry, [3]Institute of Advanced Materials, Wroclaw University of Science and Technology, Wybrzeże Wyspiańskiego 27, 50-370 Wroclaw, Poland

Email: aleksandra.kalitnik@pwr.edu.pl

Phenol-soluble modulins (PSMs) are amyloid functional peptides produced by the Gramme-positive bacteria *Staphylococcus aureus*. Amyloidogenic properties of the PSM play an essential role in bacterial biofilm formation and stabilisation [1]. The multifunctional PSM family is represented by several small amphipathic peptides characterised by differences in their sequences, fibrillation predispositions, structural plasticity, and architecture of self-produced amyloid-like structures [2]. PSMα3 has recently attracted research interest due to its unique secondary structure that forms upon fibrillation. Whereas other PSM peptides undergo conformational changes during aggregation, PSMα3 maintains its α-helical conformation even for several days of incubation, forming so-called cross-α fibrils. Those fibrils were shown to adopt the morphological, mechanical, and tinctorial characteristics of canonical cross-β-sheet amyloid architecture, but at the same time they are characterised by a different behaviour, especially during interactions with other biological structures or macromolecules. In particular, cross-interactions within the PSM peptide family participate in the stabilisation and self-destruction of biofilms [1, 2]. Moreover, it was recently shown that PSMα3 inhibits of α-synuclein aggregation and amyloid-induced toxicity by preventing monomeric protein transformation into toxic oligomers and fibrils [3].

In the current work, we investigated the *in vitro* aggregation properties of PSMα3 and its influence on human insulin aggregation. The full-length, 22-residue PSMα3 peptide was synthesised on solid support, purified with HPLC, and characterised using mass spectrometry analysis and UV-CD and ATR-FTIR spectroscopy to prove the structural correlation with the wild-type peptide. The aggregation properties of PSMa3 and its interaction with human insulin were studied *via* the Thioflavin T (ThT) fluorescence assay, CD and FTIR spectroscopy, and atomic force microscopy (AFM). Both peptides were monomerized with HFIP before the aggregation assay.

We have found that under certain conditions, PSMα3 maintains α-helical conformation up to 72 h and does not form any amyloid-like aggregates. The results obtained *via* different techniques match each other. Our findings illustrated that co-incubation of PSMα3 with human insulin for 72 h at 37 ℃ leads to inhibition of insulin fibrillation *in vitro*. The inhibitory effect of PSMα3 on insulin amyloid formation is concentration-dependent, and in particular, at concentrations of 0.031 mg/mL and higher of PSMα3 per 0.5 mg/mL of insulin, a full inhibition of insulin aggregation was observed. At concentrations of 0.0156 mg/mL, a partial dose-dependent inhibition of its fibrillation took place. The AFM data clearly proved the results of the ThT kinetic fluorescence assay.

Thus, we have demonstrated that the aggregation behaviour of PSMα3 strongly depends on incubation conditions (material, pre-treatment, dissolving procedure). Nevertheless, in the case of co-incubation with insulin, co-inhibition of the aggregation was observed independently of changes in experimental conditions.

References:
[1] Zaman M. and Andreasen M. Cross-talk between individual phenol-soluble modulins in Staphylococcus aureus biofilm enables rapid and efficient amyloid formation, *Elife*, 2020, vol. 9, pp. 1–17.
[2] Salinas N., Colletier J.P., Moshe A. and Landau M. Extreme amyloid polymorphism in Staphylococcus aureus virulent PSMα peptides, *Nature communications*, 2018, vol. 9, pp.1–9.
[3] Santos J., Gracia P., Navarro S., Peña-Díaz S., Pujols J., Cremades N., Pallarès I. and Ventura S., α-Helical peptidic scaffolds to target α-synuclein toxic species with nanomolar affinity, *Nature communications*, 2021, vol. 12, p.3752.

Peptide-polysaccharide materials in the treatment of hard-to-heal wounds

Beata Kolesinska

Lodz University of Technology, Faculty of Chemistry, Institute of Organic Chemistry, Zeromkiego 116, 90-924 Lodz

beata.kolesinska@p.lodz.pl

Chitosan and alginate derivatives are commonly used as substrates in specialist dressings. Chitosan materials exhibit hemostatic effects through the interaction of positively charged chitosan with negatively charged blood cells, forming a "pseudoclot" that blocks blood flow [1]. Alginate dressings are also used in wound care. The advantage of alginate materials is their ability to form a moist gel and provide a moist wound environment [2]. This ensures effective cleansing of the wound and accelerates the healing process. The improvement in the effectiveness of bleeding inhibition can be obtained by supplementation with compounds with hemostatic activity. The antifibrinolytic agents used include aprotinin and lysine analogs. Alginate and chitosan materials are also used as raw materials for obtaining scaffolds useful in regenerative medicine. Their fiber-forming properties allow them to obtain various fibrous structures with satisfactory mechanical strength. They can also be modified with various compounds affecting the regeneration process.

The Institute of Organic Chemistry of the Lodz University of Technology conducts research on biocompatible, multi-component materials based on polysaccharides and peptides (key fragments in the process of protein regeneration) useful in the treatment of hard-to-heal wounds, including diabetic foot syndrome [3]. The designed hybrid materials affect all stages wound healing process. In addition, they meet all the criteria of a uniform concept for the treatment of chronic wounds (TIME strategy). The diseases accompanied by the problem of difficult-to-heal wounds include vascular wounds, diabetic foot syndrome, trophic ulcers, hematological wounds, wounds in pyoderma gangrenosum, neoplastic ulcers, and wounds accompanying congenital vascular malformations. It is estimated that the problem of diabetes affects 3 million people in Poland. Diabetic foot syndrome is one of the most common causes of hospitalization among diabetic complications (4-10% of patients). The risk of ulceration in diabetics ranges from 12 to 25%. It is the most common non-traumatic cause of lower limb amputation. The risk of amputation in the diabetic population is 30-40 times higher.

As a result of the synergy between the selected set of biologically active peptides and polysaccharides, it was found that it is possible to obtain a hybrid material useful in the treatment of hard-to-heal wounds affecting all stages of the healing process: (i) hemostasis, (ii) inflammation (fragments of pro- and anti-inflammatory cytokines), (iii) proliferation, (iv) tissue remodeling and protection against bacterial infection.

The selection process of biologically active peptides is multi-stage and includes the synthesis of libraries of fragments encompassing whole proteins using the SPOT technique, performing tests allowing selection of active fragments, and finally after solid phase peptide synthesis of selected fragments using them as components of hybrid peptide-polysaccharide materials.

This allowed to find a set of protein fragments affecting all stages of wound healing:

(i) hemostasis – fragments of α and γ chain of fibrinogen, fibronectin, factor XIII;

(ii) inflammation - fragments of pro- and anti-inflammatory cytokines;

(iii) proliferation - fragments of ECM hemostasis components: collagens, elastin, growth factors;

(iv) tissue remodeling and protection against bacterial infection – κ-casein and lactoferrin fragments.

References:

[1] Paul P. Kolesinska B., Sujka W. Chitosan and Its Derivatives - Biomaterials with Diverse Biological Activity for Manifold Applications *Mini Rev. Med. Chem.*, 2019, 19, 9, 737-750

[2] Rosiak P., Latanska I., Paul P., Sujka W., Kolesinska B. Modification of Alginates to Modulate Their Physic-Chemical Properties and Obtain Biomaterials with Different Functional Properties *Molecules*, 2021, 26, 23, 7264

[3] Sierra-Sánchez Á., Kim K.H., Blasco-Morente G., Arias-Santiago S. Cellular human tissue-engineered skin substitutes investigated for deep and difficult to heal injuries *npj Regenerative Medicine*, 2021, 6, 35

Obesity and orthopedic implant treatment: case report and biomechanical analysis

Mateusz Kopec[1] , Grzegorz Szczęsny[2], Zbigniew L. Kowalewski[1]
[1]Institute of Fundamental Technological Research, Polish Academy of Sciences, Pawińskiego 5B,
02-106 Warsaw, Poland;
[2] Department of Orthopaedic Surgery and Traumatology, Medical University, 4 Lindleya Street,
02-005 Warsaw, Poland
mkopec@ippt.pan.pl

The number of overweight and obese patients in developed countries is gradually increasing. It was reported that 1287 (64%) out of 2007 adults operated on in 2017 had a body mass index (BMI) greater than 25 kg/m^2, and 26.4% even greater than 30, while the BMI of the most obese patient was as high as 57.6 kg/m^2. Such distressing statistics raised an issue related to the inadequate durability of implants used for the fixation of bone fractures. Implants for the lower-extremity fractures may not be durable enough to fit the requirements of overweight and obese patients.

This case report presents the history of a 23-year-old obese male with a BMI of 38.7, who bent the angularly stabile titanium plate stabilizing his broken lateral ankle and torn distal tibiofibular syndesmosis. Biomechanical analysis showed that the maximal static bending moment regis-tered during one-leg standing was equal to 1.55 Nm. This value was circa one-third of the max-imally admissible bending moment for this particular plate (5.34 Nm) that could be transmitted without its plastic deformation. Since dynamic forces exceed static ones several (3–12) times during typical activities, such as walking, climbing the stairs, running, and jumping, unpredict-able forces may occur and increase the risk of loosening, bending, and even breaking implants. None of these situations should have occurred for the typical patient's body mass of 75 kg, or even for the analyzed mass of the young patient (120 kg) who tried to avoid excessive loading during his daily routine. Subsequent implant bending and destabilization of the fracture shows that for the significantly high and still growing number of obese patients, a very strict physical regime should be recommended to prevent overabundant dynamic loads.

Implants for lower-extremity fractures may not be durable enough to fit the requirements of overweight and obese patients, since mechanical forces and their moments generated during body weight bearing may exceed the commonly tolerated limit values. To minimize the risk of complications in cases of physically active and insubordinate obese patients, an additional lower-limb immobilization in a plaster cast may be justified. The design of more durable implants for obese and highly active patients should also be taken into consideration in the form of implants' adaptations to the real requirements.

References:
[1] Szczęsny, G., Kopec, M., Szolc, T., Kowalewski, Z.L., Małdyk, P., Deformation of the Titanium Plate Stabilizing the Lateral Ankle Fracture Due to Its Overloading in Case of the Young, Obese Patient: Case Report Including the Biomechanical Analysis. *Diagnostics,* 2022, 12, 1479, pp. 1-10

Influence of fiber diameter and arrangement of polyurethane scaffolds on cells growth

Iwona Łopianiak[a,b,*], Mehtap Civelek[c], Michał Wojasiński[a], Beata A. Butruk-Raszeja[a], Iwona Cicha[c] and Tomasz Ciach[a,d]

[a] Laboratory of Biomedical Engineering, Faculty of Chemical and Process Engineering, Warsaw University of Technology, Waryńskiego 1, 00-645 Warsaw, Poland
[b] Doctoral School of Warsaw University of Technology, Warsaw, Poland
[c] Section of Experimental Oncology und Nanomedicine (SEON), Universitätsklinikum Erlangen, Germany
[d] Centre for Advanced Materials and Technologies CEZAMAT, Warsaw University of Technology, Poleczki 19, 02-822 Warsaw, Poland

*Corresponding author: iwona.lopianiak.dokt@pw.edu.pl

Polymeric fibrous scaffolds show the desired properties for tissue engineering applications. Due to high surface-to-volume ratio and porosity, adjustable mechanical properties and pore size, and suitable biodegradation rate are widely used in vascular, heart, muscle, and cartilage tissue regeneration. The diversity of tissues and organs makes it impossible to produce the ideal scaffold for all applications. Scaffold properties should be adapted directly to the properties of the replaced tissue[1,2]. Blood vessels are characterized by a complex, three-layered structure. Each layer is composed of different cell type, e.g. endothelial cells, smooth muscle cells, or pericytes confined by an extracellular matrix. Various distribution and organization of cells in each layer of blood vessel demand od appropriate approach to the production of vascular scaffolds. Individual layers should differ in i.e. structure, porosity, pore size, and thickness[3].

In this research, polyurethanes (PUs) fibrous materials were produced by the solution blow spinning method (SBS). The influence of SBS process parameters, such as collector rotational speed and PU solution concentration on fiber arrangement and diameter were evaluated. The properties of fibrous materials with two different average fiber diameters: 500nm and 1000nm were compared in this study. Additionally, each material was prepared in two versions: with aligned and non-aligned fibers. Moreover, the effect of fiber diameter and their arrangement in the fibrous material on pericytes growth was compared.

The results showed that fibrous scaffolds with various properties (such as fiber diameter, fiber alignment) can be produced by the SBS method. Fibrous materials properties: fiber diameter and arrangement depend on the initial SBS process parameters: polymer solution concentration and collector rotational speed, respectively. The increase of polymer solution concentration and collector rotational speed allow for obtaining fibrous materials with greater fiber diameters and homogeneously oriented (aligned) fibers. Furthermore, PUs scaffolds support pericytes proliferation, whereas the cells' growth and arrangement depend on the fibrous scaffold properties (fiber diameter and arrangement).

Summarizing, scaffolds produced by the SBS method can be adjusted directly to the intended purpose by manipulating the SBS process parameters, and are easily adaptable to cell requirements, which is of great importance in the production of complex structures such as vascular prostheses

References:
1. Jafari, M. *et al.* Polymeric scaffolds in tissue engineering: a literature review. *J. Biomed. Mater. Res. Part B Appl. Biomater.,* 2017, vol. **105**, pp. 431–459
2. Edmondson, R., Broglie, J. J., Adcock, A. F. & Yang, L. Three-dimensional cell culture systems and their applications in drug discovery and cell-based biosensors. *Assay and Drug Development Technologies,* 2014, vol. 12, pp. 207–218
3. Leal, B. B. J. *et al.* Vascular Tissue Engineering: Polymers and Methodologies for Small Caliber Vascular Grafts. *Front. Cardiovasc. Med.*, 2021, vol. **9,** pp. 376–397

Experimental evaluation of differences between planned and achieved correction in hexapod fixator system.

Bartosz Martyniuk[1], Piotr Morasiewicz[2,3], Andżelika Pajchert Kozłowska[2], Jarosław Filipiak[1]
[1]Department of Biomedical Engineering, Mechatronics and Theory of Mechanisms, Wrocław University of Science and Technology, (Łukasiewicza 7/9,50-371 Wrocław, Poland)
[2]Department and Clinic of Orthopaedic and Traumatologic Surgery, Wrocław Medical University, (Borowska 213, 50-556 Wrocław, Poland)
[3]Department of Orthopaedic and Traumatologic Surgery, Institute of Medical Sciences, University of Opole, (aleja Witosa, 26, 45-401 Opole, Poland)
Email of Corresponding Author: bartosz.martyniuk@pwr.edu.pl

The purpose of this study was an experimental assessment of changes in bone fragment position in patients with non-union of the tibia treated with a hexapod fixator. We hypothesized that the use of hexapod fixators leads to differences between the planned and actual position of bone fragments. The specific objective of the study was to investigate the difference between planned and experimental positions of bone fragments. The study was conducted in physical models of the hexapod fixator–bone fragment system.

The hexapod fixator (Smart Correction, Response Ortho) was composed of two rings (the proximal ring with an outer diameter of 245 mm and an inner diameter of 195 mm, and the distal ring with an outer diameter of 200 mm and an inner diameter of 150 mm). The two rings were connected via six struts whose length could be regulated from 140 mm to 200 mm. The fixator was mounted on a synthetic model of the left tibia (Sawbones) using Kirschner wires 1.8 mm and Schanz pins 6 mm keeping spatial configuration as close as possible to the actual configuration used in patients. Three variants of correction were analyzed in this study: 15 mm compression (configuration 1), 26 mm compression, 15∘ varus deformity correction (configuration 2), 26 mm compression, 15∘ varus deformity correction, 10∘ internal rotation deformity correction (configuration 3). The bone–fixator models were subjected to forces with the use of Maquet's model to imitate the loading forces exerted on the lower limb. This mimic weight-bearing system was based on a MTS Mini Bionix 858 universal fatigue testing system. For each configuration a force of 0 N, 25 N, 50 N, 75 N and 100 N was applied while performing correction. Displacements of bone fragments in physical model were measured using optical computer navigation system (Optotrak Certus).

A difference between the target and actual correction was observed. For compression correction differences were ranging depending on the force applied for configuration 1 from 1.5% to 13.2%, for configuration 2 from 17% to 21.3% and for configuration 3 from 13.2% to 17.9%. The differences for varus correction were for configuration 2 from 1.6% to 6.3% and for configuration 3 from 1.1% to 1.7%. The biggest differences were observed for torsional deformity correction in configuration 3 ranging from 17% to 34,4%.

Our study showed differences between the target and achieved compression of bone fragments depending on the evaluated hexapod fixator configuration in the treatment of tibial non-union. Greater planned bone fragment compression led to greater discrepancies between the target and achieved compression. Which confirms our hypothesis that there are differences between the planned and actual position of bone fragments. Our findings are consistent with other authors reports showing that there is residual deformity after performing correction with hexapod fixators. Manner et al. reported 9.3% of cases with a residual deformity following treatment with a Taylor Spatial Frame hexapod fixator [1]. Naude et al. reported a residual deformity in 29.2% of patients treated with a TrueLok-Hexapod System and in 52.4% of patients treated with a Taylor Spatial Frame [2]. The use of hexapod fixators leads to differences between the planned and actual position of bone fragments in physical models. Orthopedists must pay close attention to the fact that, in some cases of failure of initial adjustment schedule, the use of a hexapod fixator requires modifications to the initial strut-adjustment schedule.

References:
[1] M. H. et al.. Accuracy of complex lower-limb deformity correction with external fixation: a comparison of the Taylor Spatial Frame with the Ilizarov Ringfixator. J Child Orthop 2007;1:55–61.
[2]] N. J. et al. Outcomes following treatment of complex tibial fractures with circular external fixation: a comparison between the Taylor Spatial Frame and TrueLok-Hex. Strategies Trauma Limb Reconstr 2019;14:142–7.

Leveraging rheology for biomimetic materials design

Joanna Mystkowska*, Dawid Łysik
Department of Biomaterials and Medical Devices, Institute of Biomedical Engineering,
Bialystok University of Technology, Wiejska 45c, 15-351 Bialystok, Poland
*j.mystkowska@pb.edu.pl

Aims

Most biological materials are characterized by time and environment-dependent viscous and elastic properties [1]. Thus, dynamic rheological behavior should be taken into account when designing and testing new biomaterials for medical applications. Complex rheology, including compression-stiffening, and shear-stiffening, is of great interest when testing bio-related polymers, smart materials, elastomer blends and composites, etc [2]. There are some works where the development of bioprinted materials, such as cartilage matrix-based hydrogels to match the mechanical performance of native cartilage, was tested [3]. There is also a need for biomimetic materials for regenerative medicine, drug-delivery systems, tissue engineering products, artificial biofluids, elastic magnetic materials, and personal care products, where mechanical properties are concerned. In order to characterize such properties, different rheological tests have to be used. Recently, bioengineering is increasingly basing its design assumptions on guidelines derived directly from nature. In the current study, rheological characterization as a tool for biomimetic materials design was proposed.

Methods

Rheological tests of polysaccharide-based hydrogels and surface modified silicone-based composites were performed under controlled environmental conditions. The HAAKE Rheostress 6000 rheometer (Thermo Scientific, USA), with a Peltier temperature control system, in a plate-plate arrangement was used. For hydrogels, tests included dynamic viscosity assessments in the 0.1-200 1/s shear strain rate and amplitude sweep and frequency oscillation tests. For elastic composites, disk-shaped samples with a thickness of 1 mm were tested. The rheological analyzes were based on two tests, where the first one consisted of forcing a constant 10% shear strain in the material and measuring the stress response. The second test consisted of deforming the sample in an oscillating manner with a constant amplitude of 1% and a variable frequency from 0.1 to 10 Hz. Based on the obtained stress waveform, the dependence of the storage modulus G' as a function of frequency was determined.

Results

The mechanical properties of materials for medical applications become the basis for their modification, ensuring the imitation of the properties of the natural tissue they replace or the function they are to perform. In the case of biofluid substitutes, the incorporation of a polysaccharide into the hydrogel, strongly modifies biofluid rheological parameters, such as dynamic viscosity, storage modulus, and loss modulus. Some synergistic outcomes were additionally observed. For elastic materials, relaxation tests, and dynamic oscillation rheological tests show how the viscoelastic behavior of the developed silicone-based composites depends on the content of filler and the incubation conditions *in vitro*. It was observed that the powder modifier content and incubation parameters influence on relaxation module value.

Conclusion

The rheological properties of polysaccharides-modified hydrogels for oral cavity applications might be controlled in order to ensure their proper biofunctionality, e.g. in denture wearers, where it is important to ensure adequate lubrication between the mucosa and the denture plate. In the case of surface modified silicone-based composites, the stiffness change after *in vitro* tests. Additionally, the powder content in the composite influence on relaxation and storage moduli parameters. These results show that designing new soft biomaterials for medical applications should be related to research on their rheological properties.

References:

[1] Kaneda I. (ed.), Rheology of biological soft matter. Fundamentals and Applications, Springer, Tokyo, 2017.
[2] Łysik D. et al., Modulation of Biofilm Mechanics by DNA Structure and Cell Type, *ACS Biomaterials Science&Engineering*, 2022, 8, 11, 4921–4929.
[3] Kijotake E.A. et. al, The Rheology and Printability of Cartilage Matrix-Only Biomaterials, Biomolecules, 2022, 12, 846.

Influence of PEO current parameters on the obtained surface structure for a high porosity Ti6Al4V implant made by SLM method

Ada Orłowska[1*], Wojciech Kajzer[1], Karolina Goldsztajn[1], Wojciech Simka[2], Janusz Szewczenko[1]

[1]Faculty of Biomedical Engineering, Silesian University of Technology, ul. Roosevelta 40, 41-800 Zabrze, Poland
[2]Faculty of Chemistry, Silesian University of Technology, ul. Krzywoustego 6, 44-100 Gliwice, Poland

*ada.orlowska@polsl.pl

Titanium scaffolds, i.e. highly porous implants that provide space for bone tissue overgrowth into, are a technological challenge during their surface modification. The main criterion when designing the pore structure is to ensure optimal conditions for the overgrowth of bone tissue through them. The promoted pore size of ~500-700 μm, although from the point of view of bone tissue is extremely beneficial, significantly affects the penetration of the electrolyte during the process of its modification [1]. This, in turn, causes the formation of a heterogeneous passive layer, especially in the central part of the implant [2]. The aim of the research was the selection of current parameters ensuring a homogeneous surface structure for the entire volume of the implant during PEO aimed at improving the properties of the implant.

The research was carried out on a proprietary implant for the treatment of discopathy in the c4-c5 section, made of Ti6Al4V with the SLM technology at ChM Białystok Sp. z o. o. (Fig.1.). The implant was characterized by an actual porosity of ~50% and pores of ø600 μm based on a diamond mesh. The samples were subjected to the PEO process using a 0.5M $Ca(H_2PO_2)_2$ solution. The process was carried out for various current parameters (j = (12,5-100) mA/cm^2; U = (250/300) V; using the omnidirectional titanium electrode. The electrolyte was stirred using a magnetic stirrer. After modification, the samples were cleaned of electrolyte residues in an ultrasonic cleaner (5 min distilled water/5 min acetone/5 min distilled water). The samples were then cut with a precision cutter to allow evaluation of the inner part of the implant. The surface assessment was carried out using SEM.

SEM observations confirmed a significant difference between the obtained surface structure in the inner and central parts of the modified implants. Particularly unfavorable, heterogeneous structure was observed for samples modified with the use of continuous current (Fig.2.). The impulse-modified samples were characterized by a more homogeneous structure (Fig.3.). The observations showed no aggregation of electrolyte residues inside the implants.

Current parameters during the PEO process significantly affect the obtained surface structure, especially in the central part of porous implants. The use of pulsed current prevented local overheating of the sample and insufficient electrolyte replacement inside the tested element.

Fig.1. Designed implant produced by the SLM method.
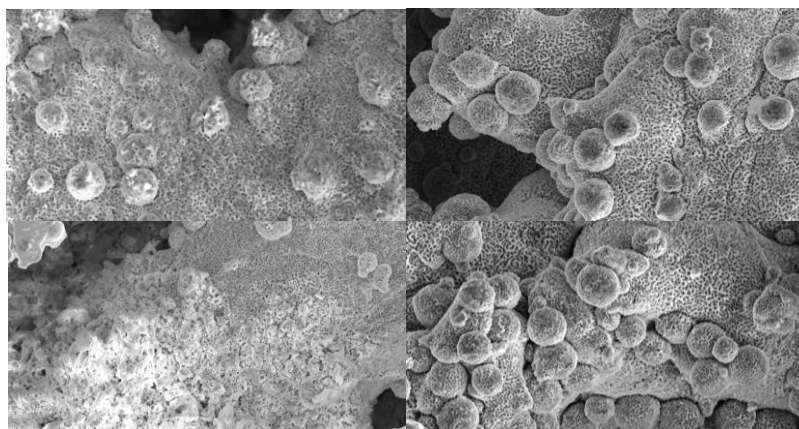
Fig.2. SEM image of the external and internal surfaces of the implant subjected to PEO treatment with continuous current for j = 50 mA/cm²; U = 250V

Fig.3. SEM image of the external and internal surfaces of the implant subjected to PEO treatment with a pulse current for j = 50 mA/cm²; U = 250V

References:

[1] Chen, Z.; et al. Influence of the pore size and porosity of selective laser melted Ti6Al4V ELI porous scaffold on cell proliferation, osteogenesis and bone ingrowth. *Mater. Sci. Eng. C* 2020, vol. *106*, 110289.

[2] Karaji, Z.G; et al., Effects of plasma electrolytic oxidation process on the mechanical properties of additively manufactured porous biomaterials. *Mater. Sci. and Eng.: C*,2017, vol. *76*, p. 406-416.

Application of ionizing radiation in synthesizing hydrogels and nanogels for biomedical applications

Janusz M. Rosiak, Renata Czechowska-Biskup, Sławomir Kadłubowski, Małgorzata Matusiak,
Alicja K. Olejnik, Bożena Rokita, Beata P. Rurarz, Radosław A. Wach, Piotr Ulański*
Institute of Applied Radiation Chemistry, Faculty of Chemistry, Lodz University of Technology,
Wróblewskiego 15, 93-590 Łódź, Poland
*piotr.ulanski@p.lodz.pl

Ionizing radiation is well known to biomaterials experts as one of the tools used for sterilization of medical devices. However, it can be also successfully applied in biomaterials synthesis, as for example in crosslinking of polyethylene-based sockets in hip prosthesis. Our team has pioneered application of ionizing radiation in synthesizing soft and swellable polymer-based biomaterials, i.e., hydrogels. While many hydrogel-based or hydrogel-containing medical devices are on the market (soft contact lenses, hydrogel dressings, transdermal drug delivery devices, etc.), classical methods for synthesizing hydrogels for biomedical purposes have two major drawbacks. Firstly, they involve application of monomers, crosslinking agents and initiators, which are usually toxic and difficult to completely remove from the final product. Secondly, sterilization of the product must be performed as a separate procedure. In contrast, radiation synthesis of hydrogels requires only two compounds as the substrates – a biocompatible, hydrophilic polymer and water. The action of ionizing radiation induces crosslinking of macromolecules, a clean and waste-free process that leads to the formation of macroscopic, three-dimensional stable hydrogel. Moreover, radiation causes concomitant sterilization of the product, so that synthesis and sterilization can occur in the same technological step, in the final packaging, significantly simplifying the production and lowering its costs. Hydrogel dressings based on this technology [1] are currently manufactured Poland and in several other countries on an industrial scale, and are standard equipment for the US Marine Corps units.

Our studies have demonstrated that ionizing radiation is also an excellent tool for synthesizing nanoscale gel particles – internally crosslinked macromolecules called nanogels, which may be perceived as frozen polymer coils or soft macromolecular nanocages. A short but powerful pulse of high-energy electrons applied to a polymer solution can simultaneously create many free radicals along each macromolecule. Subsequent recombination of these radicals within the same chain leads to the formation of stable covalent bonds between the chain segments, thus forming the nanogels. The method is universal and it allows to control the main product properties (mass, size, density) while retaining the chemical structure of the polymer substrate.

Nanogels are excellent candidates for nanocarriers of drugs, genes and radioisotopes. For instance, nanogels obtained by radiation technique have been demonstrated to cross the blood-brain barrier while carrying a drug to treat Alzheimer's disease [2]. Our team is currently involved in designing a nanogel-based platform, which can be a robust basis for developing nanocarriers dedicated for particular medical applications. In our lab, we elaborated procedures for synthesizing poly(acrylic acid)-based nanogels of various sizes, which can be further modified to serve as selective radioisotope nanocarriers for theranostics of prostate cancer. In vitro studies on cell lines indicate high selectivity of this nanoradiopharmaceutical in targeting cancer cells [3].

References:
[1] Rosiak J., Rucińska-Rybus A., Pękala W., A Method of Manufacturing Hydrogel Dressings, US Patent 4,871,490.
[2] (a) Picone P., Ditta L.A., Sabatino M.A., Militello V., San Biagio P.L., Di Giacinto M.L., Cristaldi L., Nuzzo D., Dispenza C., Giacomazza D., Di Carlo M., Ionizing Radiation-Engineered Nanogels as Insulin Nanocarriers for the Development of a New Strategy for the Treatment of Alzheimer's Disease. *Biomaterials*, 2016, vol. 80, pp. 179–94; (b) Picone P., Sabatino M.A., Ditta L.A., Amato A., San Biagio P.L., Mulè F., Giacomazza D., Dispenza C., Di Carlo M., Nose-to-Brain Delivery of Insulin Enhanced by a Nanogel Carrier. *J. Control. Release*, 2018, vol. 270, pp. 23-36.
[3] (a) Matusiak M., Rurarz B.P., Kadłubowski S., Wolszczak M., Karczmarczyk U., Maurin M., Kolesińska B., Ulański P., Synthesis and Properties of Targeted Radioisotope Carriers Based on Poly(Acrylic Acid) Nanogels, *Pharmaceutics*, 2021, vol. 13, art. no. 1240; (b) Ashfaq, A., An, J.-C., Ulański, P., Al-Sheikhly, M., On the Mechanism and Kinetics of Synthesizing Polymer Nanogels by Ionizing Radiation-Induced Intramolecular Crosslinking of Macromolecules, *Pharmaceutics*, 2021, vol. 13, art. no. 1765.

The cardiovascular stents biofunctionalized with anti-inflammatory interleukins could modify the course of inflammation and prevent future in-stent restenosis

Przemysław Sareło[1], Beata Sobieszczańska[2], Edyta Wysokińska[3], Marlena Gąsior-Głogowska[1], Anna Szagdaj[1], Ewa Zioło[3], Wojciech Kałas[3], Magdalena Wawrzyńska[4], Halina Podbielska[1], Marta Kopaczyńska[1]

[1]Department of Biomedical Engineering, Faculty of Fundamental Problems of Technology, Wrocław University of Science and Technology, Wybrzeże Stanisława Wyspiańskiego 27, 50-370 Wrocław, Poland; [2]Department of Microbiology, Faculty of Medicine, Wrocław Medical University, Wybrzeże Ludwika Paustera 1, 50-367 Wrocław, Poland; [3]Department of Experimental Oncology, Ludwik Hirszfeld Institute of Immunology and Experimental Therapy, Polish Academy of Sciences, Rudolfa Weigla 12, 53-114 Wrocław, Poland; [4]Center of Preclinical Studies, Wrocław Medical University, Karola Marcinkowskiego 1, 50-368 Wrocław, Poland

przemyslaw.sarelo@pwr.edu.pl

The mechanisms underlying in-stent restenosis (ISR), defined as re-reduction of the vessel lumen after previous percutaneous coronary intervention (PCI), have not been fully elucidated. Among many, acute inflammation with accompanying accumulation of monocytes in the subendothelial space is considered [1]. Moreover, this condition is superimposed on chronic inflammation associated with progressive atherosclerosis [2]. An active inflammatory process triggers a series of vascular cells responses (including endothelial cells dysfunctions as well as phenotypic transformation and migration of vascular smooth muscle cells), that result in hypertrophied neointima formation. The blood flow through the diseased coronary artery could be afresh restricted and if left untreated could be fatal [1]. Thus, the attempts to extinguish inflammation are currently being studied as they may prove to be a novel, effective therapeutic strategy for the prevention of ISR [3].

In the study, the step-by-step procedure of selected anti-inflammatory interleukins functionalized polydopamine-based coating synthesis was reported. The physico-chemical properties of proposed biomaterial were assessed by appropriate techniques (e.g., attenuated total reflectance Fourier transform infrared spectroscopy – ATR-FTIR and atomic force microscopy – AFM). There were also performed studies to evaluate the biological activity of the coating in reference to selected cells, whose dysfunction promotes the development of atherosclerosis and ISR (e.g., viability and proliferation of endothelial cells, thrombogenicity by monocyte adherence, cells proinflammatory response, macrophages changes of polarization).

By the ATR-FTIR spectroscopy and AFM examination the incorporation of interleukins into the coating was confirmed, thus effectiveness of functionalization was proved. The gradual release of interleukins from the coating allowed to deliver the deficient cytokines, whose low serum levels were regarded as ISR risk factor. The proposed coating promoted endothelialization of stent surface in the initial stage after PCI, which turned out to be consistent with present treatment strategies. The limitation of selected pro-inflammatory interleukins daily release by coating-interacted-endothelium significantly reduced another risk factor of ISR, that is the inflammatory activation of endothelium. By assessing the changes in macrophages differentiation, the coating immunological activity was confirmed, what proved that the binding procedure did not impair biological properties of the interleukin.

Therefore, it can be concluded that biological action of proposed anti-inflammatory coating modifies the course of inflammation-dependent cellular responses, thereby probability of restenosis can be reduced to a minimum.

References:
[1] Clare J., Ganly J., Bursill C., Sumer H., Kingshott P., de Haan J. The Mechanisms of Restenosis and Relevance to Next Generation Stent Design. *Biomolecules*, 2022, vol. 12, no. 3, pp. 1–26.
[2] Milutinović A., Šuput D., Zorc-Pleskovič R. Pathogenesis of Atherosclerosis in the Tunica Intima, Media, and Adventitia of Coronary Arteries: An Updated Review. *Bosnian Journal of Basic Medical Sciences*, 2020, vol. 20, no. 1, pp. 21–30.
[3] Sareło P., Sobieszczańska B., Wysokińska E., Gąsior-Głogowska M., Kałas W., Podbielska H., Wawrzyńska M., Kopaczyńska M. In vitro examinations of the anti-inflammatory interleukin functionalized polydopamine based biomaterial as a potential coating for cardiovascular stents. *Biocybernetics and Biomedical Engineering*, 2023, vol. 43, pp. 369–385.

Atomic layer deposition Ta$_2$O$_5$ films on NiTi shape memory alloys for cardiovascular applications

Anna Taratuta, Zbigniew Paszenda, Marcin Basiaga
Faculty of Biomedical Engineering, Silesian Univeristy of Technology, Roosevelta 40, Zabrze, Poland
marcin.basiaga@polsl.pl

Currently, research in the field of biomedical engineering is focused on the search for new, advanced materials. A relatively new group of materials, focusing the attention of researchers, are the so-called "smart" materials. "Smart" materials differ from "classic" in that they have the ability to finally and actively adapt to changing external conditions. Shape Memory Alloys (SMA) are considered to be one of the most promising "smart" materials. They constitute a unique group of alloys characterized by the ability to remember the given shape, i.e., subjected to permanent deformations under appropriate conditions, return to their original shape. The shape memory phenomenon was observed in alloys based on copper, silver, gold, nickel, iron, cadmium and others. At present, NiTi alloys are the most common. Research on these alloys has been intensively conducted since the 1980s. The special properties of these materials have made many researchers from various fields interested in these alloys. Their mechanical properties were well recognized. Corrosion phenomena were studied to a lesser extent, in particular with regard to the effects of shape memory and superelasticity as well as biocompatibility [1-3]. Despite the involvement of many scientific centers in the world, the issue of NiTi alloys for medical applications is based on partial research. There are no studies synthesizing comprehensive issues of corrosion and biocompatibility in relation to specific forms of medical devices intended for long-term use. Against this background, comprehensive assessment of the results obtained by individual authors is difficult to generalize. Therefore, the proposed work was develop conditions for the production of surface layers with physicochemical properties adequate to the specificity of the cardiovascular system.

Thus, the main goal of the research was to determine the correlation between the structure and physicochemical properties of the layers (shaped by the technological conditions of the process) applied to the substrates of NiTi alloy intended for contact with blood, and their hemocompatibility. The first stage of the work implementation was involve the development of conditions for the deposition of surface layers Ta2O5 using the ALD (Atomic Layer Deposition). The use of this type of surface treatment is dictated by the need to ensure invariable geometric, structural and mechanical properties of the metal substrate subjected to surface treatment processes. Comprehensive tests for their corrosion resistance were carried out for the surface layers produced under conditions simulating the circulatory system environment. In particular, pitting and crevice corrosion tests were carried out. Next, for selected variants of surface treatment, also tests of the chemical and phase structure of the produced layers, their mechanical properties, surface topography, and physical properties were carried out. In the final stage, for the samples prepared in this way, in vitro biological tests, based on the ISO 10993 standard, which were divided into the general assessment of biocompatibility and the hemocompatibility test under the conditions of potential, post-project use. The following tests were carried out as part of the biocompatibility assessment: determination of inflammatory cytokines of selected agents using the Luminex test, in vitro tests on the immune response of cells immunocompetent in direct contact with the materials. In turn, as part of the hemocompatibility tests, they will be carried out test for activation of the blood coagulation cascade and analysis of the immune response. The scope of the research was allow a comprehensive analysis of the impact of the structure and physicochemical properties of surface layers on the processes occurring on the surface of implants after their introduction into the blood system. Obtained results may form the basis for the development of more detailed criteria for the assessment of the final quality of medical devices used in the cardiovascular system, which will ensure the required biocompatibility of implants and contribute to minimizing the risk of postoperative complications.

References:
[1] Hodgson D.E., Krumme R.C., [in:] Pelton A., Hodgson D., Duerig T. (eds.): Proceedings I International Conference On Shape Memory and Superelastic Technologies, SMST 94, SMST Proceedings, Pacific Grove, CA, 1994, p. 371.
[2] Tyber J., McCormick J., Gall K., DesRoches R., Maier H. J., Abdel Maksoud A.: Structural Engineering with NiTi. I: Basic Materials Characterization, Journal of Engineering Mechanics, Vol. 133, No. 9, 2007.
[3] McCormick J., Tyber J., DesRoches R., Gall K., Maier H.J.: Structural Engineer-ing with NiTi. II: Mechanical Behavior and Scaling, Journal of Engineering Mechanics, Vol. 133, No. 9, 2017.

Assessment of proliferative potential, DNA repair activity and level of apoptosis of cells exposed to metallic biomaterials used for the production of implants

Marta Walczyńska[1,2], Marta Kamińska[1], Madalena Walkowiak-Przybyło[1,3], Piotr Komorowski[1,4], Marcin Elgalal[4,5], Krzysztof Makowski[4,6], and Bogdan Walkowiak[1,4]

[1]Department of Biophysics, Institute of Materials Science and Engineering, Lodz University of Technology, Stefanowskiego1/15, Lodz, Poland; [2]Department of Medical Imaging Techniques, Medical University of Lodz, Lindleya 6, Lodz, Poland; [3]Aflofarm Farmacja Polska Sp. z o.o., Partyzancka 133/151, Pabianice, Poland; [4]Laboratories of Bionanopark, Bionanopark Sp. z o.o. Lodz, Poland; [5]II Department of Radiology and Diagnostic Imaging, Medical University of Lodz, Pomorska 251, Lodz, Poland. [6]Biotechnika, Lukasinskiego 4/238, Lodz, Poland

bogdan.walkowiak@p.lodz.pl

Introduction: There are numerous reports of neoplastic lesions in the vicinity of implants or in distant sites, but temporally correlated with implantation. Such reports mainly concern the implantation of dental implants, which are performed in the largest number, and squamous cell carcinoma is one of the main types of cancer located in the vicinity of such implants [1]. The occurrence of malignancies after hip arthroplasty in the vicinity of endoprostheses has also been described [2]. At present, there are no indisputable data on the promotion of carcinogenesis by implants used in orthopedics, and the problem of accelerated tumor induction in the area of implantation is still poorly understood and unclear. The aim of the present study was a preliminary assessment of the risk of carcinogenesis induced by metallic biomaterials intended for orthopedic implants. Recently, we published a preliminary assessment of changes in the expression of tumor-promoting genes in chondrocytes exposed to metallic biomaterials [3]. The current report is an analytical summary of changes in the proliferation potential, DNA damage repair activity and level of apoptosis of primary and neoplastic cells (chondrocytes and osteoblasts) exposed to commonly used metallic biomaterials.

Materials and Methods: The tests were carried out for four commonly used biomaterials: medical steel (AISI 316L), titanium alloys (Ti6Al4V and Ti6Al7Nb) and cobalt-chromium-molybdenum alloy (CoCrMo). Four cell lines were used: primary (HO-f) and neoplastic (Saos-2) osteoblasts as well as primary (HC-a) and neoplastic (SW 1353) chondrocytes. The parameters were assessed using the Apoptosis, DNA Damage, and Cell Proliferation kit (Becton Dickinson) and the BD Accuri C6 Plus flow cytometer (Becton Dickinson). All experiments were performed in duplicate, collecting 5000 events each.

Results and Conclusions: The obtained results were presented in the form of dot plots as in the attached figure (example results for HO-f primary osteoblasts).
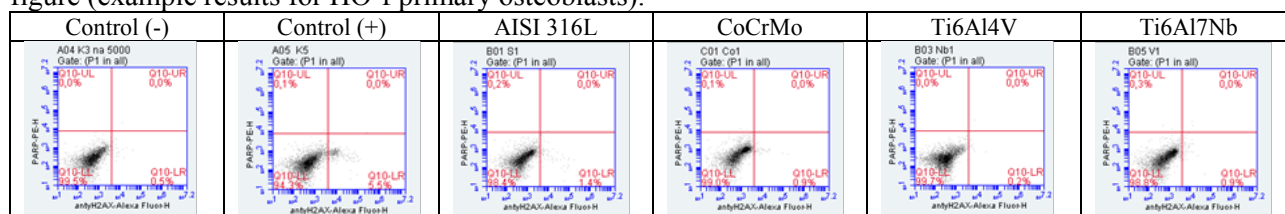
The percentage of cancer cells (Saos-2 and SW 1353) showing the process of repairing damaged DNA is noticeably higher compared to primary cells (HO-f and HC-a). This may be due to both more frequent damage in cancer cells, as well as a more intensive process of repairing damaged DNA in these cells - which could explain the better survival of cancer cells, even with a reduced proliferative potential. Damage and repair of damaged DNA in primary cells was observed at a low level.

References:
[1] Jeelani S., Rajkumar E. et al.: Squamous cell carcinoma and dental implants: A systematic review of case reports. J Pharm Bioallied Sci. (2015), 7(2), S378–S380.
[2] Levasic V., Milosev I. et al.: Risk of cancer after primary total hip replacement: The influence of bearings, cementation and the material of the stem. Acta Orthop. (2018), 89(2), 234–239.
[3] Magdalena Walkowiak-Przybyło: May metallic biomaterials used for orthopedic implants promote carcinogenesis? Preliminary transcriptomic research on human chondrocytes. Engineering of Biomaterials (2020), 157, 15-19.

Surface modification of NiTi shape memory alloy in low temperature plasma in terms of implant applications

Justyna Witkowska[1*], Tomasz Borowski[1], Tomasz Płociński[1], Janusz Kamiński[1], Dorota Moszczyńska[1], Emilia Choińska[1], Agnieszka Sowińska[2], Jerzy Sobiecki[1], Tadeusz Wierzchoń[1]

[1]Warsaw University of Technology, Faculty of Materials Science and Engineering, Warsaw, Poland
[2] Pathology Department, Children's Memorial Health Institute, Warsaw, Poland
*justyna.witkowska@pw.edu.pl

The NiTi alloy with a chemical composition close to equiatomic, is increasingly used in medicine due to its unique properties, such as shape memory and superelasticity [1]. However, its use for long-term implants raises concerns due to the high content of nickel, which can have toxic, allergenic, and even carcinogenic effects on the human body. Therefore, various surface engineering methods are employed to enhance the corrosion resistance of NiTi alloy and modify its biological properties [2]. The intended use determines the biological properties that the surface must exhibit. Other requirements are imposed on cardiac implants, which must primarily be athrombogenic and ensure proper endothelialization, and other requirements are imposed on bone implants, where good osseointegration of the implant with the patient's bone is crucial.

In the first stage, the aim of the study was to produce and investigate the properties of innovative composite layers (a-C:N:H+TiO_2) on NiTi alloy, consisting of outer coating of amorphous hydrogenated carbon doped with nitrogen and titanium dioxide (rutile) layer, compared to titanium dioxide (TiO_2) layers and the NiTi alloy in initial state. Oxidizing and nitriding processes were carried out using low-temperature plasma under glow-discharge conditions at temperatures up to 300°C, ensuring the preservation of NiTi alloy properties. The a-C:N:H carbon coatings were synthesized using the RFCVD method. The properties of the produced layers were examined in terms of microstructure, chemical composition, corrosion resistance, surface topography, wettability, surface free energy, and biological properties regarding hemocompatibility. In the second stage of the studies the bioactivity of the produced oxidized layers were also evaluated. It was verified by the spontaneous biomimetic growth of apatite deposits from simulated body fluid (SBF) solution.

The obtained research results indicated that the formation of surface layers such as TiO_2 (rutile) and a-C:N:H+TiO_2 on NiTi shape memory alloy improves its functional properties, including biological properties. Specifically, it enhances corrosion resistance, limits the release of nickel ions into the biological environment, reduces platelet adhesion and aggregation on the surface, and ensures proper endothelialization. The results are promising in terms of proposing a new material solution for the use of NiTi shape memory alloys in long-term cardiac implants. Further studies of the bioactivity of the oxidized layers, understood as the ability to induce biomimetic growth of calcium phosphates, showed that titanium dioxide (TiO_2) layers increased the bioactivity of the shape memory alloy. The apatite deposits formed faster on the modified surface compared to the initial state. The presence of calcium-deficient hydroxyapatite (CDHA) among the calcium phosphates in the biomimetic layer produced in vitro indicates a potential better bioactivity also in vivo, as the SBF solution used resembles both the composition and pH of human body fluids. Better proliferation of osteoblasts was also demonstrated on the modified surface. This is an extremely important aspect in the potential use of a shape memory alloy for the production of bone implants for long-term use, because better bioactivity translates into faster osseointegration of the implant with the patient's bone.

The obtained results showed the potential of the low-temperature plasma treatments in terms of shaping the biocompatibility of NiTi shape memory alloys. The surface modification via processes under glow discharge conditions improve the functional properties of the NiTi alloy. The appropriate combination and planning of hybrid processes allow for the achievement of desired biological properties, depending on the potential use for cardiological or bone implants.

References:
[1] Biesiekierski A., Wang J., Abdel-Hady Gepreel M.,Wen C.: A new look at biomedical Ti-based shape memory alloys. Acta Biomaterialia 2012, vol. 8, no. 5, pp. 1661–1669.
[2] Shabalovskaya S., Anderegg J., Van Humbeeck, J.: Critical overview of Nitinol surfaces and their modifications for medical applications. Acta Biomaterialia, 2008, vol. 4, no. 3, pp. 447-467.

Flexible neural electrode prototype for intracranial electrostimulation

Natalia Zalewska, Matthias Nawrocki, Mikołaj Kubiak, Rafał Laskowski, Aleksandra Zieminska, Karolina Cysewska*

Laboratory of Functional Materials, Faculty of Electronics, Telecommunications and Informatics, and Advance Materials Centre, Gdańsk University of Technology, ul. Narutowicza 11/12, 80-233 Gdańsk, Poland

*karolina.cysewska@pg.edu.pl

Currently, one thousand million people suffer from neurological issues, such as vision loss and paralysis due to neural path degradation, epilepsy and Parkinson's disease. The introduction of electrodes within the neural tissue can improve the patient outcomes for these diseases in most cases. Most electrodes available on the market today are based on pure metals such as platinum (Pt) or gold (Au). Their rigid structure leads to their poor integration with the tissue environment and a reduction in the effective lifetime of the electrode[1]. Therefore, there is a need to develop a new, more compatible type of electrode for this purpose.

In this work, the prototype of flexible, Au and/or polymer-based electrodes was developed. In order to obtain stable and stretchable conductive paths, Au and/or conducting polymer such as poly(3,4-ethylenedioxythiophene) polystyrene sulfonate (PEDOT:PSS) were deposited on the polydimethylsiloxane (PDMS) substrate. PDMS reveals tissue-like elastic modulus, exhibits lower inflammatory response compared to the other flexible materials as electrode substrate[2]. PEDOT:PSS is a commercially available, highly biocompatible conducting polymer. Several tasks were performed in order to obtain a prototype of the electrode (a) design of molds for PDMS preparation for 3D printing, (b) development of procedure for modification of PDMS surface, (c) design of masks for the path preparation, (d) deposition of the conducting paths (Au – by sputtering, PEDOT:PSS – by drop-casting method), (e) development of the electrical connections and isolation. In the end, basic electrical interface parameters of the electrode such as impedance, potential window, double-layer capacitance, charge storage capacitance, and charge injection limit were determined in the simulated body fluid at the body temperature. The parameters of the flexible vs. rigid commercial electrode were determined and discussed.

The procedure for surface modification of PDMS was developed and included using of the O_2 plasma and silane-based chemicals. The tests showed that it was possible to provide uniform and highly adhered conducting Au and/or PEDOT:PSS layer on the surface of the PDMS, which was stable even after the electrochemical measurements. The electrical interface parameters of the developed electrode prototype were the order of values similar to those of commercially used electrodes.

Currently, the biggest challenge of the development of the flexible electrode is to provide highly adhered conducting paths on its surface. The problem is significant especially in the case of PDMS surface because of its high hydrophobic properties. The work presents full procedure of the surface modification of PDMS to enhance the adhesion of the conductive path to the surface of the substrate for the both Au and commercial PEDOT:PSS.

References:
[1] Y. Cho, H. Shin, J. Park, S. Lee, Micromachines 12 (2021) 1552.
[2] M. Gori, G. Vadalà, S.M. Giannitelli, V. Denaro, G. di Pino, Frontiers in Bioengineering and Biotechnology 9 (2021) 411.

Integrating Electrospinning and 3D Printing of Modified PBS Copolyester for Multiscale Tubular Structures Resembling Blood Vessels

Moein Zarei, Miroslawa El Fray*.
Department of Polymer and Biomaterials Science, West Pomeranian University of Technology in Szczecin, al. Piastów 45, 71-311 , Szczecin, Poland
Email: *mirfray@zut.edu.pl

Biological organs and tissues, including blood vessels, possess intricate multilayered structure that necessitate the use of suitable biomaterials and various processing techniques to achieve such sophisticated hierarchical architectures[1]. Recently, new biodegradable poly(butylene succinate-dilinoleic succinate-ethylene glycol succinate) (PBS-DLS-PEG) copolymers were synthesized through melt polycondensation, resulting in good processability and tailored physico-chemical properties[2]. To emulate the multilayered structure of vascular walls, we investigate the combination of fused filament fabrication (FFF) and electrospinning techniques, enabling the creation of intricate architectures with precision and fidelity.

The architecture of blood vessels comprises three distinct layers with varying cell types, thicknesses, and functionalities. To replicate these structures, each layer is engineered using different techniques. The middle layer with a diameter of 5 mm, akin to that of a muscular artery, which is the thickest, is fabricated through 3D printing using 1.75 mm filament made from tailored PBS-DLS-PEG copolymers. The outer layer, consisting of connective fibrous tissue in natural blood vessels, is engineered using electrospinning with the same PBS-DLS-PEG copolymers. The lumen, crucial for promoting endothelialization and blood compatibility, is created using perfusion coating with gelatin. The results of this study encompass a comprehensive characterization of the physicochemical and biological properties of the materials, as well as the architectural and mechanical features of the fabricated tubular multiscale graft. The engineered multilayered vascular graft exhibited robust layer attachment and demonstrated excellent mechanical performance, including compliance and leakage properties, highlighting its considerable potential for vascular graft applications. This study introduces a novel approach in the realm of biomaterials and implants, offering promising avenues for the advancement of vascular tissue engineering and regenerative medicine.

References:
[1] O'Connor C, Brady E, Zheng Y, Moore E, Stevens KR. Engineering the multiscale complexity of vascular networks. Nature Reviews Materials 2022 7:9 2022;7:702–16. https://doi.org/10.1038/s41578-022-00447-8.
[2] Moein Zarei, Beata Michalkiewicz, Miroslawa El Fray. The effect of segmental composition of bio-based PBS-DLS-PEG copolymers on their physico-chemical properties and processability by 3D printing and electrospinning. ChemRxiv 2022. https://doi.org/10.26434/chemrxiv-2022-6m6sm.

Dynamic network formation of pH-tunable chitosan functionalized by catechol

Joanna Żur-Pińska[1], Julien Es Sayed[2], Armin Amirsadeghi[2], Małgorzata Włodarczyk-Biegun[1,2]

[1]Biotechnology Centre, The Silesian University of Technology, B. Krzywoustego 8, 44-100, Gliwice, Poland
[2]Zernike Institute for Advanced Materials, University of Groningen, Nijenborgh 4, Groningen, 9747 AG, The Netherlands
m.k.wlodarczyk@rug.nl, malgorzata.wlodarczyk-biegun@polsl.pl

Aims: 3D printing has great potential in the biomedical engineering field, but its usage is limited by the availability of suitable (bio)inks that can meet the required physicochemical and cytocompatibility criteria [1]. One promising approach is using printable hydrogels that contain metal-based dynamic bonds. To date, most studies on that topic were based on PEG grafted with dopamine cross-linked with iron [1,2]. In this study, we proposed a novel ink based on quaternized chitosan-catechol due to its unique properties and enhanced adhesion capabilities which promote cell attachment and growth. Catechol groups can be employed in metal-induced cross-linking mechanisms to form reversible bonds [2]. The stoichiometry of complex formation is tightly controlled by pH with the typical level required to establish bis- and tris-complexes reported as above neutral or slightly basic (7.0-9.1). The dynamic network formed between catechol groups, and divalent or trivalent metal ions can be further oxidized by sodium periodate to form covalent bonds [1,2].

Methods: The influence of different molar ratios, solvents, and pH on the gel formation and self-healing properties of catechol-Fe^{3+} and catechol-Cu^{2+} polymer networks were analyzed. The gelation kinetics of quaternized chitosan-catechol mixtures at a different concentration range from 2.5-7.5% (w/v) with Fe^{3+} and Cu^{2+} metal ions were analyzed using a rotational rheometer (TA Instruments HR20) by frequency sweep oscillatory test. The final stiffness and time-dependent response of the obtained hydrogels were analyzed in a time sweep test. Recovery of stiffness and cohesiveness after failure was checked by a thixotropy test induced by shear strain and simple tearing of the gel. The filament printability evaluation was analyzed by 3D printing (GeSIM, BioScaffolder 3.3), and the cytocompatibility of the proposed inks was verified by using mouse fibroblasts NIH 3T3.

Results: Quaternized chitosan-catechol inks cross-linked with Fe^{3+} and Cu^{2+} ions were developed and characterized by rheology. The most beneficial molar ratio which allows for maximizing the coordination degree of complexation for both metals was established as 3:1 (catechol:metal). The immediate cross-linking indicated by a rapid color and mechanical properties change after increasing pH in the range of 7.15-11 was observed for both systems. The most suitable inks were chosen for extrusion printing. The cell culture study confirmed that developed inks are non-cytotoxic.

Conclusion: New inks for 3D printing have been developed using modified chitosan cross-linked with two different metals. The self-healable hydrogels proposed in this study have been shown to possess good mechanical properties and biocompatibility with fibroblasts NIH 3T3, indicating their potential for use in tissue engineering applications. The polymer networks can be further modified to optimize their properties.
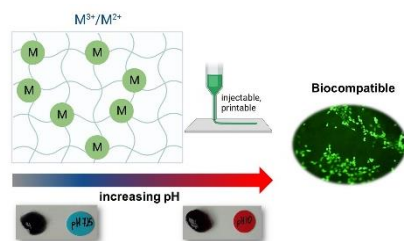
Fig. 1. The properties of quaternized chitosan-catechol hydrogels cross-linked with metals.

References:
[1] Włodarczyk-Biegun M.K., Paez J.I., Villiou M., Feng J., del Campo A. Printability study of metal ion crosslinked PEG-catechol based inks, *Biofabrication*, 2020, vol. 12, no. 035009, pp. 1-17.
[2] Holten-Andersen N., Harrington M.J., Birkedal H., Lee B.P., Messersmith P.B., Lee K.Y.C., Waite J.H. pH-induced metal-ligand cross-links inspired by mussel yield self-healing polymer network with near-covalent elastic moduli, *PNAS*, 2011, vol. 108, no. 7, pp. 2651-2655.

Chapter IV

Biomaterials for Controlled Delivery of Biologically Active Substances

Session organizers:

Prof. Elżbieta Pamuła, AGH University of Science and Technology in Kraków
Prof. Alina Sionkowska, Nicolaus Copernicus University in Toruń

3D bioprinting of alginate-gelatin scaffolds with incorporated BMP-2 encapsulated PLGA microspheres for enhancing osteoporotic repair

Onyedikachi Azuama[1], Małgorzata K. Włodarczyk-Biegun[1,2]

[1]Biotechnology Center, Silesian University of Technology. ul. B. Krzywoustego 8, 44-100, Gliwice, Poland.
[2]Polymer Science, Zernike Institute for Advanced Materials University of Groningen Nijenborgh 4, 9747 AG Groningen.
m.k.wlodarczyk@rug.nl, Malgorzata.Wlodarczyk-Biegun@polsl.pl

INTRODUCTION: Osteoporosis is a disorder affecting millions of patients, with pathophysiology characterised by excessive bone resorption against bone formation. Often, patients with bone defects require surgical bone grafts, though with limitations like multiple required surgeries, morbidity, and limited quantity of donor tissues [1]. Tissue engineering is a means to obtain biomaterial constructs with adequate bio-functional and mechanical properties that can restore function of damaged tissues. Most times, scaffolds are insufficient to induce osteogenesis, but combination with bioactive molecules like growth factors or small signalling molecules, can improve success of bone regeneration [2].

AIM: The objective of this study was to develop a mechanically stable and biofunctional 3D-printed scaffold reinforced with PLGA-microparticles, to enhance bone regeneration in osteoporotic defect model.

METHODS: PLGA (poly(lactic-co-glycolic acid)) microspheres were prepared by double emulsion solvent extraction (w/o/w) and then characterised morphologically by Scanning electron Microscope. Next, it was included into cell laden alginate-gelatine based bioink. Scaffolds were 3D printed using extrusion-based printing technique (GeSim BioScaffold Printer BS3.2). This bio-ink physical properties were further assessed via rheological analysis. 3D bioprinted constructs were analysed in respect to degradation rate and subsequent monitoring of cell viability and osteogenic differentiation via live/dead stain and alkaline phosphatase activity.

RESULTS: Printable alginate-gelatin based construct was obtained and stability of scaffold was tuned by the interplay of different cross-linking approaches. However, constructs were more stable in tissue culture medium compared to Phosphate buffered saline medium. Also, the addition of PLGA microspheres enhanced the viscosity of the biomaterial ink.

CONCLUSIONS: We are currently developing a tuneable strategy for the fabrication of alginate-gelatine bioink possessing enhanced osteogenic differentiation potential by incorporation of microspheres into bioink. In future BMP-2 will be incorporated into PLGA microspheres to enhance the success of bone regeneration.
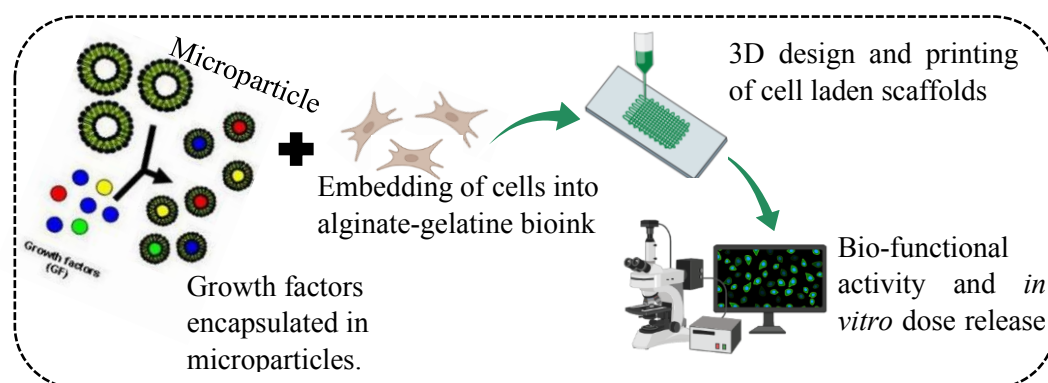
Figure 1. Graphical representation of 3D bioprinting of alginate- gelatin scaffolds with incorporated BMP-2 encapsulated PLGA microspheres for enhancing osteoporotic repair.

REFERENCES

[1] García-García, P., Reyes, R., Segredo-Morales, E., Pérez-Herrero, E., Delgado, A., & Évora, C. PLGA-BMP-2 and PLA-17β-Estradiol Microspheres Reinforcing a Composite Hydrogel for Bone Regeneration in Osteoporosis. *Pharmaceutics,* 2019, vol. 11, pp. 648.

[2] Segredo-Morales, E., García-García, P., Reyes, R., Pérez-Herrero, E., Delgado, A., & Évora, C. Bone regeneration in osteoporosis by delivery BMP-2 and PRGF from tetronic–alginate composite thermogel. *International Journal of Pharmaceutics*, (2018), vol. 543(1–2), pp. 160–168.

Hydrophobic tobramycin encapsulated in PLGA microparticles for pulmonary drug delivery

Karolina Knap[1], Gabriela Markowicz[1], Konrad Kwiecień[1], Anna Moskwik[1], Dorota Ochońska[2], Katarzyna Reczyńska-Kolman[1], Monika Brzychczy-Włoch[2], Elżbieta Pamuła[1]

[1] AGH University of Science and Technology, Faculty of Materials Science and Ceramics, Department of Biomaterials and Composites, Al. Mickiewicza 30, 30-059 Kraków, Poland
[2] Jagiellonian University Medical College, Faculty of Medicine, Chair of Microbiology, Department of Molecular Medical Microbiology, ul. Czysta 18 , 31-121 Kraków, Poland
kknap@agh.edu.pl

Aims

Pulmonary drug delivery has many advantages such as a large surface area, excellent lung vascularization, and high doses delivered directly to the infected site. The most widely used synthetic degradable polymer to manufacture drug carriers is poly(lactide-*co*-glycolide) (PLGA), however, due to its hydrophobic character it is not suitable to encapsulate hydrophilic drugs, e.g. tobramycin (Tob) [1]. Ernst et al. [2] tried to encapsulate Tob in PLGA microparticles (MPs). The results showed a relatively low encapsulation efficiency of around 3% and drug loading of about 0.15%. In our studies, we modified tobramycin to a hydrophobic form using dioctylsulfosuccinate (AOT) and encapsulated in PLGA MPs in different feed ratios (TobAOT:PLGA=1:10, TobAOT:PLGA=1:5, TobAOT:PLGA=1:3). The size, morphology, encapsulation efficiency (EE), drug loading (DL), cytotoxicity, and antibacterial activity of the MPs were characterized.

Methods

PLGA MPs loaded with TobAOT were manufactured using oil in water emulsification, where oil phase: PLGA and TobAOT were dissolved in dichloromethane, and water phase: poly(vinyl alcohol) was dissolved in water. The morphology and size of MPs were characterized by scanning electron microscope. The parameters of DL and EE were evaluated using an orto-pthaldialdehyd (OPA) assay. The cytotoxicity was evaluated by AlamarBlue assay and Live/Dead staining against BEAS-2B epithelial lung cells. The antibacterial activity was tested in contact with *Staphylococcus aureus* using the Kirby-Bauer method.

Results

We successfully obtained spherical MPs unloaded and loaded with TobAOT. The size, EE, DL, and bacterial zone inhibition are presented in Tab.1. The MPs are not cytotoxic in contact with BEAS-2B cells in low concentrations.

Tab.1. Size, EE, DL of MPs and inhibition zone of bacteria growth.

	Geometric diameter (μm)	EE (%)	DL (%)	Bacterial zone inhibition (mm)
PLGA unloaded	1.3 ± 0.5	-	-	0
TobAOT:PLGA=1:10	2.1 ± 0.9	19.1 ± 4.2	1.7 ± 0.3	0
TobAOT:PLGA=1:5	2.6 ± 1.3	15.1 ± 3.2	2.5 ± 0.4	9
TobAOT:PLGA=1:3	2.4 ± 1.4	95.0 ± 18.9	21.9 ± 3.6	28

Conclusion

MPs based on PLGA loaded with TobAOT seem to be promising carriers for pulmonary delivery for the treatment of bacterial respiratory lung infections. However, it is necessary to evaluate aerodynamic properties of MPs and perform more advanced *in vitro* studies in co-cultures of lung epithelial cells and alveolar macrophages.

Acknowledgments

References:

[1] K. Knap, K. Kwiecień, K. Reczyńska-Kolman, and E. Pamuła, "Inhalable microparticles as drug delivery systems to the lungs in a dry powder formulations," *Regen. Biomater.*, vol. 10, p. rbac099, Jan. 2023, doi: 10.1093/rb/rbac099.
[2] J. Ernst *et al.*, "Polyester-based particles to overcome the obstacles of mucus and biofilms in the lung for tobramycin application under static and dynamic fluidic conditions," *Eur. J. Pharm. Biopharm.*, vol. 131, pp. 120–129, Oct. 2018, doi: 10.1016/j.ejpb.2018.07.025.

Novel polyanhydrides as potential carriers of azithromycin to the lungs

Konrad Kwiecień[1*], Karolina Knap[1], Dorota Ochońska[2], Joanna Płonka[3], Daria Niewolik[4], Iwona Pudełko[1], Alicja Kazek-Kęsik[3], Katarzyna Reczyńska-Kolman[1], Monika Brzychczy-Włoch[2], Katarzyna Jaszcz[4], Elżbieta Pamuła[1].

[1]Department of Biomaterials and Composites, Faculty of Materials Science and Ceramics, AGH University of Science and Technology, Al. Mickiewicza 30, 30-059 Kraków, Poland
[2]Department of Molecular Medical Microbiology, Chair of Microbiology, Faculty of Medicine, Jagiellonian University Medical College, 18 Czysta Street, 31-121 Kraków, Poland
[3]Silesian University of Technology, Faculty of Chemistry, Department of Inorganic Chemistry, Analytical Chemistry and Electrochemistry, ul. Krzywoustego 6, Gliwice 44-100, Poland
[4]Silesian University of Technology, Faculty of Chemistry, Department of Physical Chemistry and Technology of Polymers, ul. M. Strzody 9, 44-100 Gliwice, Poland
*kkwiecien@agh.edu.pl

Systemic administration of antibiotics has a limited use in the treatment of lung bacterial infections, as there is limited bioavailability of the drug in alveoli. Therefore, inhalable formulations are designed to deliver drugs directly to the lungs, in the form of, e.g., dry powders [1]. Several polymers are considered for this purpose. Among others, copolymers of poly(sebacic anhydride) (PSA) and poly(ethylene glycol) (PEG), namely (PSA-PEG)s are considered thanks to the fast degradation rate. This study aimed to develop a powder from PSA-PEG microparticles (MPs) loaded with a macrolide antibiotic azithromycin (AZ), and to characterize its physicochemical, aerodynamic, and biological properties.

Copolymers of PSA and two PEGs of different molar mass (250 and 600 Da, respectively), namely: PSA-PEG250 and PSA-PEG600 were synthesized by polycondensation. Then, MPs were manufactured using solid-in-oil-in-water emulsification, freeze-dried and investigated with optical microscopy and scanning electron microscopy (SEM) to assess their morphology and size ditribution, and zeta potential measurement to evaluate the surface charge. AZ loading efficiency was assessed by HPLC measurements of supernatants after the manufacturing process. Carr's index (IC), Hausner ratio (HR), and median aerodynamic diameters were calculated based on tapped and untapped densities as indicators of flowability and aerodynamic properties estimation. To assess the cytocompatibility of the powders, in vitro test on A549 and BEAS-2B human lung epithelial cells after 24 hours incubation with MPs dispersed in culture medium. The antibacterial properties were evaluated by Kirby-Bauer test against *Staphylococcus aureus*.

The manufactured MPs were spherical and of regular shape. Particle size measurement showed that the most of MPs have diameters smaller than 5 μm. The powders showed low tapped densities which resulted in even smaller aerodynamic and also the assessed IC and HR values indicated fair to good flowability that was better for a higher drug loading. We assume that the encapsulation efficiency was nearly 100%, as no trace of AZ was detected by the HPLC. The zeta potential of the MPs was negative and the charge was partly reduced in with the higher AZ content. No cytotoxic effect was noticed in *in vitro* tests at the concentration up to 100 μg/ml. Kirby-Bauer tests showed increasing bactericidal effects with increasing concentration. For the highest drug loading, the inhibitory action was observed for 50 μg/ml.

In this study, we described the use MPs-based powders from novel polyanhydrides and their potential for the pulmonary delivery of antibiotics. Physicochemical, aerodynamic, and biological evaluation showed that the chosen formulations are promising to be used as inhalable drug delivery systems in the future. However, further research in terms of aerodynamic properties as well as *in vivo* toxicity and efficacy have to be tested.

References:
[1] A. K. Thakur, D. K. Chellappan, K. Dua, M. Mehta, S. Satija, and I. Singh, "Patented therapeutic drug delivery strategies for targeting pulmonary diseases," Expert Opin. Ther. Pat., vol. 30, no. 5, pp. 375–387, 2020.

Microcarrier-based delivery systems of the drugs with enhanced bioavailability, targetability and stimulus triggered release

Elżbieta Pamuła

AGH University of Krakow, Faculty of Materials Science and Ceramics,
Department of Biomaterials and Composites, Al. Mickiewicza 30, 30-059 Kraków, Poland
*epamula@agh.edu.pl

Drug delivery systems (DDSs) are engineered devices designed for the targeted transfer and/or controlled release of biologically active molecules to the required site of action in the body. In most cases, the drug is encapsulated within a biocompatible shell, providing protection against degradation and loss of activity. Different biomaterials, for example natural or synthetic polymers, lipids, metals, or metal oxides, can be used to produce carriers in DDSs. The main advantages of DDSs include improved bioavailability, prolonged drug circulation, control over drug release kinetics, and a reduced risk of severe side effects. Another benefit of DDSs is related to the cost effectiveness of the development of the formulations based on already existing drugs compared to the development of entirely new active pharmaceutical ingredients (APIs).

In our group, we are working on lipid and polymer microparticles to be used as inhalable dry powder formulations [1]. So far we have developed innovative, inhalable stimuli-sensitive drug carriers that are intended to improve the efficacy of lung cancer therapy through guided accumulation directly at the tumour site and controlled drug delivery triggered by an alternating magnetic field resulting in a local increase in temperature [2]. Such drug delivery carriers are in the form of solid lipid microparticles composed of fatty acids loaded with superparamagnetic iron oxide nanoparticles and paclitaxel. The microparticles fulfil various criteria including appropriate aerodynamic properties, melting temperature suitable for hyperthermia conditions, high drug loading efficiency, sufficient mobility in the magnetic field, and enhanced *in vitro* efficacy as studied in contact with healthy and cancerous lung epithelial cells in hyperthermia conditions.

Recently we are working on polymer drug delivery systems of antibiotics and quorum sensing inhibitors for the treatment of bacterial infections in patients with chronic obstructive pulmonary disease (COPD) exacerbations [3]. Such systems are based on fast-degrading polyanhydride microparticles /microcapsules loaded with antibiotics (e.g., gentamycin, tobramycin, azithromycin) and quorum-sensing inhibitors (e.g., curcumin, linolenic acid). The microparticles are designed to ensure an appropriate size for inhalation, degrade within a few days, and release drug cargo, which is capable of killing bacteria causing COPD and prevent biofilm formation. The system is cytocompatible with lung epithelial cells, as shown by *in vitro* tests.

References:
[1] K. Knap, K. Kwiecień, K. Reczyńska-Kolman, and E. Pamuła, "Inhalable microparticles as drug delivery systems to the lungs in a dry powder formulations," *Regen. Biomater.*, vol. 10, p. rbac099, Jan. 2023, doi: 10.1093/rb/rbac099.
[3] K. Reczyńska, M. Marszałek, A. Zarzycki, W. Reczyński, K. Kornaus, E. Pamuła, W. Chrzanowski, Superparamagnetic iron oxide nanoparticles modified with silica layers as potential agents for lung cancer treatment, *Nanomaterials*, 2020, 10(6), art. no. 1076, 1–16. DOI: 10.3390/nano10061076
[3] K. Kwiecień, K. Reczyńska-Kolman, D. Niewolik, K. Jaszcz, E. Pamuła, Poly(sebacic anhydride) microparticles loaded with curcumin for pulmonary purposes, Engineering of Biomaterials, 2021, 162, 7-12, doi:10.34821/eng.biomat.162.2021.7-12

3D Bioprinting with Porcine Extracellular Matrix: Future of Meniscus Injuries Treatment

Filip Porzucek1, Julia Semba1,2, Monika Mankowska1, Adam Mieloch1, Anna Mleczko1, Adam Augustyniak1, Piotr Cywoniuk1, Tomasz Szymański1,3, Jakub Dalibor Rybka1*
[1] Center for Advanced Technology, Adam Mickiewicz University, Poznan, Poland
[2] Faculty of Biology, Adam Mickiewicz University, Poznan, Poland
[3] Faculty of Chemistry, Adam Mickiewicz University, Poznan, Poland
*jrybka@amu.edu.pl

Aims

In the knee, the meniscus is essential for articular surface protection, shock absorption, and stress transmission. In the general population, it causes injuries at a rate of 0.7 per 1000 individuals [1]. The meniscus's potential to regenerate is restricted to the outer, vascularized zone due while the inner zone lack helaing potential. Existing treatment options are insufficient, thus novel alternatives that mimic the physiological characteristics of the meniscus are explored [2].

In this study, we present an innovative method to manufacture bioink from porcine menisci (decellularize extracellular matrix - dECM), that is designed specifically for 3D bioprinting of meniscal implants. ECM is a heterogeneous connective network that provides mechanical stability and contains biochemical cues required for tissue development and homeostasis. Recent research has shown that ECM-based scaffolds may function as an inductive template for repair and functional reconstruction, foster tissue-specific remodeling, and create a favorable regenerative environment [3]. However to avoid an immune response, adequate ECM treatment is necessary.

Methods

The three crucial steps for ECM extraction were: the extraction of water- and acid-soluble ECM components, protein digestion, and final decellularization, which combined DNase treatment and extraction in $scCO_2$. The acquired dECM underwent DNA, GAG, and collagen content analysis, as well as microbiological investigation. The rheological characteristics were tested followed by SEM imaging and printing accuracy measurements. Human adipose-derived mesenchymal stem cells (hMSC-AT) were mixed with bioink and 3D bioprinted into constructs for the biological study. Based on cell viability and morphological analysis using the LIVE/DEAD assay at four time intervals (1, 10, 20, and 30 days), the biocompatibility of the produced bioinks was evaluated.

Results

GAGs and collagen content were greatly maintained during the dECM extraction process, yet the DNA content gradually decreased. By changing the pH, gelation of the dECM was induced in room temperature. The printing accuracy was good. Gealtine and cellulose nanocrystals were added to improve the stiffness, which also produced larger channels and more porosity. Only a few dead cells were seen throughout the course of the 30 days following 3D bioprinting with hMSC-AT, showing high bioink biocompatibility. The presence of spindle-shaped cells and visible cell elongation, which point to hMSC-AT differentiation toward chorndocytes, were observed.

Conclusion

The purpose of this research was to provide a reproducible method for extracting porcine meniscal ECM while maintaining its biocompatibility and native features. It also aimed to provide a stimulating environment for cell proliferation and differentiation toward a meniscus-like phenotype. This work presents a comprehensive rheological and biological evaluation along with a complete description of dECM manufacturing and formulation into bioink for meniscus tissue engineering.

References:

[1] Logerstedt, D. S. et al. Knee pain and mobility impairments: Meniscal and articular cartilage lesions Revision 2018. J. Orthop. Sport. Phys. Ther. 48, A1–A50 (2018).
[2] Doral, M. N., Bilge, O., Huri, G., Turhan, E. & Verdonk, R. Modern treatment of meniscal tears. *EFORT Open Rev.* 3, 260–268 (2018).
[3] Yi, S., Ding, F., Gong, L. & Gu, X. Extracellular Matrix Scaffolds for Tissue Engineering and Regenerative Medicine. *Curr. Stem Cell Res. Ther.* 12, 233–246 (2017).

Alginate-based composites as versatile biomaterials for biomedical applications

Pawel Sikorski

Department of Physics, Norwegian University of Science and Technology, NTNU, Trondheim, Norway.

Abstract

Composites based on biopolymers such as alginate and mineral phases such as calcium phosphate or calcium carbonate have gained significant attention in the field of biomaterials. These composites can be easily formed using chemical or enzymatic mineralization and are investigated as scaffolds, in cell encapsulation applications, for 3D printing, drug delivery and more. The presence of the biopolymer component, particularly alginate, significantly influences the crystallization of calcium phosphate (CaP) within these materials. Alginate, known for its calcium binding properties, affects both the nucleation and crystal growth processes during composite formation, as well as the formation and transformation of amorphous CaP phases. Therefore, the study of crystallization phenomena is important in understanding the behavior and characteristics of these composites. I will highlights the potential applications and advantages of biopolymer-CaP composites and describe how the interplay between biopolymers, small molecule additives, calcium and phosphate ions can be used to manipulate the properties of alginate gels and hydrogel-based composites. This includes novel strategies to form hydrogels, control hydrogel dissolution and developing methods to study mineralization, and also drug and ion delivery strategies using these types of materials. By understanding these mechanisms, we are able to unlock new possibilities for tailoring the properties and behavior of biopolymer-based composites for biomaterials science applications.

References:
[1] Competitive ligand exchange of crosslinking ions for ionotropic hydrogel formation DC Bassett, AG Håti, TB Melø, BT Stokke, P SikorskiJournal of Materials Chemistry B, 2016, 4, 6175-6182
[2] Stabilisation of amorphous calcium phosphate in polyethylene glycol hydrogels. M Schweikle, SH Bjørnøy, ATJ van Helvoort, HJ Haugen, P Sikorski, Hanna Tiainen. Acta biomaterialia 2019, 90, 132-145
[3] Formation of hydroxyapatite via transformation of amorphous calcium phosphate in the presence of alginate additives S Ucar, SH Bjørnøy, DC Bassett, BL Strand, P Sikorski, JP Andreassen. Crystal Growth & Design, 2019, 19, 7077-7087

The release of Salicin from the membranes based on the blend of chitosan and hyaluronic acid

Alina Sionkowska, Katarzyna Lewandowska, Marzanna Kurzawa
Nicolaus Copernicus University in Toruń
Faculty of Chemistry
Gagarin 7, 87-100 Toruń, Poland
alinas@umk.pl

Salicin (2-(hydroxymethyl)phenyl; β-d-glucopyranoside) is a compound which can be found in willow bark and leaves. The willow bark extract has anti-inflammatory and antiseptic properties [1,2]. Polymers and biopolymers have played an integral role in the advancement of active substance delivery technology by providing a controlled release of active agents in constant doses over desired periods [3]. Still, there is a need for the preparation of new drug delivery systems for active substances crucial in biomedical and cosmetic applications.

In this work, the membranes based on the blends of chitosan, and hyaluronic acid with salicin as active agents were obtained by solution casting method. The membranes have been characterized using FTIR spectroscopy and the surface was observed using optical and AFM microscopy. The released salicin concentration was detected by the HPLC method after different period of time. The release was studied in pH 5.5 which is related to the pH of the human skin.

The profile of the release of salicin has been shown in Fig. 1. As it can be seen, after 15 min the release of the salicin reached the maximum.
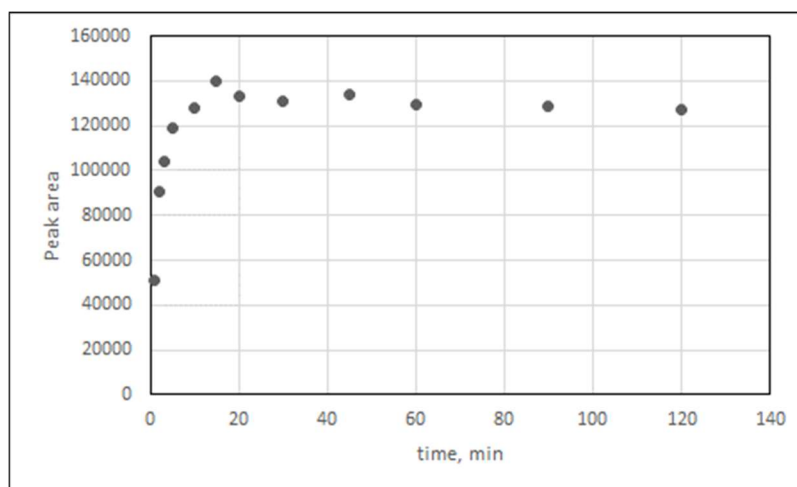
Fig. 1. The profile of salicin release

Our results showed that the release of salicin from the membranes based on the blends of chitosan, and hyaluronic acid is sufficient for applications in cosmetic beauty masks and wound healing materials.

References:
[1] Gopaul, R.; Knaggs, H.; Lephart, J.; Holley, K.; Gibson, E. Original Contribution: An evaluation of the effect of a topical product containing salicin on the visible signs of human skin aging. J. Cosmet. Dermatol. **2010**, 9, 196–291
[2] Shakibaei, M.; Allaway, D.; Nebrich, S.; Mobasheri, A. Botanical Extracts from Rosehip (Rosa canina), Willow Bark (Salix alba), and Nettle Leaf (Urtica dioica) Suppress IL-1β-Induced NF-κB Activation in Canine Articular Chondrocytes. Evid. Based Complement. Altern. Med. **2012**, 2012, 1–16.
[3] Sionkowska, A. Current Research on the Blends of Natural and Synthetic Polymers as New Biomaterials: Review. Prog. Polym. Sci. **2011**, 36, 1254–1276.

Capsaicin-loaded microdroplets for alleviating the symptoms of burning mouth syndrome

Daria Zaytseva-Zotova[1], Lea Lecomte[1], Nadin Elkafas[1], Frozan Haideri[1], Alejandro Barrantes[1],
P. Bano Singh[2], Hanna Tiainen[1]
[1]University of Oslo, Norway, [2]Polytech Nantes, France
hanna.tiainen@odont.uio.no

INTRODUCTION: Burning mouth syndrome (BMS) is a chronic intraoral burning sensation, which develops without any oral mucosa injury. BMS affects approximately 3.7% of the normal population and is considered as a nociplastic pain caused by an altered activity of the peripheral nociceptors [1-2]. Capsaicin (CAP), an alkaloid found in chili peppers, is an agonist of TRPV1 receptors involved in BMS pathogenesis. Although CAP is a well-recognised topical analgesic and is currently used to treat BMS, efficacy of its formulations in the oral cavity is limited since CAP quickly washes out by the flow of saliva and tongue movements. Therefore, novel strategies for CAP delivery in the oral cavity should be investigated. The aim of this study was to develop and characterise a novel CAP delivery system with mucoadhesive properties and evaluate its cytotoxicity *in vitro*.

METHODS: The CAP delivery system was generated by Pickering emulsion technique. CAP (Sigma-Aldrich) was dissolved in a food-grade rapeseed oil and mixed with $CaCO_3$ nanoparticles (~0.8 μm [3]) dispersed in water (or buffer). The mixture was sonicated (60 sec), manually shaken (30 sec) and then left on a rotary shaker to mature at 4 °C for 1 h. Various oil:water:$CaCO_3$ ratios were tested. The obtained microdroplets were coated with alginate (100-300 cP, Sigma-Aldrich) by mixing the emulsion with 0.5-4% (w/v) alginate solution in 1:1 ratio. Phosphomolybdic acid assay was used to characterise CAP encapsulation efficacy, while combination of FTIR spectroscopy and SEM imaging was used to assess phase stability of $CaCO_3$ nanoparticles. Primary human gingival fibroblasts (hGF; ATCC) and keratinocytes (hGK; ATCC) were exposed to various concentrations of the freshly prepared microdroplets. Acute cytotoxicity, cell metabolic activity and cell morphology were evaluated after 24 hours using LDH assay, resazurin assay and confocal microscopy (phalloidin/DAPI).

RESULTS: Oil, water and $CaCO_3$ particles were mixed at various ratios to determine optimal conditions at which oil microdroplets can be formed. Spherically shaped oil droplets were obtained at oil volume fractions $\varphi \leq 0.4$, and that ≥ 250 mg of $CaCO_3$ particles per 1 ml of oil was needed to stabilise the droplets. Size of the droplet correlated with φ, with high φ yielding larger particles. The resulting droplets were not stable during storage in aqueous environment since the vaterite $CaCO_3$ nanoparticles slowly underwent polymorphic transformation to larger calcite particles. This compromised the stability of the oil droplets. Coating the microdroplets with alginate immediately after emulsification improved droplets stability in water and increase their lifetime > 1 month. Next, microdroplets loaded with high concentrations of CAP (37.5 mM) were prepared. Encapsulation efficacy was found to be 97.9%. Neither blank nor CAP-loaded microdroplets exhibited cytotoxic effects in either hGF or hGK.

CONCLUSION: Taken together, our preliminary experiments show that the suggested encapsulation strategy allows fabrication of stable microdroplets containing high concentrations of CAP. Further studies are required to fully optimise and characterise the developed CAP-delivery system and its mucoadhesive potential.

REFERENCES:
[1] Y.F. Liu et al., *Oral Dis*, 2018, 24, 325-334.
[2] V.I. Madariaga, *J Oral Rehabil*, 2020, 47, 1590-1605.
[3] D.B. Trushina et al., *Cryst Growth Des*, 2016, 16, 1311-1319.

Chapter V

Biomodelling and Machine Learning in Cancer Diagnosis and Prediction of Metastases

Session organizers:

Prof. Andrzej Świerniak, Silesian University of Technology
Prof. Krzysztof Fujarewicz, Silesian University of Technology

Time delays in a model of CAR-T therapy for glioblastoma

Urszula Foryś, Magdalena Szafrańska

Institute of Applied Mathematics & Mechanics, University of Warsaw, Banacha 2, 02-092 Warsaw, Poland

urszula@mimuw.edu.pl

Chimeric Antigen Receptor T (CAR-T) cell therapy occurred successful against some leukaemias and lymphomas. This was the motivation for clinical trials using this therapy in other cancers, for example in glioblastoma, which is a type of primary brain tumor. As this tumor is highly aggressive and located in a very sensitive organ, the researchers still try to find a therapy that will allow for cure or at least extends the patient's life. To get better insight how the CAR-T therapy should be applied in solid tumors (like glioblastoma), in [1] two mathematical models of this therapy were proposed. Simpler model is two-dimensional and describes the interactions of tumor cells and CAR-T cells. Next, the authors of [1] described so-called "dual CART-T cells model" with two localizations of CAR-T cells: at the tumor site and outside. This model is four-dimensional and after a systematic study of both models the authors concluded that the dual model gives more chances for the therapy to be successful. In [2], more deep mathematical analysis of the simpler model is presented.

It is obvious that simple two-dimensional model could be considered as an oversimplification. On the other hand, four-dimensional model has very similar qualitative dynamics and the main differences are quantitative. Our main idea was to propose a bridge between the two models introducing time delay into the term describing stimulation of CAR-T cells in the presence of cancer cells in the simpler model.

We studied the model dynamics with respect to increasing delay, first analyzing the case when only one initial portion of CAR-T cells is applied, through the constant treatment (as the first approximation as it is simpler from the point of view of mathematical analysis), ending with the impulsive treatment, as it was done in [2].

We hope that the results obtained by us can be useful in further considerations related to CAR-T cells treatment in solid tumors, especially in glioblastoma, which is our main interest throughout this research project.

References:
[1] León-Triana O., Perez-Martinez A., Ramirez-Orellana M. and Perez-Garcia V. Dual-target CAR-Ts with on- and off-tumour activity may override immune suppression in solid cancers: A mathematical proof of concept, *Cancers,* 2021, 13(4).
[2] Bodnar M., Foryś U., Piotrowska M.J., Bodzioch M., Romero-Rosales J.A., and Belmonte-Beitia J. On the analysis of a mathematical model of CAR-T cells therapy for glioblastoma: insight from a mathematical model, *Int. J. Appl. Math. Comput. Sci.*, 2023, to appear.

Harnessing artificial intelligence for the prediction of lung cancer survival, based on integrated multiomic data

Roman Jaksik, Jarosław Śmieja
Silesian University of Technology, Akademicka 2A, 44-100 Gliwice
roman.jaksik@polsl.pl

Lung cancer is responsible for the highest number of cancer-related deaths, which is primarily attributed to the ineffectiveness of screening programs and the late emergence of symptoms, typically associated with advanced stages of the disease. The considerable heterogeneity of lung cancer has often been linked to its molecular characteristics, opening up opportunities to employ machine learning techniques for aiding in diagnosis and the development of personalized treatments.

The main difficulty in a successful application of machine learning methods for survival prediction is the extraction of features from raw data and selection of those which have the predictive potential. Features from various datasets can be incompatible or contain in-complete data, leading to inconsistent conclusions about the quality of the methods developed. This is especially evident in studies that involve multiple -omic datasets, with a goal to combine information obtained using various measurement techniques [1]. Additionally some of the features are too specific, being observable only in individual patients e.g. somatic mutations, which leads to a sparse predictor matrix that contains mostly zeros.

The main goal of this study is to identify which -omics dataset or combination of them, provide the most relevant information for the prognosis of lung cancer survival. Secondary goal is to determine the best feature aggregation strategy for the -omics datasets that are characterized by a sparse predictor matrix.

To achieve both goals, we utilized multiple datasets encompassing various omics data to evaluate their potential for predicting the 2-year survival of lung adenocarcinoma. By incorporating clinical and molecular data from lung cancer patients, we developed several classifiers based on mRNA and microRNA expression levels, somatic mutation positions, changes in DNA copy number, DNA methylation levels and additional features that are based on occurrence frequencies of specific alteration types. Additionally, we explored different techniques for data aggregation and feature selection, assessing their impact on classification accuracy.

The findings of our research not only demonstrate the effective utilization of molecular data in predicting 2-year survival in lung adenocarcinoma (AUC=0.85), but also reveal that information pertaining to gene expression changes, methylation patterns, and mutations offers superior predictive capabilities compared to copy number alterations and data derived from microRNA studies. Furthermore, we investigated the performance of various dimensionality reduction methods on the challenging copy number variation dataset, ultimately concluding that aggregating genes and gene sets yields the most favorable classification results.

References:
[1] Gao, Y., Zhou, R., Lyu, Q.: Multiomics and machine learning in lung cancer prognosis. *Journal of thoracic disease* 12, 4531-4535 (2020),

Parameters estimation of a mathematical model for the metastasis process

Krzysztof Łakomiec, Emilia Kozłowska, Agata Wilk, Krzysztof Fujarewicz
Silesian University of Technology, ul. Akademicka 2A, 44-100 Gliwice
Krzysztof.lakomiec@polsl.pl

Aims

The time of metastasis, i.e., the appearance of secondary tumors in cancer disease is an important prognostic factor. It can be used to assess the prognosis of the disease and the overall survival of the patient. Being able to predict this time using clinical data could help guide the physician to select the appropriate cancer therapy for a given case. To predict the time of metastasis, one can use mathematical modelling. The main effort arising in this case consists on finding (estimation) the values of the model parameters. The objective of this work has been estimation of parameters of a developed mathematical model for the cancer metastasis process using clinical data obtained from the National Institute of Oncology in Gliwice (NIO).

Methods

Analyzed in this work mathematical model of the metastasis process is composed of three ordinary differential equations. To find values of the model parameters, a gradient minimization of the quadratic objective function was used. Gradient of the objective function with respect to estimated parameters was calculated using adjoint sensitivity analysis method, which was successfully used in our previous work [1]. Objective function defined in our work compares the size of the simulated secondary tumor and the assumed size of detectable tumor. In our analysis we assumed that detectable tumor needs to have a volume equal to 1.77 cm^3. The estimation process was performed using clinical data acquired from NIO containing times of detection the secondary tumors for 37 patients.

Results

Simulation of the model using estimated parameters shows a large discrepancy between growth of the primary and secondary tumors. Additionally, using analyzed model with estimated parameters we can predict when the secondary tumor can be detectable in each patient (see Figure 1).
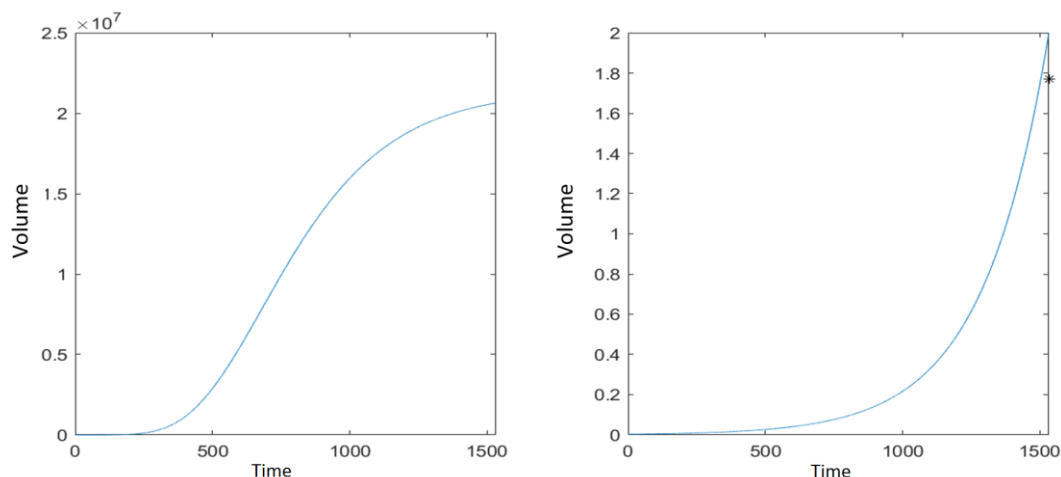
Figure 1. Simulation of the analyzed model for one patient using estimated parameters; left - simulation of the primary tumor, right - simulation of the secondary tumor

Conclusions

The obtained in this work results can be used to further study the effect of clinical data on metastasis process. In our future works we plan to build a so-called hybrid mathematical model of metastasis where some of the model parameters will be a function of clinical data.

References:
[1] K Łakomiec, S Kumala, R Hancock, J Rzeszowska-Wolny, K Fujarewicz, Modeling the repair of DNA strand breaks caused by γ-radiation in a minichromosome, Physical biology 11 (4), 2014, 045003

Chapter VI

Electromagnetics in Biology and Medicine

Session organizer:

Prof. Sławomir Hausman, Lodz University of Technology

Influence of radiofrequency electromagnetic fields on health and electrosensitivity in the clinical practice of Polish physicians

Gabriela Kanclerz, Jakub Popielak, Kamila Undas, Grzegorz Tatoń
Jagiellonian University Medical College, Chair of Physiology, Department of Biophysics
Email of the corresponding author: zelazny.kanclerz@student.uj.edu.pl

The exact influence of non-ionizing electromagnetic fields (EF) on health is not determined yet; only the thermal effects on tissues had been confirmed. [1] In the literature, there are many reports about people who complain about the negative effects of these fields on their health. Because radiofrequency EF is emitted by most electronic devices, these symptoms are often persistent and difficult to avoid. In some countries, the presence of mentioned symptoms, called electrosensitivity, is treated as impairment or disability. The prevalence of electrosensitivity symptoms has often been investigated by means of surveys among physicians. There are no studies available to check the prevalence of this phenomenon in Poland.

In this study, an 18-question survey consisting of questions about demographic data, clinical specialty and internship, as well as experience with patients complaining of negative symptoms associated with non-ionizing EF, was distributed among physicians. The goal was not only to investigate the prevalence of symptoms of exposure to EF, but also to define the exact symptoms and devices that caused them. Physicians were also asked whether, in their opinion, nationwide information campaigns on the influence of EF on health are needed and if they would like to participate in training on this topic themselves. The questionnaires were distributed in two ways: on paper and in electronic form.

So far a total of 171 questionnaires have been collected, 118 of them in paper form. There was no significant difference between the answers collected on the paper and on-line. The mean age of the responders was 33 ± 6 years and 102 (59.65%) of them were women. The respondents were specialized in 34 different fields, most often in internal medicine (37, 23.42%), endocrinology, and neurology (17, 10.76%). Most of them (112, 65.50%) admitted patients mainly in large cities, more than 500 thousands of citizens. Almost half (73, 42.69%) of the physicians asked declare that they admit patients who suffer from the negative impact of EF on health, in most cases patients with those symptoms account for less than 1% of all patients (55, 75.34%). 57 (33.33%) of physicians admit patients whose main reason for a doctor's visit are negative symptoms of exposure to EF and 55 (32.16%) consult patients with significant difficulty in daily life caused by these symptoms. Most of them (50, 68.49%) meet such patients less than once a year, but the rest claim that this occurs more often, even a couple times a month (7, 9.57%). When comparing the group of physicians who admit patients with negative symptoms of exposure to non-ionizing EF and the rest of the responders, the physicians in the first group were more likely to be a professor (8.22% vs 0.58%), have a Ph.D. (23.29% vs 8.19%) or more than one specialization (24.66% vs 7.02%), as well as completed medical specialty (58.90% vs 23.39%). The most common symptoms of exposure to non-ionizing EF in clinician practice are headache (54, 73.97%), fatigue (29, 39.73%) and difficulty in concentration (28, 38.36%). The most common devices pointed as harmful were: cell phone (49, 67.12%), cell phone base station, and Wi-Fi router (both 19, 26.03%). Only slightly above one-third of the respondents (68, 39.77%) declare that they have sufficient knowledge about the impact of EF on health. Less than half of them (77, 45.03%) believe that radiofrequency EF with an intensity that meets generally accepted standards does not have a negative impact on health. Almost half of the respondents (83, 48.54%) believe that symptoms attributed to the impact of EF have a psychosomatic background. The vast majority of respondents (121, 70.76%) believe that national information campaigns regarding the influence of EF on health should be implemented and most of them (97, 56.73%) would like to attend a seminar on this topic.

The research presented is the first to try to determine the Polish physicians experiences with electrosensitive patients. As it turns out, the phenomenon is present in everyday clinical practice of almost half of Polish physicians, and therefore, it should be better investigated.

References:
[1] Saliev T., Begimbetova D., Masoud AR., Matkarimov B. *Biological effects of non-ionizing electromagnetic fields: Two sides of a coin,* Progress in Biophysics and Molecular Biology, 2019, vol. 141, pp. 25-36.

Prevalence of Electromagnetic Hypersensitivity in Poland in 2022

Grzegorz Tatoń, Artur Kacprzyk, Rafał Pawlak, Tomasz Rok

Department of Biophysics, Faculty od Medicine, Jagiellonian University Medical College, Św. Łazarza 16, 31-530 Kraków

g.taton@uj.edu.pl

One of the problems associated with the development of modern technologies, especially wireless communication, is that there are a certain number of people in every society who believe that the development of such technologies adversely affects their health. These beliefs most often result from the fear of adverse effects of electromagnetic field (EMF) generated by electrotechnical devices. The phenomenon in which some people perceive themselves as particularly sensitive to the adverse effects of EMF is called electromagnetic hypersensitivity, electrosensitivity (EHS), and, most correctly according to the recommendations of the World Health Organisation, idiopathic environmental intolerance attributed to electromagnetic fields (IEI-EHS).

In many countries, studies of EHS are carried out mainly to estimate the number of vulnerable people in the context of determining methods of dealing with this phenomenon. Such estimates were not carried out in our country until 2018. In 2018 and 2020, we conducted the first studies of this kind [1,2], and they were repeated last year in twelve selected cities in Poland.

The study was conducted as a CATI (computer assisted telephone interview) survey. It was attended by 2200 people living in Białystok, Kielce, Kraków, Lublin, Łódź, Opole, Poznań, Rzeszów, Tarnów, Warsaw, Wałbrzych and Wrocław.

The questionnaire consisted of three questions that define the characteristics of the respondent (age, gender, education) and ten questions to determine whether he or she feels sensitive to EMF. They also examined symptoms associated with deterioration of well-being, the type of devices associated with them, and possible sensitivity to other factors.

The most important result obtained is the upper limit of the prevalence of EHS in the population studied. It was estimated at 1.6%. Interesting results were also obtained by analysing the frequency of sensitivity to environmental factors other than EMF, such as noise or environmental pollution, and by analysing the prevalence of sensitivity to some selected allergens. It turns out that people who perceive themselves as EHS are significantly more likely to also be sensitive to other environmental factors and allergens. The same conclusion was reached in the previous studies.

The devices most frequently indicated to negatively affect the well-being of the respondents were: mobile phone (35.2%), TV set (13.9%) and computer (13.2%). The most commonly indicated EMF-related symptoms are headache (63.0%), fatigue (14.8%) and irritability (9.9%).

The prevalence of EMF decreased significantly compared to the previous study from 2020 [1,2] (1.6% versus 1.9% respectively, $p < 0.05$). However, this change may be due to differences in the populations studied and not due to a real decrement. The population representative for the entire Polish society was studied in 2020, while last year's survey included only the residents of selected cities.

In the latest study, as in the previous one, the mobile phone was the device most frequently associated with symptoms of EHS, and the most frequently indicated symptom was headache.

The prevalence of EHS assessed in our studies is at the same level as that observed in other countries.

[1] Tatoń G, Kacprzyk A, Rok T, Wasik A, Siwek M, Is the hypersensitivity to electromagnetic fields caused by a physical mechanism or is it a psychological problem? Przegląd elektrotechniczny, 2022, 99(1): 215-19

[2] Tatoń G, Kacprzyk A, Rok T, Pytlarz M, Pawlak R, Rokita E, A survey on electromagnetic hypersensitivity: the example from Poland, Electromagnetic Biology and Medicine, 2022, 41(1): 52-59

Chapter VII

Hybrid Analysis of Multimodal Medical Data

Session organizer:

Prof. Ewa Piętka, Silesian University of Technology

Analysis of physiological response during synchronization and pseudosynchronization tests using rhythmic auditory stimulation

Damian Kania[1], Patrycja Romaniszyn-Kania[2], Aleksandra Tuszy[2], Monika Bugdol[2], Mirosław Czak[2], Bruce Turner[3], Karol Bibrowicz[4], Tomasz Szurmik[5], Andrzej W. Mitas[2]

[1] Institute of Physiotherapy and Health Sciences, The Jerzy Kukuczka Academy of Physical Education in Katowice, Mikołowska 72A, 40-065 Katowice, Poland
[2] Faculty of Biomedical Engineering, Silesian University of Technology, Roosevelta 40, 41-800 Zabrze, Poland
[3] dBs Music, HE Music Faculty, 17 St Thomas St, Redcliffe, Bristol, BS1 6JS, UK
[4] Science and Research Center of Body Posture, College of Education and Therapy in Poznań, 61-473 Poznań, Poland
[5] Faculty of Arts and Educational Science, University of Silesia, ul. Bielska 62, 43-400, Cieszyn, Poland
Corresponding Author: aleksandra.tuszy@gmail.com

Sensorimotor synchronization (SMS) is coordinating rhythmic movements with external rhythm. One musical ability with a neural basis is beat perception and synchronization (BPS), defined as the ability to perceive the rhythm in music and synchronize body movements with it [1,2]. Pseudosynchronization, on the other hand, occurs when participants believe they are synchronizing to an externally controlled rhythm but, in fact, control ("produce") the tones with their own tapping. In other words, the tones provide auditory feedback on the taps, particularly on their tempo and variability [3].

Aims: The present study aimed to examine synchronization errors as a response of test subjects to a metrorhythmic stimuli in the context of synchronous and pseudosynchronous stimulation.

Methods: 19 healthy subjects participated in the study. The research protocol consisted of two parts. In both cases, the research's essence was the measurement of synchronization errors and physiological response in the form of recorded EMG signals from the upper and lower limbs, respectively. At the beginning of the conducted experiments, the subjects were asked to fill out a music preference questionnaire (MPQ) on music education and involvement in music-related activities. During study 1, the subjects performed an adaptation of the finger tapping test (FTT), which involves rhythmically tapping the index finger of the dominant hand on a single, well-defined key of a keyboard, in such a way as to synchronize with the metrorhythmic stimulus being asked (pseudosynchronization), for one minute. The following elements of the research protocol were Study 2, during which the subject's task was to try to synchronize heel taps on the ground with the rhythm of the metrorhythmic stimulus being set, at a predefined and personalized pace, i.e., to perform the so-called heel stomping test (HST). Tests were performed three times - (1) with the preferred pacing frequency, (2) accelerated by 5%, and (3) slowed by 5% relative to baseline pacing.

Results: Based on the analysis, statistically significant differences ($p<0.05$) were shown in EMG signal parameters, depending on musical education, musical and sports activity, both during the synchronization and pseudosynchronization test with the metrorhythmic stimulus. Correlations of EMG signal parameters with synchronization errors and metrorhythmic stimulus rate were also analyzed. Positive and negative correlations were shown for individual muscle groups in successive trials, depending on the set rate. For both FTT and HST, the correlated parameters were repeated. It was also proven that the mentioned three differential variables affect the values of synchronization errors only in the HST trial.

Conclusion: Based on the literature analysis and the authors' best knowledge, there are no similar scientific reports on errors of synchronization and pseudosynchronization in FTT and HST tests using metrorhythmic stimuli of different tempos. The obtained results allowed us to conclude the relevance of music in human life. It is not so much the musical education that is important during synchronization tests but the musical activity of the individual itself. The presented research results will be reflected in further research work and in developing a system to support the rehabilitation of people with motor dysfunctions.

References:
[1] Nettl B. An Ethnomusicologist Contemplates Universals in Musical Sound and Musical Culture. *The origins of music*, 2000, pp. 463-472
[2] McNeill W. H. Keeping together in time: Dance and drill in human history. *Harvard University Press*, 1997
[3] Flach R. The transition from synchronization to continuation tapping. *Human Movement Science*, 2005, vol. 24, no. 4, pp. 465-483

NLP Methods Applied in Computer-Aided Diagnostics of Body Image in Head and Neck Cancer

Stella Maćkowska[1], Klaudia Barańska[1], Agnieszka Różańska[1], Elwira Gliwska[2], Dominik Spinczyk[1]

[1]Department of Medical Informatics and Artificial Intelligence, Silesian University of Technology, Roosevelta 40, 41-800 Zabrze, Poland

[2]Cancer Epidemiology and Primary Prevention Department, M. Sklodowska-Curie National Research Institute of Oncology, 02-781 Warsaw, Poland

stella.mackowska@polsl.pl

Cancer is one of the leading causes of death worldwide. Head and neck cancers are often treated with medical interventions that affect appearance and may interfere with patients' self-perception of their own bodies [1]. Due to the invasive nature of the treatment this cancer disturbs patient's body image. Psychological assessment of a patient's condition and mood can be supported by tools of Natural Language Processing. It offers immediate data extraction and analysis of target data. It is used in many fields of medicine, in particular in psychiatry, psychology, and oncology field. Some researchers [2] focus on analyzing the clinical cancer patients records to identify the treatment methods ordinated to the patient and to manage the patient's medical documentation to tailor the process of further therapy. The aim of the authors in this paper is to proposes the method using NLP techniques to detect some morphological traits in patients' notes that may create a linguistic profile of a person with cancer and to determine the sentiment. Such analysis would allow the experts to tailor appropriate psychological therapy.

The authors proposed an automatic method based on NLP, including vocabulary and sentiment analysis. It includes determining the frequency of using verbs, verb tense references, adjectives (both positive and negative), and the intensity of using word 'MY' in relation to body to find out how the patients' concerns about their appearance. The text analysis investigate some characteristic tokens used by cancer patients. We proposed a list of words embraces body image that can support treatment application tailored for special needs. SAS Viya analytic software with open architecture was used for the analysis. We used text parsing, which provides us with Start/Stop list, stemming the terms to their basic form, and part of speech tagging to retrieve morphological features. Next, we calculated the number of analyzed features, and detected characteristic tokens. The study used a hybrid model approach, weighing the sentiment derived from the dictionary of emotions and the machine learning algorithm: deep recursive network. We used the traditional model of sentiment based on terms from the general sentiment vocabulary, created by Wilson, Wiebe, and Hoffman [3]. In the machine learning part, a deep recursive network with 5 hidden layers using LSTM cells was used. As property vectors, we used 100-element pre-learned global property vectors developed according to the GloVe method. The research group included 50 cancer patients, who prepared short notes about their body image.

The total number of adjectives was 191, of which 138 negative and 53 positive. Patients present some level of body image concerns as they use more adjectives with negative connotations. The overall number of verbs included 270 tags, where 105 stands for the verb "to be". We registered 7 past forms of this verb, 89 referring to the present and 9 to the future. The number of verbs related to states, actions, and verbs of perception is 163. In this group there are 25 tags in the past form and 140 in the present. The analysis detected 36 words MY. Patients used plenty of negative words, mainly related to face, skin and hair, signaling concerns regarding the loss of attractive appearance. They often referred to their bodies as ugly, old, dry, skinny, wrinkled, sick, devastated, weak, and disgusting. They also put their concerns towards the skin, often characterized as dry, transparent, pale, rough, with rash, and allergic. The analysis of sentiment resulted in 29 negative patients' attitude towards their body, 10 positive, and 11 neutral. They usually had difficulties with accepting hair loss and their fatal condition. Generally speaking, participants feel unattractive and mainly talk about death, pain, fear, and cachexia.

The developed method using NLP elements enables the quantitative determination of selected patient attributes. The proposed method tries to quantitatively analyze a specific research area: the perception of the body. A large part of psychological research in oncology focuses on the patient's well-being and quality of life. The developed method can support the assessment of the patient's condition by direct personnel who have daily contact with the patient. The method can generally contribute to a better understanding of the patient's psychology. We can use it for a specific patient as well as statistically for a research group.

References:
1. Clarke S., Newell R., Thompson A., et al. 2014. Appearance concerns and psychosocial adjustment following head and neck cancer: A cross-sectional study and nine-month follow-up. Psychology, Health & Medicine, doi: 10.1080/13548506.2013.855319.
2. Zeng J., Banerjee I., Solomon H., et al. 2021. Natural Language Processing to Identify Cancer Treatments With Electronic Medical Records. JCO Clinical Cancer Informatics(5):379–393.
3. Tanveer A., Schramm D., Sokolova M., et al. 2013. Can I hear you? Sentiment analysis on medical forums. In pages 667–673.

Hybrid System for Acquisition and Processing of Multimodal Signal: Population Study on Normal and Distorted Pronunciation of Sibilants in Polish Preschool Children

Joanna Trzaskalik[1], Ewa Kwaśniok[2], Zuzanna Miodońska[3], Michał Kręcichwost[3], Agata Sage[3], Paweł Badura[3]

[1] Jesuit University Ignatianum in Krakow, Kopernika 26, 31-501 Kraków, Poland
[2] Center for Human Health and Development "Therapy", Kłodnicka 2, 41-706 Ruda Śląska, Poland
[3] Faculty of Biomedical Engineering, Silesian University of Technology, Roosevelta 40, Zabrze, Poland
pawel.badura@polsl.pl

Aims. This paper presents the population study in research on computer-aided speech diagnosis and therapy in children. The project aims to broaden knowledge on sigmatism (a pronunciation disorder related to the non-normative realization of phonemes called sibilants: /s, z, ts, dz/, /ʃ, ʒ, ʧ, ʤ/, /ɕ, ʑ, ʨ, ʥ/) and discover interconnections between articulation (normal and distorted pronunciation features), acoustics, and position and motion of articulators. This report presents the sigmatism prevalence observed in the study.

Methods. The data were collected between October 2021 and May 2023 during speech therapy examinations performed by two speech-language pathologists over a group of 150 children aged 5–8 in five kindergartens and one primary school in Katowice, Mysłowice, Ruda Śląska, and Zabrze, Poland. Each examination was supported by two recording sessions involving a dedicated multimodal data acquisition device described in detail in [1] (Fig. 1). The device was safely and comfortably fixed on the speaker's head to record a 15-channel audio signal and a double-camera stereovision stream. The diagnoses were prepared using a dedicated questionnaire containing 196 fields. It enabled a thorough analysis of anatomical and articulation features observed during relaxed speech and speech therapy exercises [2].

Fig. 1. Multimodal data acquisition device used in the study [1].

Results. Table 1 presents normal pronunciation rates (NPR) in the research group. That covers only children assessed as featuring normal pronunciation in all the articulation features defined for a given phone (11-12), e.g., mediality of the articulators, place of the articulation, or voicing. The results were consistent within each series of sibilants: from 18-20% in /s, z, ts, dz/, 23-25% in /ʃ, ʒ, ʧ, ʤ/ to 33-35% in /ɕ, ʑ, ʨ, ʥ/. Dentalization (NPR at 61.9%) and mediality of the mandible (70.9%) were the features assessed overall as normative in the smallest number of participants.

	NPR		NPR		NPR
/s/	19,0%	/ʃ/	25,0%	/ɕ/	34,7%
/z/	19,3%	/ʒ/	24,7%	/ʑ/	33,3%
/ts/	19,0%	/ʧ/	25,0%	/ʨ/	35,3%
/dz/	18,3%	/ʤ/	23,7%	/ʥ/	34,3%

Tab. 1. Normal pronunciation rates (NPR) in individual sibilants, aggregated across various articulation cues.

Conclusion. We report that between 65 and 82% of Polish preschool children featured distorted pronunciation depending on the sibilant. However, these results came from a relatively strict rule to assess phoneme pronunciation as normal: no pronunciation disorder was observed in any of ca. a dozen articulation features per phoneme. We aim to use our extensive speech database supported by hybrid audio-video data for computer-aided speech diagnosis.

References:
[1] Krecichwost M., Sage A., Miodonska Z. and Badura P. 4D Multimodal Speaker Model for Remote Speech Diagnosis, *IEEE Access*, 2022, vol. 10, pp. 93187-93202, DOI: 10.1109/ACCESS.2022.3203572.
[2] Ostapiuk B. Dyslalia. On the study of the pronunciation quality in speech therapy, (PL) Dyslalia. O badaniu jakości wymowy w logopedii, 2013, Szczecin, Wydawnictwo Naukowe Uniwersytetu Szczecińskiego.

Multimodal data acquisition, registration, and analysis system for monitoring chronic skin wounds

Agata M. Wijata[1], Maria Bieńkowska[1], Marcin Rudzki[1], Jacek Andrzejewski[1], Damian Kurach[2], Marcin Sprawka[3] and Jan Juszczyk [1]

[1] Faculty of Biomedical Engineering, Silesian University of Technology, Roosevelta 40, Zabrze, Poland
[2] EXQDEV, Konarskiego 50, Częstochowa, Poland
[3] Woundscanning Sp. z o.o., 75 Pułku Piechoty 1, Chorzów, Poland

Agata.Wijata@polsl.pl

Aims

A chronic wound is a loss of skin because of a disease or an injury that cannot be healed [1]. Diagnosis and treatment of chronic skin wounds is an interdisciplinary medical problem, the incidence of which increases with the aging of the society. The presence of a chronic wound adversely affects not only the patient's physical health but also his/her mental state, as well as generates significant costs caused by the extended therapeutic process (related not only to the treatment of the wound). Therefore, developing tools for treatment monitoring enable objective assessment of the wound surface area, volume, or inflammation, which is of paramount practical importance. This work aims to present a stand that allows the collection of image data, which can be further applied to evaluate the patient's wound condition.

Methods

The multimodal wound scanner consists of three cameras: photo camera (2592x1944 px), thermal camera (320x240 px), and depth camera (320x240 px) rigidly mounted together. Different resolutions of the captured data require a calibration protocol for determining the transformations for image co-registration and making image fusion possible. The transformations are calculated based on checkerboard images (8x9 black and white squares) captured by each camera. The checkerboard is heated to get proper contrast for the thermal image (checkerboard elements have different infrared absorption) without affecting the other two modalities. Characteristic points (corners) are determined from the checkerboard image [2], then the transformation matrices (translation, rotation, and scaling) are calculated [3] and used to match the RGB photos of the wound to its thermal image. The result of the fusion of both modalities is then matched with the depth-camera intensity image in order to apply texture to the point cloud. After the alignment and calibration, the system is ready to acquire the image of the wound, which can finally be utilized to estimate the wound's volume [1].

Results

The verification of the system was carried out based on phantom wounds that were modeled in the Blender software and then printed using a 3D printer. Wound phantoms' areas and volumes were 7.80, 4.06, 1.58 cm^2 and 2.34, 0.48, 0.17 cm^3, respectively. For each wound we collected 4 sets (by 90° rotation of the wound) of multimodal data. The mean errors of area and volume determination for each wound were: 2.28%, 7.64%, 3.16% and 12.82%, 10.00%, 10.29% respectively, at the distance 15 cm from the measuring device. For greater distances, the error values increase, i.e., for a 55 cm distance the error is less than 15% for the area and 25% for volume.

Conclusion

The results show that even small wounds can be accurately assessed, which allows for quantifying the changes that take place during the diagnostic and therapeutic process. The distance between the device and the wound affects the measurement error. Also, the created visual and thermal medical documentation enables long-term comparisons and drawing conclusions about the impact of the implemented treatment pathway.

Acknowledgments

References:

[1] Juszczyk JM, and others. Wound 3D geometrical feature estimation using Poisson reconstruction, IEEE Access, 2021, vol. 9, pp. 7894–7907

[2] Geiger A, and others. Automatic camera and range sensor calibration using a single shot, IEEE ICRA 2012, pp. 3936–3943

[3] Woloshuk A, and others. Development of a multimodal image registration and fusion technique for visualising and monitoring chronic skin wounds, in ITIB 2019, pp. 138–149

Chapter VIII

Information Content Analysis in Cardiovascular and Respiratory Systems

Session organizer:

Prof. Gerard Cybulski, Warsaw University of Technology

Electrophysiological Activity Models as a Background for Non-Uniform Signal Sampling

Piotr Augustyniak
AGH University of Krakow, 30 Mickiewicz Ave., 30-059 Krakow
august@agh.edu.pl

Non-uniform sampling is commonly agreed to be more adequate and economic for digital representation of variable-bandwidth phenomena than commonly used regular (i.e. constant interval) sampling. Various statistical models have been proposed depending on the signal to either limit acquisition time and cost (e.g. magnetic resonance tomography) or reduce data volume (e.g. seismic record of an earthquake). In case of electrophysiological activity records, besides of intrinsically irregular time sequences such as RR intervals in ECG, non-uniform representation may rely on physiological limitations of known signal sources. Therefore, we propose to replace statistical approach such as compressed sensing (CS) [1] by electrophysiological activity models [2] as a background for non-uniform signal sampling.

Among several approaches, we considered to compare three models driving the non-uniform sampling process of the ECG based on: (1) expected sequence of variable-bandwidth events (VBE), (2) perceptual features of the displayed record (PFE) and (3) diagnostic parameters' equivalence (DPE) between the uniform and non-uniform variants of the record. The VBE assumes the use of signal segmentation i.e. delineation of several P, QRS and T waves, calculating individual bandwidth of each wave type and employing the wave borders to stepwise adaptation of the signal bandwidth and, consequently, sampling frequency. The PFE method uses an eyetracker applied to interpreting human expert to reveal regions of interest and focus time as representative to distribution of medical content of displayed record. The DPE requires the use of automatic ECG interpretation procedure applied to both original and forward-reverse non-uniform transform to quantitatively compare distortions of medical content and optimize local sampling interval.

To express the quantitative result of comparison we used the cross-correlation (CC) coefficient and the compression ratio (CR) of the number of samples in non-uniform and uniform representation. Since the cross-correlation function is only defined for simultaneously sampled signals, we first applied the cubic spline interpolation with regular sampling to non-uniform signals. Besides, the CSE Multilead Database with 125 annotated and segmented ECG signals was used as reference data and the MTrace (M4Medical, Poland) 12-leads electrocardiograph with external record interpretation (according to EN 1064) completed the test setup. With all 125 ECG files, each composed of 15 leads of 10-s ECG strips we got the following average results:

Method	Compression ratio (CR)		Cross-correlation (CC) [%]	
	avg.	std.	avg.	std.
CS [1]	2.9	1.35	95.4	1.53
VBE	3.1	0.98	94.1	1.88
PFE	4.7	1.13	97.8	1.03
DPE	5.1	1.04	99.1	0.57

The results show questionable advantage of using VBE over regular CS. Indeed, calculation of local bandwidth with the spectral features of P, QRS and T waves is based on statistics similar to CS, and additional loss of correlation is due to wave delineation inaccuracy. On the contrary, the advantage of PFE and in particular of DPE over regular CS is remarkable. Our comparison of these method reveals better performance of DPE in both compression ratio and cross-correlation, but at the same time one should also mention the drawbacks of both methods: PFE uses a heuristic perceptual model depending on participating experts-volunteers and DPE requires manufacturer-specific ECG interpretation procedure and a computationally expensive optimization loop. The approach proposed for ECG records may easily be extended to other electrophysiological signals.

References:
[1] D.L. Donoho. Compressed sensing, IEEE *Transactions on Information Theory*, 52(4):1289–1306, 2006,
[2] P. Augustyniak Adaptive Sampling of the Electrocardiogram Based on Generalized Perceptual Features. *Sensors* 2020, 20, 373;

Bipolar Leads in ECG Conceal the Dark Side of the Moon

Teodor Buchner[1], Sebastian Wildowicz[1], Tomasz Gradowski[1], Judyta Sobiech[1], Kazimierz Pęczalski[2],
Maryla Zajdel[1], Mirela Graczyk[1]
Warsaw University of Technology, [1]Faculty of Physics, [2]Faculty of Mechatronics
teodor.buchner@pw.edu.pl

Information content of the ECG is a problem which remains open, despite more than 100 years of its history. Of particular importance is the inverse problem - a precise localization of cardiac sources, from the surface measurements. The existing solutions to this cardiac imaging problem still exhibit poor convergence. It is typically attributed to unsatisfactory numerical procedures. The underlying theory is, however, rarely challenged. Virtually all existing theories of the ECG assume, that the tissue should be described using Maxwell equations. Our approach takes into account the actual mesoscopic structure (anatomy) of living matter and its molecular nature, which leads to extreme simplification [1]. The validity of this approach is under experimental verification - so far successful [2,3]. The aim of this study is to show an alternative description of the sources of bipolar ECG measurements, taking well known pathologies of the ECG as an example.

We present a method to synthetise the ECG from cellular potentials using the concept of activation functions (c.f. Fig 1), which summarize the electric effect of the tissue underneath the electrode. Potential of the electrode is just a convolution of activation function and potential of a typical cardiac cell. We study the conditions, required to regenerate the morphologies of typical pathologies, such as ventricular ectopy or ischemia. A crucial factor is the precedence of electrode potentials which decides on such quantities as the QRS morphology; in particular the electric axis.

We demonstrate, how the novel interpretation allows to easily deduce the important details, concerning the localization of the sources, which produced certain morphology of the ECG. Specifically the nature of various mirror effects is explained. One convincing example is given by the symptoms of posterior wall myocardial infarction, which is diagnosed in precordial leads, which are actually the farthest from the actual source of pathology. We note, that the shape of the visible ECG does not reveal the complete time course of activity of the heart, as due to the bipolar nature of measurements, only the asymmetry of cardiac potentials is envisaged, with respect to finite CMRR. Hence, an important part of information on the electric activity in cardiac cycle remains invisible, until pathological conditions reveal it. It occurs that an important part of the ECG is on the dark side of the moon. We also note, that the actual paths of biopotential propagation should be measured using modern measurement techniques.
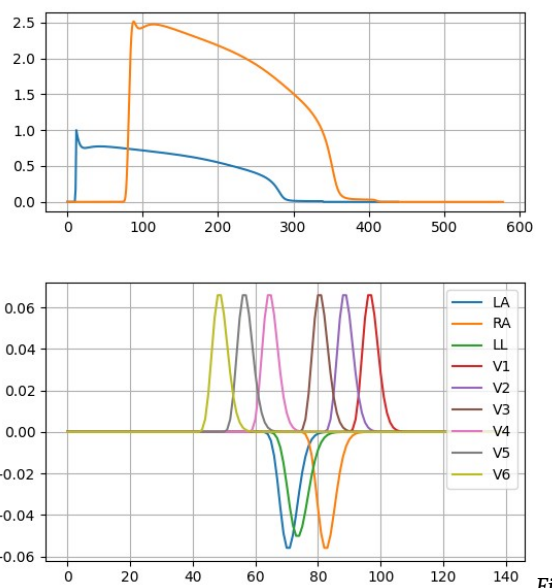
Fig. 1 Example of cell potential and electrode potential (top) and activation functions for 12 lead ECG (bottom).

We conclude, that molecular theory of biopotential provides a useful tool, which brings not only better compliance with the underlying physics, but also alleviates the interpretation of the ECG and allows for better localization of the exact source of pathology. This localization is entirely based on plain physics and does not require any computationally and formally demanding theories.

References:
[1] Buchner T., Molekularna Teoria Biopotencjału, Oficyna Wydawnicza Politechniki Warszawskiej, 2022.
[2] Buchner T, Zajdel M, Pęczalski K, Nowak P. Finite velocity of ECG signal propagation: preliminary theory, results of a pilot experiment and consequences for medical diagnosis. *Sci Rep.* 2023,13(1), 4716.
[3] Buchner T. On the physical nature of biopotentials, their propagation and measurement. *Physica A*, 2019, 525, 85–95.

HEART RATE ASYMMETRY IN RESPIRATORY PHASES

Grzegorz Graff [1], Dorota Wejer [2], Beata Graff [3], Krzysztof Narkiewicz [3] and
Danuta Makowiec [4]

[1] Gdańsk University of Technology & BioTechMed Center, Faculty of Applied Physics and Mathematics,
Narutowicza 11/12, 80-233 Gdańsk, Poland
[2] University of Gdańsk, Faculty of Mathematics, Physics and Informatics,
Institute of Experimental Physics, Wita Stwosza 57, 80-308 Gdańsk, Poland
[3] Medical University of Gdańsk, Department of Hypertension and Diabetology, M. Skłodowskiej-Curie 3a,
80-210 Gdańsk, Poland
[4] University of Gdańsk, Faculty of Mathematics, Physics and Informatics, Institute of Theoretical Physics
and Astrophysics, Wita Stwosza 57, 80-308 Gdańsk, Poland

grzegorz.graff@pg.edu.pl

Heart rate asymmetry (HRA) is a physiological phenomenon related to unequal contribution of decelerations and accelerations to heart rate variability, but its mechanism has not yet been fully explained yet (cf. [1,2] and references therein). The significant influence of breathing on heart rhythm prompted us to investigate HRA in respiratory phases. We considered 20-minute recordings of ECG and respiration of 18 healthy adults (age: 45 ± 14). Each consecutive pair of RR intervals was assigned to one of 8 states corresponding to the phase of breathing: inspiration or expiration, and two possible breathing phase transitions: from inspiration to expiration or from expiration to inspiration. All subjects were examined in supine position and had a regular breathing pattern. Poincaré plots for pairs of RR intervals in subsequent respiratory states were obtained and analyzed by a use of Guzik's Index, Porta Index as well as their generalization: Multistructure Index (cf. [3]). The value of Guzik Index computed for the considered group without taking into account the respiratory phases was significantly different from 50% (Student's t-test: p= 0,085), which means presence of asymmetry for healthy subjects. On the other hand, for Porta Index the difference was not statistically significant (p=0,338). However, we observed that there are significant differences between values of asymmetry indices in dependence of the respiratory state. In particular these differences were observed (for both indices) between phases (IN EX EX) and (EX EX IN) as well as (EX IN IN) and (IN IN EX). The Multistructure Index MI(q) is a function of one control parameter q. The values of MI(q) were determined for q in $[-10, 10]$. The results confirmed our findings for Guzik and Porta Index. What is more, we observed completely different type of behavior of MI(q) in many phases for large values of q, for example between (IN EX EX) and (EX IN EX).

Concluding, we found that the asymmetry (measured by considered indices) is strongly influenced by the respiratory phase. As asymmetry is reduced with aging and pathology (type 1 diabetes, CHF, and others), more detailed insight into asymmetry in dependence of respiratory phases might be helpful in identifying pathological states.

References:

[1] G. Graff, B. Graff, A. Kaczkowska, D. Makowiec, J. Amigo, J. Piskorski, P. Guzik, Ordinal pattern statistics for the assessment of heart rate variability. *The European Physical Journal-Special Topics,* 2013, vol. 222(2), 525-534.
[2] P. Guzik, J. Piskorski, Asymmetric properties of heart rate microstructure, *Journal of Medical Science,* 2020, vol. 89 (2), 121-131.
[3] D. Makowiec, B. Graff, Z. R. Struzik, Multistructure index in revealing complexity of regulatory mechanisms of human cardiovascular system at rest and orthostatic stress in healthy humans, *Physica A: Statistical Mechanics and its Applications,* 2017, 468, 809-824.

Numerical modelling of myocardial bridge covering dynamic shape of the human coronary artery

Bartłomiej Melka[1*], Krzysztof Psiuk-Maksymowicz[2], Damian Borys[2], Ziemowit Ostrowski[1], Marek Rojczyk[1], Maria Gracka[1], Wojciech P. Adamczyk[1], Ryszard A. Bialecki[1]

[1]Department of Thermal Technology, Silesian University of Technology
[2]Department of Systems Biology and Engineering, Silesian University of Technology
[*]Bartlomiej.Melka@polsl.pl

Nowadays, cardiovascular diseases are the main reason of death globally. The presented research focuses on the myocardial bridge (MB) which is qualified as one of the cardiovascular diseases. MB is a congenital pathology while one of the main coronary arteries or its part is placed under the heart muscle structure (in the myocardium). The mentioned pathology could cause none or one or even a few of the mentioned symptoms: angina, myocardial ischemia, acute coronary syndrome, left ventricular dysfunction, arrhythmia, and even sudden cardiac death [1]. Therefore, a deeper understanding and improvement of the diagnostic procedures connected with MB could improve therapy planning and treatment methods.

One of the noninvasive techniques allowing diagnosis and assessment of the MB influence on the patient's condition is computer modelling. Mathematical modelling called Computational Fluid Dynamics (CFD) solving governing equations based on mass and momentum conservation principles allows to estimate the 3D blood flow field. 3D field analysis allows also estimating the indicators such as Wall Shear Stress (WSS) and Oscillatory Shear Index (OSI) which point to the regions where plaque deposition is the most probable. In the presented research CFD technique also covered the dynamic geometry of the investigated blood vessel of the specific patient. It was possible on the basis of a few images coming from computer tomography during the heart cycle. Eight medical images after the segmentation procedure were used as the input to the software (ANTS) which on the basis of the diffeomorphism technique allowed to estimate the 3D vector field of the deformations from one image to another [2]. Using these results, the numerical mesh used in the CFD software could be transformed during the heart cycle by applying smoothing and remeshing approaches for the dynamic mesh. The linear interpolation of the shapes was applied in the time steps between the instants when the medical images were available. Dynamic mesh is also connected with the blood vessel volume change, including the blood accumulation and its release during the specific parts of the heart cycle.

The presented results indicated consistency between the places where the plaque was deposited and regions with high OSI and low WSS values. Additionally, implementing dynamic mesh in the CFD calculation increases the accuracy of the results.

The developed methodology and calculation tools could be implemented in clinical practice as noninvasive diagnostic methods and prognostic tools for MB in terms of potential atherosclerosis. The results from CFD simulations could also be used as a therapy planning tool allowing estimation of the artery performance after invasive treatment. Therefore, the development of mathematic modelling for cardiovascular medicine could be a crucial step in the coming years for this branch.

References:
[1] Lee MS, Chen CH. Myocardial bridging: an up-to-date review, *The Journal of invasive cardiology,* 2015, vol. 27(11), pp. 521-528
[2] Avants BB, Tustison NJ, Stauffer M, Song G, Wu B, Gee JC, The Insight ToolKit image registration framework, *Frontiers in Neuroinformatics,* 2014, vol. 8, pp. 1–13

Cough - about novelties in diagnosis and monitoring. What do we know about it? Initial literature studies and experimental and clinical studies on volunteers.

Krzysztof Jakub Pałko[1], Dominika Szuberla[2], Włodzimierz Łukasik[2], Elżbieta Magdalena Grabczak[3], Rafał Krenke[3] and Tadeusz Pałko[2]

[1]Nalecz Institute of Biocybernetics and Biomedical Engineering, Polish Academy of Sciences (IBBE PAS), Ks. Trojdena 4 st., 02-109 Warsaw, Poland
[2]Warsaw University of Technology (WUT), Faculty of Mechatronics, Institute of Metrology and Biomedical Engineering, A. Boboli 8 St., 02-525 Warsaw, Poland
[3]Department of Internal Medicine, Pulmonary Diseases and Allergy, Medical University of Warsaw (MUW), Banacha 1a, 02-097 Warsaw, Poland
krzysztof.palko@ibib.waw.pl

Aim: Cough is a symptom accompanying various types of diseases[1], both of infectious origin - primarily the upper respiratory tract (such as colds and flu, etc.) and in chronic diseases (including tuberculosis, whooping cough, obstructive airway diseases, lung cancer, among others), sometimes also the result of reflux disease or allergies. Despite many years of research and construction work carried out in many medical and engineering and technical centers around the world, it's hard to find the device that could meet all the physicians expectations. The aims of this work were to conduct a literature query on comparison of the used diagnostic methods and their analysis of measurement signals, and to conduct preliminary research by using digital recorders of vibroacoustic cough signals (developed by WUT as part of the collaboration between WUT, MUW and IBBE PAS and which resulting in two diploma (Master's and Engineer's) theses were defended), intended for both experimental and clinical purposes.

Methods: At first, a literature review in particular in the years 2019-2023 (using Pubmed, Google Scholar, Web of Science, Research Gate and Academia.edu) was done as a more or less systematic way of collecting and synthesizing previous research. Next, the WUT devices were adapted to work with an accelerometer microsensor for vibration recording, and the other with a microphone for sound recording. Another important aspect of this work was the numerical (digital) analysis and parametric characterization of these signals.

Results: The main results of the work were in the literature query on the monitoring and analysis of diagnostic signals of cough (about 300 publications) and in verification of the correct operation of the developed measuring devices, as well as in the initial registration of the acoustic and acceleration (vibration intensity) signals along with checking the possibility of their further analysis. An integral part of the subject was conducting tests on volunteers at MUW in Warsaw. A numerical (digital) analysis was carried out. For the characterization of the diagnostic signals, the following parameters were selected: intensity (signal amplitude, instantaneous value), frequency of coughing incidents, their duration, time shift of the microphone signal relative to the accelerometer signal, power spectral density of the signals, as well as the total number of coughing incidents during its duration. Five volunteers were registered. Each measurement lasted approximately 40 minutes. Recordings took place on two synchronized devices.

Conclusions: There was a variety of cough monitoring methods in use, recently quite developed during the ongoing COVID-19 pandemic caused by the SARS-CoV-2 coronavirus (including the most widely used Leicester Automatic Cough Monitor (LCM)[2] and the Vitalograph VitaloJAK[3]). The obtained results of the conducted experimental and clinical studies confirmed the adopted assumptions, the correct operation of the developed devices and the sufficiently adequate quality of the recorded vibroacoustic signals, suitable for further numerical processing and analysis as well as their reliable characterization. The preliminary tests are very promising and the common scientific collaboration will be continued.

References:
[1] Sharma S, Hashmi MF, Alhajjaj MS. Cough. [Updated 2023 Feb 19]. In: *StatPearls* [Internet]. Treasure Island (FL): StatPearls Publishing, 2023. Available from: https://www.ncbi.nlm.nih.gov/books/NBK493221/.
[2] Birring SS, Fleming T, Matos S, Raj AA, Evans DH, Pavord ID. The Leicester Cough Monitor: preliminary validation of an automated cough detection system in chronic cough. *Eur Respir J.* 2008, vol. 31, no. 5, pp. 1013-8, doi: 10.1183/09031936.00057407.
[3] https://vitalograph.com/intl/clinical-trials/product-solutions/vitalojak/ (available on May 31st , 2023).

Chapter IX

Mathematical and Computational Modeling in Physiology, Medicine and Biomedical Engineering

Session organizers:

Prof. Jan Poleszczuk, Nalecz Institute of Biocybernetics and Biomedical Engineering
Prof. Jacek Waniewski, Nalecz Institute of Biocybernetics and Biomedical Engineering

Detection of medial vascular calcification in chronic kidney disease based on the pulse wave analysis in the frequency domain

U. Białończyk [1*], M. Dębowska [1], L. Dai [2,3], AR. Qureshi [3], M. Söderberg [4], B. Lindholm [3], P. Stenvinkel [3], J. Poleszczuk [1]

[1] Nalecz Institute of Biocybernetics and Biomedical Engineering, Polish Academy of Sciences, Ul. Ks. Trojadena 4 02-109 Warsaw, Poland, [2] Aging Research Center, Department of Neurobiology, Care Sciences and Society, Karolinska Institutet and Stockholm University, Stockholm, Sweden, [3] Renal Medicine and Baxter Novum, Department of Clinical Science, Intervention and Technology, Karolinska Institutet, Stockholm, Sweden, [4] Pathology, Clinical Pharmacology and Safety Sciences, AstraZeneca R&D
[*] corresponding author, ubialonczyk@ibib.waw.pl

Background: Medial vascular calcification (mVC), particularly prevalent in patients with chronic kidney disease (CKD), is a pathological deposition of minerals in the medial layer of the vessel wall and is associated with an increased risk of cardiovascular disease [1]. Currently, computed tomography, although imperfect, is viewed as a gold standard for calcification detection [1]. Several therapeutic strategies have been proposed to slow down the progression of vascular calcification [2]. For this reason, a cost-effective and non-invasive procedure of mVC assessment which could be used for CKD patients in a clinical routine is needed. The aim of the study was to test whether in-depth analysis of non-invasively recorded peripheral pulse waves can serve as an effective mVC biomarker.

Methods: The study included 97 CKD patients with information about mVC and pulse wave measurements in the brachial artery. Pulse waves (PW) were analysed in the frequency domain to obtain features which, together with traditional mVC risk factors (RF), such as age, sex, or body mass index, were used to build various generalized linear models for mVC prediction. The classifiers with the best scores in terms of balanced accuracy were combined in an ensemble establishing the final model. The gain in performance obtained by using PW and RF features together was additionally assessed by building similar models without pulse wave features and with pulse wave features only.

Results: The final, ensembled model, assessed using a leave-one-out cross-validation process, achieved a balanced accuracy equal to 0.87, an accuracy of 0.93, an AUC ROC of 0.91, and an F-score of 0.96. Apart from the features associated with pulse waves, the selected variables included age, sex, body mass index, heart rate, and diastolic blood pressure. The classifier built with the use of both PW and RF features outperformed the classifiers deprived of either one of the two groups of variables which is shown in Table 1.

Conclusions: Analysis of non-invasively recorded peripheral pulse waveforms combined with traditional risk factors, can help to detect mVC in CKD patients and thus, possibly introduce risk-lowering therapeutic strategies at earlier disease stages.

Table 1: Performance metrics of the built ensembles. AUC – area under the receiver operating characteristic curve, PW only – the model with pulse wave associated features only, RF only – the model with traditional risk factors only, PW and RF – the model with all of the analyzed features. The latter outperformed the other classifiers which is highlighted by the bolded values.

Model	Precision	Recall	Specificity	Accuracy	Balanced accuracy	F-score	AUC
PW only	0.95	0.90	0.78	0.88	0.84	0.92	0.87
RF only	0.92	0.96	0.61	0.90	0.79	0.94	0.84
PW and RF	**0.95**	**0.96**	**0.78**	**0.93**	**0.87**	**0.96**	**0.91**

[1] C. Marreiros, C. Viegas, and D. Simes, "Targeting a Silent Disease: Vascular Calcification in Chronic Kidney Disease.," *Int J Mol Sci*, vol. 23, no. 24, Dec. 2022, doi: 10.3390/ijms232416114.

[2] S. C. Ren *et al.*, "Vascular Calcification in Chronic Kidney Disease: An Update and Perspective," *Aging and Disease*, vol. 13, no. 3. International Society on Aging and Disease, pp. 673–697, May 18, 2022. doi: 10.14336/AD.2021.1024.

A Mathematical Model for Transport in Poroelastic Materials

Roman Cherniha[1], Joanna Stachowska-Pietka[2], Jacek Waniewski[2]

[1] School of Mathematical Sciences, University of Nottingham, Nottingham NG7 2RD, UK
[2] Nalecz Institute of Biocybernetics and Biomedical Engineering, Trojdena 4, Warsaw, Poland
Email: r.m.cherniha@gmail.com

Fluid and solute transport in poroelastic materials (biological tissue is an example) is studied. Mathematical modeling of such transport is a complicated problem because the specimen volume under special conditions might change due to swelling or shrinking and the transport processes are nonlinearly linked. The tensorial character of the variables adds also substantial complication in both theoretical and experimental investigations of the transport in poroelastic materials (PEM). Therefore, developing and solving adequate mathematical models is an important and still open problem.

Using modern foundations of the poroelastic theory [1], the basic nonlinear model for PEM with the variable volume was constructed. We consider PEM that consists of pores of two different sizes ('small' and 'large') with fluid and solid material (matrix); molecules of essentially different sizes are dissolved in fluid phase and transported through pores. We assume that fluid is incompressible and there are no internal sources/sinks. The governing equations of the model consist of continuity equations reflecting classical physical laws (with the extended Darcy's law, Newtonian law). The stress-strain relationship was described by the generalized Terzaghi stress tensor with an additional quadratic term involving a parameter κ. A simplified version of this model was studied earlier in [2]. To derive some analytical results, the one-dimensional (in space) version of the model was studied in detail. As a result, multiparameter families of exact solutions were constructed. In particular, the steady-state solutions of the model were calculated that describe the profiles of the material deformation u, intra-pore fluid hydrostatic pressure, solutes concentration as a distance from the tissue surface.

The obtained results have been illustrated using typical parameters that corresponds to the healthy tissue (interstitium) that became in contact with hypertonic fluid (glucose 3.86%) as used in peritoneal dialysis. Tissue with a slightly negative interstitial hydrostatic pressure, containing albumin and glucose was considered. The albumin void volume was assumed 40% of the fluid void volume available for glucose. The impact of osmotic and hydrostatic pressure (40 mmHg) exerted at the tissue surface by the dialysis solution was assumed. The obtained results showed changes of the tissue size caused by fluid in which tissue was immersed. Different deformations u (depending on the parameter κ) were predicted for healthy tissue, **Figure 1.** The deformations were not pronounced in case of materials with higher stiffness (as in tumor tissue).

Since the results obtained for the one-dimensional model are promising, our work is in progress to study the model in the case of two and three space variables.
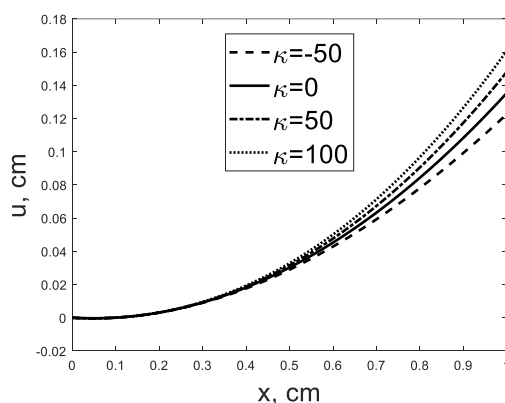
Figure 1. Deformation of tissue as a function of present tissue width of 1 cm for κ=-50, 0, 50, 100.

[1] Loret B. and F.M.F. Simoes, Biomechanical aspects of soft tissue 2017, Boca Raton: CRC Press.
[2] Cherniha R. et al A Mathematical Model for Transport in Poroelastic Materials with Variable Volume: Derivation, Lie Symmetry Analysis, and Examples, *Symmetry*, 2020, vol. 12, no. 3: 396.

Distributed delays in a simple neuronal population model of decision making

Urszula Foryś, Marek Bodnar, Emad Attia.
Institute of Applied Mathematics & Mechanics, University of Warsaw, Banacha 2, 02-092 Warsaw, Poland
Prince Sattam Bin Abdulaziz University, Al-Kharj 16278, Saudi Arabia
urszula@mimuw.edu.pl

Decision making is one of our brain daily activity. Mathematical modeling of such processes has not so long history, but variety of approaches can be found in the literature. One of such approaches is based on neuronal competition models. In our previous articles [1, 2] we proposed a model describing interactions between two neuronal populations where time delay was responsible for ambiguity in perception [1], also in the context of elderly [2].

Time delay introduced in [1, 2] was discrete, for simplification. However, it is obvious that in nature the same constant time delay appearing each time when the specific process occurs is not possible. Distributed delays seem to reflect nature much better. This was our motivation to study the model with distributed delays.

In our analysis we found conditions of instability which are independent of assumed distributions. However, finding such general results in the context of stability occurred impossible. Hence, we focused on some specific types of distributions. First, we considered the distribution with kernel being decreasing and convex (meaning that smaller delays are more probable than larger ones). Next we studied non-shifted Erlang, ending with the shifted Erlang distribution. For all the mentioned distributions we found conditions of stability, and for Erlang distributions we were able to calculate threshold delays for which stability is lost. In the figure below we see the bifurcation with respect to $a = 2/\tau$, where τ is the average delay in Erlang distribution with parameters a and $n = 2$.
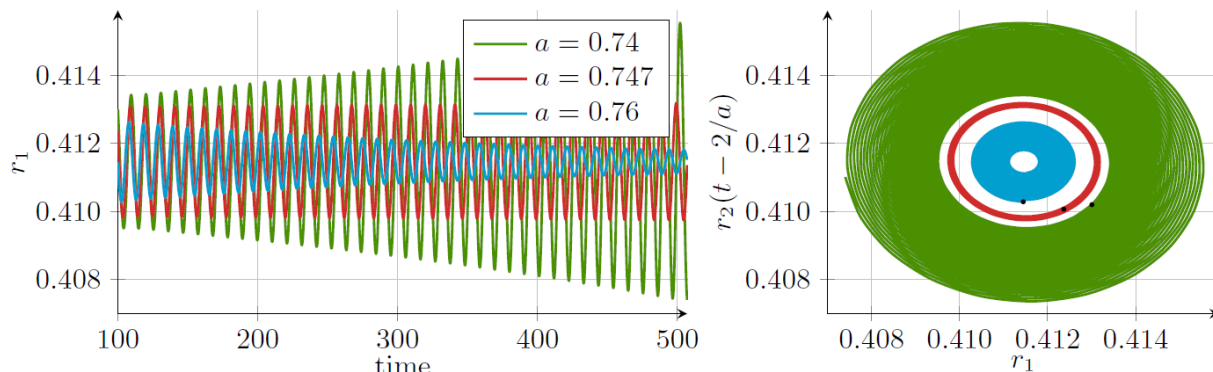
As it is stated in [1], "cortical networks operate on the edge of instability, in which oscillations can appear". Hence, models with time delays (which typically lead to a Hopf bifurcation and instability for larger delays) seem to be a good mathematical approach in describing perceptual decision-making. We hope our study can bring new ideas in mathematical modeling of decision-making processes and would allow for better understanding of these processes.

References:
[1] Bielczyk N.Z., Piskała K., Płomecka M., Radziński P., Todorova L., and Foryś U. Time-delay model of perceptual decision making in cortical networks, *PloS One*, 2019, vol. 14, no. 2, e0211885.
[2] Foryś U., Bielczyk N.Z., Piskała K., Płomecka M., and Poleszczuk J. Impact of time delay in perceptual decision-making: Neuronal population modeling approach, *Complexity*, 2017, ID 4391587.

A numerical algorithm for reducing the time of HIFU thermal ablation of large tissue volumes and its experimental verification

Lukasz Fura, Tamara Kujawska
Institute of Fundamental Technological Research Polish Academy of Sciences,
Pawińskiego St. 5B; 02-106 Warsaw, Poland
lfura@ippt.pan.pl

The standard HIFU (High Intensity Focused Ultrasound) thermal ablation procedure of large tissue volumes requires multiple sonications and a constant long cooling time, usually about 60 seconds [1] between successive sonications, which significantly prolongs the ablation process. Therefore, the objective of this study was to develop a numerical algorithm to shorten HIFU ablation time that can be applied to any spatial scanning plan. Numerically generated procedures for large-volume ablation have been verified experimentally on ex vivo samples.

The developed algorithm consists in calculating using the k-wave toolbox the space-time distribution of sound pressure in the pulsed beam generated by the HIFU transducer and propagated in the two-layer system of water-tissue media, and then determining the power density of the heat sources and the evolution of the thermal field using the pseudo-spectral k- space method. Based on the calculated spatial-temporal distribution of temperature at a given time step, the spatial distribution of thermal dose in the assumed system is calculated. According to these distributions, assuming the threshold of irreversible thermal damage to the tissue CEM43 = 240 min and the maximum allowable temperature in the system during sonication (60°C), the beam duty cycle was selected, thus creating a numerical proportional controller used in HIFU thermal ablation. The algorithm outputs for a given spatial plan of ablation, the adjusted values of the duty cycle at a given moment of time, the moment of transition to the next sonication target, and the predicted spatial distribution of the necrotic lesion being formed. The calculated size of necrotic changes was experimentally verified.

Two cylinders with diameters of 5 mm and 9 mm and a height of about 10 mm, for which the standard procedure consisting of 3 s of sonication and 60 s of cooling takes 8.45 min and 30.5 min, respectively, were scheduled for ablation using a reduced-time algorithm. The developed algorithm reduced the time of the mentioned ablation procedures to 1.17 min and 2.98 min, so to about 13.8% and 9.7% of the time of the standard procedure. The average difference in length and diameter between experimentally and numerically obtained necrotic lesions using the developed algorithm was 1.7 mm and 0.6 mm, respectively.

The developed algorithm made it possible to shorten the ablation time by about 7 times and 11 times, respectively, and to predict with good accuracy the size of the expected necrotic lesion, so it has the potential to be applied in clinical practice in the future.

References:
[1] Experimental evaluation of the near-field and far-field heating of focused ultrasound using the thermal dose concept. Ultrasonics. 2021;116:106513.

Mathematical modeling unveils potential synergy between CAIX suppression and immune checkpoint inhibitors

Julia Grajek, Jan Poleszczuk

Nalecz Institute of Biocybernetics and Biomedical Engineering Polish Academy of Sciences

Ks. Trojdena 4, 02-109 Warsaw

jgrajek@ibib.waw.pl

Immune checkpoint inhibitors (ICIs) have revolutionized the treatment of solid malignancies. However, immunotherapy resistance constitutes a significant challenge, with less than half of the patients responding to the treatment. In this study, we investigated carbonic anhydrase IX (CAIX) as a driver of this resistance and explored the potential synergy between CAIX inhibition and ICIs.

We built a differential equation model of tumor-immune interactions, informed by pre-clinical data and insights from our previous modeling approach [1,2]. The model considers treatment with the CAIX inhibitor SLC-0111 alone and in combination with anti-PD-1 and anti-CTLA-4 therapies. Given certain constraints, the model has two distinct steady states: one tumor-free equilibrium and one positive equilibrium indicating stable disease. Our simulations revealed that tumors lacking CAIX expression tended towards elimination when faced with an efficient immune response, whereas CAIX-expressing tumors stabilized near the positive equilibrium. Importantly, we demonstrated that short-term combination therapy with a CAIX inhibitor and immunotherapy could shift the asymptotic behavior of the original model from stable disease to tumor eradication.

Concluding, we have developed a model that reproduces experimental findings and enables the investigation of combination therapies. Our model suggests that transient CAIX inhibition combined with immunotherapy may induce durable tumor regression. Furthermore, simulations indicate that anti-CAIX reduces the fraction of cancer stem cells, making it thus a combination therapy target for treatments that struggle with stem cell removal, such as chemotherapy.

References:

[1] Grajek J, Kather NL, Poleszczuk J, An in silico model to study the impact of carbonic anhydrase IX expression on tumour growth and anti-PD-1 therapy, Journal of the Royal Society Interface, 20(198), 2023, 1742-5662, doi: https://do i.org/10.1098/rsif.2022.0654

[2] Shawn C. Chafe et al. "Targeting Hypoxia-Induced Carbonic Anhydrase IX Enhances Immune-Checkpoint Blockade Locally and Systemically". Cancer Immunology Research 7, pp. 1064–1078. ISSN: 2326-6066. DOI:0 . 1158 / 2326 - 6066 . CIR - 18 - 0657.

Digital twin architecture for remote trajectory planning and control of a rehabilitation exoskeleton

Filip Gwardecki, Warsaw University of Technology
Piotr Falkowski, ŁUKASIEWICZ Research Network – Industrial Research Institute for Automation and Measurements PIAP, Warsaw University of Technology
ŁUKASIEWICZ Research Network – Industrial Research Institute for Automation and Measurements PIAP, Al. Jerozolimskie 202, 02-486 Warsaw, Poland
Warsaw University of Technology, Nowowiejska 24, 00-665 Warsaw, Poland
piotr.falkowski@piap.lukasiewicz.gov.pl

The digital twin technology enables taking better real-time decisions for the operator than just based on visual observations. This technology was developed primarily for industrial applications. However, it gained popularity in modern healthcare – mainly by twinning the patients. Nevertheless, digital twinning rehabilitation devices can enable active supervision of patients during kinesiotherapy [1].

For this reason, a digital twin of the *ExoReha*, the 3D-printed rehabilitation exoskeleton for the upper extremity, was designed in the *Robot Operating System* environment. Its structure consists of rigid elements with five degrees of freedom. Among these, three are driven (two mobilising a shoulder joint and one mobilising elbow flexion/extension) with the servomotors with integrated encoders. The shoulder rotation and pronation/supination are not supported but can be measured with magnetic linear encoders. Moreover, the device contains adjustable transitional connections measured with potentiometers. The research was focused on developing the architecture and applications of a digital twin for an upper limb rehabilitation exoskeleton. Its main aim was to enable remote monitoring of a patient and programming the desired trajectories.

The designed digital twin consists of three interconnected nodes. The first one, running on a *Raspberry Pi 4B*, is responsible for controlling the drives via the CAN bus. It receives the desired position data for the actuated rotations and publishes the actual motor encoder readings, and control torques in real time. The second node, implemented using the rosserial package, runs on an *STM32* microcontroller and processes measurements from the sensory system. The last node is located on the physiotherapist's computer and provides a user interface for controlling the exoskeleton. The entire system is integrated into the *Gazebo* physics engine, which visualises, simulates the exoskeleton's behaviour, and determines the forces and moments during exercise.

The presented digital twin architecture enables a safe remote control over the exoskeleton. The physiotherapist operating a system can also benefit from an active view of the patient's current position and estimated joint forces. This contributes to providing remote rehabilitation, which is particularly important for people affected with severe impairments. This not only increases accessibility to rehabilitation services but also reduces the need for on-site therapy sessions and the associated costs. Furthermore, the detailed collected information can be used to design more effective rehabilitation programs, leading to fully autonomous rehabilitation. The data could become a base to train artificial neural networks for self-reliant physiotherapy sessions. Moreover, the digital twin can be transferred to virtual reality, increasing patient engagement and improving feedback from the physiotherapist [1].

References:
[1] Falkowski P, Osiak T, Wilk J, Prokopiuk N, Leczkowski B, Pilat Z, Rzymkowski C. Study on the Applicability of Digital Twins for Home Remote Motor Rehabilitation. *Sensors*. 2023; 23(2):911.

Numerical simulations and experimental research of hemolysis in atherosclerosis

Krystian Jędrzejczak[1], Arkadiusz Antonowicz[1,2], Krzysztof Wojtas[1], Wojciech Orciuch[1], Michał Kozłowski[3],
Łukasz Makowski[1]

[1] Faculty of Chemical and Process Engineering, Warsaw University of Technology, Waryńskiego 1,
00‑645 Warsaw, Poland

[2] Eurotek International Ltd., Skrzetuskiego 6, 02‑726 Warsaw, Poland

[3] Department of Cardiology and Structural Heart Diseases, Medical University of Silesia, Ziołowa 47,
40‑635 Katowice, Poland

Email of Corresponding Author: krystian.jedrzejczak.dokt@pw.edu.pl

According to the World Health Organization, cardiovascular diseases are one of the leading causes of death worldwide. One of the most common circulatory system diseases is atherosclerosis, caused by the deposition of cholesterol deposits in the space of blood vessels, causing a reduction in the cross-sectional area of the blood vessel and consequently leading to hemolysis or blockage of blood flow through the vessel. Engineers can help understand the mechanisms involved in the hemolysis of blood induced by high shear stresses in the area of cholesterol constrictions. Today's medical equipment allows imaging of individual blood vessels with sufficient accuracy to create numerical grids for CFD software and to print blood vessel models necessary for experimental flow field measurements using µPIV equipment. The study aims to describe the relationship between the shape of the cholesterol stenosis and the risk of hemolysis.

The research was carried out both *in silico* and experimentally. µPIV measurements were used to validate the results obtained in the CFD simulation. A solution of water, glycerin, and sodium iodide was used to obtain a fluid with rheology similar to blood [1] and a refractive index identical to the three-dimensional model obtained from 3D printing [2]. The dynamic viscosity was measured using an Anton Paar MCR302 rotational rheometer. The density was measured using a pycnometer. It was decided to adjust the kinematic viscosity [1] due to the need to add NaI to obtain the appropriate refractive index. µPIV measurements were made possible by adding seed particles with surface-deposited Rhodamine B [2]. The system for µPIV measurements consisted of a syringe pump, a laser, the measured system, and a microscope with a camera. The obtained flow field distributions were then compared with the results of CFD simulations.

Apart from the flow field numerical simulations, the hemolysis of blood was analyzed by implementing a blood rheology model based on population balance [3], which enables the modeling of blood hemolysis and physiological processes related to agglomeration and deagglomeration of red blood cells depending on local shear stresses. Based on several numerical simulations for a wide range of variants of cholesterol stenoses, the relationship between the shape of the stenosis and the risk of hemolysis was developed.

The measurement system was developed to study the flow field for blood flows similar to those in the human circulatory system. Possibilities of a new blood rheological model based on population balance in modeling physiological processes, including hemolysis, were presented. Furthermore, the usefulness of 3D printing in biomedical issues was demonstrated. Finally, the obtained correlations will allow for a better understanding of the mechanisms responsible for blood hemolysis in patients with atherosclerosis and help clinicians diagnose during medical practice.

References:
[1] M. R. Najjari, J. A. Hinke, K. V. Bulusu, and M. W. Plesniak, "On the rheology of refractive-index-matched, non-Newtonian blood-analog fluids for PIV experiments," Experiments in Fluids, vol. 57, no. 6. Springer Verlag, Jun. 01, 2016. doi: 10.1007/s00348-016-2185-x.
[2] A. Antonowicz, K. Wojtas, Ł. Makowski, W. Orciuch, and M. Kozłowski, "Particle Image Velocimetry of 3D-Printed Anatomical Blood Vascular Models Affected by Atherosclerosis," Materials, vol. 16, no. 3, p. 1055, Jan. 2023, doi: 10.3390/ma16031055.
[3] K. Jędrzejczak, Ł. Makowski, and W. Orciuch, "Model of blood rheology including hemolysis based on population balance," Commun Nonlinear Sci Numer Simul, vol. 116, p. 106802, Jan. 2023, doi: 10.1016/J.CNSNS.2022.106802.

Recommendation system in medical applications

Anna Kasperczuk (1a), Agnieszka Dardzińska-Głębocka (1b)Institution
1 Faculty of Mechanical Engineering, Institute of Biomedical Engineering(1a)
Institute of Mechanical Engineering(1b), Bialystok University of Technology,
a.kasperczuk@pb.edu.pl

Inflammatory Bowel Diseases (IBD), among which Ulcerative Colitis (UC) and Crohn's disease (CD) can be distinguished, are the subject of many studies. Despite many years of research on IBD, they are still of interest to scientists today.CD and UC have been known by doctors for many years. One of the first clear descriptions of UC in the medical literature was Wilkes' work published in 1859. Crohn's disease was officially described later by the research team, which included Crohn, Ginzburg and Gordon Oppenheimer, in 1932 [1].

It is important to look for new factors that differentiate the disorder and check the relationship between them. The obtained information will help to better understand UC and CD. Our paper attempts to model the medical diagnostic process, based on logistic model, which helps in the correct classification of the two subtypes of IBD [2].

In order to test the accuracy of the constructed logistic model, a matrix of error was used. We use some statistics, [3] (Sensitivity (TPR), Specificity (TNR)).

In the first group, UC was diagnosed (N = 86, women N = 32, men N = 54), while in the second group patients with CD (N = 66, women N = 32, men N = 34) where diagnosed. The age in the study group was 38.05 ± 16.57, where the average age of women was 35.97 ± 15.56 and for men was respectively 39.57 ± 17.19. The mean age in the CD group was 34.42 ± 14.30 (mean age of women 36.19 ± 16.90, men 32.76 ± 11.34). The mean age in the group of UC patients was 40.84 ± 17.70 (mean age of women 35.75 ± 14.37, men 43.85 ± 18.88).

The constructed model was trained on 90% of available patient cases, while it was tested on 10% of all available cases (cross-validation method). The cross-validation method (10-fold) was used to select specific model parameters. The results presented below refer to the model constructed after introducing variables that were significantly different in the analyzed groups. These variables were previously subjected to significance tests. For the proposed model OR values significantly different from 1 were obtained for the attribute current/past smoker (OR = 0.012, 95% CI: $0.001 \div 0.023$). This means that smokers are more likely to suffer from CD. Another feature is blood in the stool. In this case, OR = 14.454, 95% CI: $14.324 \div 14.658$, which means that the phenomenon of bloody stools is much more likely to signify UC than CD. The occurrence of stools with blood increases the likelihood of UC by about 15 times. In the case of MCV, an increase in its value should qualify the patient for ulcerative colitis. Similar results were obtained for PLT, monocytes, eosinophils, basophils. In the case of neutrophils, an increase in their values should cause the patient to be classified in the group with CD disease.

This paper proposes a way of combining two approaches to data analysis (statistical analysis and exploration algorithms) by using statistical methods to search for significantly important knowledge, which is then directly applied to exploration methods. Our study included 152 patients with CD or UC. The data collected included not only biochemical blood parameters, but also very subjective information such as interview data. The built-in classification model was able to assign patients to the appropriate group with very high precision (sensitivity = 0.84, specificity =0.74, AUC = 0.93). The constructed model was able to distinguish ulcerative colitis from Crohn's disease.

References:
[1] Connelly, T.M.; Koltun W.A. The cancer "fear" in IBD patients: is it still real? J Gastrointest Surg 2014, 18, pp. 213-218.
[2] Daniluk, J.; Daniluk, U.; Reszec, J.; Rusak, M.; Dabrowska, M.; Dabrowski, A. Protective effect of cigarette smoke on
the course of dextran sulfate sodium-induced colitis is accompanied by lymphocyte subpopulation changes in the blood and colon. Int J Colorectal Dis 2017, 32, 1551-1559.
[3] Kasperczuk, A.; Dardzinska, A. Comparative evaluation of the different data mining techniques used for the medical database. Acta Mech Autom 2016, 10, 233-238.

Numerical models and measurement validation
for inverse estimation of local stiffness of human artery walls

Ziemowit Ostrowski[1], Aleksander Sinek[1,2], Mateusz Mesek[1,2], Marek Rojczyk[1],
Jan Juszczyk[3], Ewa Piętka[3], Wojciech P. Adamczyk[1], Jacob Sturdy[2], Friederike Schäfer[2],
Bartłomiej Melka[1], Adam Golda[4], Michał Nowok[4], Leif Rune Hellevik[2], Ryszard Białecki[1]

[1]Silesian University of Technology, Department of Thermal Technology,
Konarskiego 22, 44-100 Gliwice, Poland
[2]Norwegian University of Science and Technology, Department of Structural Engineering,
Richard Birkelands vei 1a, NO-7491 Trondheim, Norway
[3]Silesian University of Technology, Department of Informatics and Medical Devices,
Roosevelta 40, 41-800 Zabrze, Poland
[4]Gliwice Municipal Hospital No. 4, Cardiology Ward,
Zygmunta Starego 20, 44-100 Gliwice, Poland
ziemowit.ostrowski@polsl.pl

Increased stiffness of the artery wall, by reducing the absorption ability of pressure pulse, is changing the way how reflected pressure waves are propagated, and in turn is increasing the pumping work of the left ventricle. This causes, among others, the damage of tissues and organs, hypertension, or cardiac hypertrophy. Therefore arterial stiffness has been established as a predictor of cardiovascular risk. A non-invasive method for estimating local arterial stiffness is proposed. The currently available methods focus on estimating Pulse Wave Velocity (PWV), a carotid-femoral technique, but it has limited diagnostic power due to a lack of indication of local variations in stiffness along the arterial tree.

The purpose of the research is to propose and validate the method that is based solely on the ultrasound-measured displacements of the artery wall itself, followed by an inverse estimation of its mechanical properties. The research aims to solve the inverse problem of the fluid-structure interaction (FSI) task of blood flow in deforming blood vessels. The method is tested for both full 3D (CFD-FSI) and 1D numerical models.
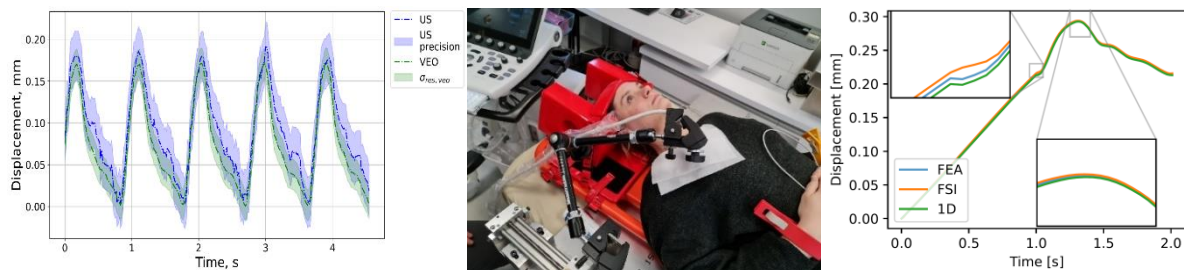
Fig. 1. Comparison of ultrasound (US) and optical (VEO) measured deformation and their uncertainties [1] (left). Medical experiment – ultrasound measurements of deformations of the carotid artery *(centre)*. Modelled deformation of inner artery wall at mid-length for full 3D & 1D models for nonlinear hyperelastic Holzapfel-Gasser-Ogden material model (right).

A novelty in this research is the idea of determining the stiffness of the elastic channel by solving the problem of inverse CFD-FSI and the method of measuring deformation using an ultrasound device. Unlike in most works, the arterial wall is modelled using advanced hyperelastic material models, that describe better the behaviour of the arterial wall tissue.

References:
[1] A. Sinek, M. Mesek, M. Rojczyk, J. Juszczyk, W.P. Adamczyk, J. Sturdy, B. Melka, A. Golda, M. Nowok, Z. Ostrowski, R. Białecki Evaluating the precision and reproducibility of non-invasive deformation measurements in an arterial phantom, *Measurement*, 2023, vol. 216, pp.112904

Hybrid (physical-computational) modeling approach to study valvular heart diseases

Raman Pasledni[1], Maciej Kozarski[1], Jeremi Mizerski[2], Piotr Okrzeja[1], Marek Darowski[1], Krzysztof Zieliński[1]

[1] Nalecz Institute of Biocybernetics and Biomedical Engineering, Polish Academy of Sciences, Ks. Trojdena 4, 02109 Warsaw, Poland

[2] Department of Cardiac Surgery SPSW im. Papieża Jana Pawła II w Zamościu, Aleje Jana Pawła II 10 22-400 Zamość, Poland

e-mail: rpasledni@ibib.waw.pl

Aims: Valvular heart disease (VHD) is a frequent cause of mortality in the world. The most common VHD are aortic stenosis (AS) and mitral regurgitation (MR) [1]. To understand and evaluate the impact of VHD on the hemodynamics of the circulatory system, it is first necessary to create models of heart valve diseases. Therefore, the main aim of the study was to develop physical models of VHD, such as AS and MR. Another important aspect of the study was the use of these physical models of VHD in a hybrid (physical-computational) cardiovascular simulator [2] to modeling cases of heart failure. The severity of VHD was analyzed in terms of transvalvular pressure gradient, aortic valve area (AVA) and mitral regurgitant orifice area (MRA).

Methods: In this study, physical models of valve regurgitation and valve stenosis were developed. The valve regurgitation model is a special mechanical device that acts as a bypass for the heart valve. In addition, to simulate varying degrees of severity of valvular regurgitation, it is possible to change diaphragms with different diameters of the passage orifice (0.2 – 0.8 cm with a step of 0.1 cm). The physical model of valve stenosis is a mechanical device that allows to place diaphragms with different orifice diameters (0.4 - 1.6 cm with a step of 0.2 cm) near the heart valve. Björk-Shiley mechanical heart valves were used as aortic and mitral valves. The simulation was performed on a hybrid simulator with installed physical models of VHD.
The Gorlin equation was used to quantify the degree of AS and MR. According to which AVA is calculated by the formula:

$$AVA = \frac{Q_{mean}}{44.3 * \sqrt{\Delta P_{mean}}}$$

where Q_{mean} is mean aortic valve flow, ΔP_{mean} - mean transaortic gradient.
The Gorlin equation for calculating MVA is as follows:

$$MRA = \left(\frac{RV}{RT}\right) / C\sqrt{SPG}$$

where MRA – mean mitral regurgitant orifice area, RV - regurgitant volume, RT – regurgitant time, SPG - mean systolic pressure gradient between the left ventricle and left atrium, C is a constant.

Results: The preliminary simulation results showed that the system is behaving correctly. In the case of AS, left ventricular pressure increased and aortic pressure decreased with increasing severity of AS. The mean pulmonary arterial pressure was increased due to an increase in left ventricular preload. The calculated values of AVA are in line with the American Heart Association (AHA) guidelines. In the case of MR, left ventricular pressure decreased and left atrial pressure increased with increasing severity of MR. The relative measurement error of the MRA decreases with the severity of MR, i.e. with an increase in the diameter of the mitral valve regurgitation orifice.

Conclusions: The hybrid cardiovascular simulator was adapted to perform simulations of the circulatory system using two artificial valves – mitral and aortic. Two physical models of VHD were developed, namely valve stenosis and regurgitation. The simulation results are generally consistent with clinical data.

References:
[1] Iung B, Delgado V, Rosenhek R, et al. Contemporary Presentation and Management of Valvular Heart Disease: The EURObservational Research Programme Valvular Heart Disease II Survey. Circulation. 2019;140(14):1156-1169.
[2] Darowski M, Kozarski M, Ferrari G, et al. A new hybrid (hydro-numerical) model of the circulatory system. Bull. Pol. Ac. Tech. 2013;**61**(4):993–1003.

Simulation of the long-term effect of bicarbonate profiling in hemodialysis

Mauro Pietribiasi, Jacek Waniewski, John K. Leypoldt
Nalecz Institute of Biocybernetics and Biomedical Engineering PAS (Trojdena 4, 02-109 Warsaw)
mpietribiasi@ibib.waw.pl

The delivery of bicarbonate to chronic end-stage renal disease patients is a fundamental component of hemodialysis (HD) treatment. The failing kidneys lose the capacity to preserve the acid-base equilibrium of bodily fluids and chronic acidemia is developed. During HD bicarbonate levels are restored via diffusion from the dialysis fluid, replenishing the main acid-base buffer of the body. It was observed by several authors that blood bicarbonate concentration (C_B) increases primarily in the first 90 minutes of HD, and bicarbonate transport during the rest of the session elicits more endogenous organic acid production to neutralize it. Therefore, Marano et a recently presented a bicarbonate profiling protocol aimed at achieving a more linear increase in C_B during an HD session while reaching the same C_B post-HD [1]. This was done through 8 steps of increasing dialysis fluid bicarbonate concentration (C_D), from 25 to 32 mEq/L. We used a computational model to predict the long-term effect of such a protocol on C_B and pH, and compared it with another suggested, simpler, protocol.

The model simulates the transport of bicarbonate and dissolved CO_2 from the dialyzer to an arteriovenous fistula, and its impact on the many variables defining the acid-base equilibrium is predicted solving a system of biochemical and biophysical equations in each of four body compartments (venous and arterial blood pools, interstitial spaces and tissue cells, lungs capillaries) [2]. Model and patient's parameters were based on the average of data collected in a recent clinical study carried out in Warsaw. We simulated a standard treatment (C_D = 32 mEq/L), Marano's protocol (Treatment A), and a new protocol (Treatment B) involving a single step increase after 2 hours (C_D from 28 to 32 mEq/L). Four consecutive weeks of thrice-weekly HD were simulated for each protocol.

The model predicted a stable cycle, with the same pre-HD C_B reached before each new week, for each treatment. Because of a lower C_B reached at the end of each session compared to the standard treatment, pre-HD C_B for Treatment A was consistently lower as well, by 1.4 mEq/L and for Treatment B by 0.27 mEq/L. Bicarbonate mass exchanged in each session is reported in Table 1.

Table 1. Bicarbonate mass transferred during the sessions of the first week (in mEq). Values in the following weeks were similar.

	HD1	HD2	HD3
Standard	229.59	198.33	196.76
Treatment A	204.29	195.71	195.01
Treatment B	223.95	197.34	195.93

The simulation of Treatment B resulted in an intradialytic profile of C_B closer to a linear increase compared to the standard treatment, while delivering to the patient a similar amount of buffer base and reaching similar post-HD C_B values. Numerically, the differences in concentrations and transported mass between treatments are small enough to cast doubts on their clinical significance. Both simulated protocols resulted in stable acid-base equilibrium after a month of therapy. In conclusion, all factors being equal, the relative complexity of Treatment A makes the more practical Treatment B a viable alternative to obtain a more regular increase of blood bicarbonate during the HD session.

References:
[1] S. Marano, M. Marano and F. J. Gennari, "A New Approach to Bicarbonate Addition During Hemodialysis: Testing Model Predictions in a Patient Cohort," in IEEE Access, vol. 10, pp. 17473-17483, 2022.
[2] S.E. Rees and S. Andreassen, Mathematical Models of Oxygen and Carbon Dioxide Storage and Transport: The Acid-Base Chemistry of Blood. *Crit Rev Biomed Eng* 33(3), 209-264 2005.

Prediction of VO$_2$peak using cardiorespiratory parameters from treadmill maximal exercise test up to 85% of maximal heart rate

Maciej Rosoł[1*], Marcel Młyńczak[1], Monika Petelczyc[2], Jakub S. Gąsior[3], Gerard Cybulski[1]

[1] Faculty of Mechatronics, Warsaw University of Technology
[2] Faculty of Physics, Warsaw University of Technology
[3] Department of Pediatric Cardiology and General Pediatrics, Medical University of Warsaw
*maciej.rosol.dokt@pw.edu.pl

Treadmill Maximal Exercise Test (TMET) is a popular method for the assessment of athlete's maximum oxygen uptake, response to effort and monitoring of the training progress. As maximal test, it is performed until exhaustion and poses an unnecessary risk of injury, therefore, new methods and tools for accurate but less-fatiguing assessments are developed. In this paper, we analyzed the possibility to predict VO$_2$peak using cardiorespiratory parameters based on the part of the TMET up to 85% of maximal heart rate (HR), as well as the importance of including respiratory measurement in ramp exercise testing in terms of VO$_2$peak prediction. The analysis was performed using 371 TMET recordings previously published by *Mongin et al.* [1,2]. The population of the study was limited to the subjects aged between 18 and 40 years old excluding individuals outlying in terms of height, weight and VO$_2$peak (based on interquartile range method). Cardiac (based on HR) and respiratory (based on respiratory rate and pulmonary ventilation) parameters were calculated from the start of the TMET until each subject reached 85% of their maximal HR. For each recording, the VO$_2$peak was predicted two times. The first prediction was made according to approach 1 (A1) with only demographic (age, weight, height, sex) and cardiac parameters as input data for the machine learning model, and another was done based on approach 2 (A2) with all previously used parameters as well as respiratory ones as input data. It was undertaken to examine whether the inclusion of respiratory-based parameters improves the quality of the prediction and thus to evaluate the predictive utility of respiratory parameters in the presented setting. Various machine learning models, including Support Vector Regression, Random Forests, Lasso and Ridge regression, Artificial Neural Networks and others, were tested for prediction. The predictions were assessed using the mean absolute percentage error (MAPE), mean absolute error (MAE) and R^2 score (metrics). The 10-fold cross-validation technique was used to estimate the prediction results, where after each iteration the metrics were calculated and stored. Metrics for both datasets were compared using Wilcoxon signed-rank test to check whether including respiratory parameters improves the prediction of VO$_2$peak. The significance level was set to 0.05. Analysis was performed using Python version 3.9.13. The mean $\pm$ standard deviation of metrics values obtained from the cross-validation for both modeling approaches and the p-values obtained from the Wilcoxon signed-rank test are presented in Table 1.

Table 1. Statistics of prediction performance results obtained in the analysis of two approaches considered.

	MAPE	MAE	R^2 score
A1	11.87 ± 1.78	5.21 ± 0.64	0.31 ± 0.14
A2	11.04 ± 1.75	4.85 ± 0.60	0.41 ± 0.13
p-value	0.014 *	<0.001 ***	0.002 **

All metrics were significantly better for the models incorporating respiratory-based parameters as their input. Thus, it might be said that including the respiratory parameters improves the quality of the prediction of the VO$_2$peak (in particular, the improvement in the R2 score is over 30%). Those results emphasize the importance of monitoring respiratory activity during ramp exercise tests. The VO$_2$peak might be estimated based on the cardiorespiratory parameters, but the accuracy of the prediction needs further improvement to be used in everyday practice. The main limitation of this study is a small number of analyzed recording and lack of typically used HRV parameters included in the analysis as raw ECG signals were not available. The possibility of a more accurate prediction needs further investigation preferably with a wider range of HRV parameters for the first approach as well as with causal or information domain parameters quantifying cardiorespiratory dependencies for the second approach.

References:
[1] Mongin, D., et al. (2021). Treadmill Maximal Exercise Tests from the Exercise Physiology and Human Performance Lab of the University of Malaga (version 1.0.1). PhysioNet. https://doi.org/10.13026/7ezk-j442 [Accessed: 29.05.2023].
[2] Mongin, D., et al. (2021). Heart rate recovery to assess fitness: comparison of different calculation methods in a large cross-sectional study, Research in Sports Medicine, DOI: 10.1080/15438627.2021.1954513

On the minimal model for enzymatic cleavage of glucose polymers during peritoneal dialysis with icodextrin – based dialysis fluid

Joanna Stachowska-Pietka[1], Jacek Waniewski[1], Anna Olszowska[2], Elvia Garcia-Lopez[3], Zofia Wankowicz[2], Bengt Lindholm[3]

[1] Nalecz Institute of Biocybernetics and Biomedical Engineering, Polish Academy of Sciences, Ks. Trojdena 4, 02-109 Warsaw, Poland. [2] Military Institute of Medicine, Central Hospital of the Ministry of Public Defence, Warsaw, Poland. [3] Department of Clinical Science, Intervention and Technology, Division of Renal Medicine and Baxter Novum, Karolinska Institutet, Stockholm, Sweden.
Email of Corresponding Author: jwaniewski@ibib.waw.pl

A mixture of glucose polymers, called icodextrin, is applied as an osmotic agent during peritoneal dialysis (PD) with prolonged effect on ultrafiltration to the peritoneal cavity. Glucose polymers (dextrins) are cleaved in blood and body fluids by the enzyme alpha-amylase, which can leak also to dialysis fluid in the peritoneal cavity from blood. Two attempts to model the activity of alpha-amylase in icodextrin-based dialysis fluid were presented previously, and both were adjusted to the measured icodextrin fractions [1, 2]. We present here a simple model of fluid and mass transport during PD combined with the reduction of icodextrin fractions' concentrations related to the enzyme activity. The previous models assumed more sophisticated patterns of cleavage with the products accumulated in two lowest fractions [1], or possibly in any fraction of molecules with lower molecular mass (MW) than the cleaved molecule [2]. Our model allows for estimation of the removal of each fraction from the peritoneal cavity by transport mechanisms (diffusion to the tissue and convective absorption to the tissue and by lymphatic vessels) and by its cleavage to polymers of lower MW attributed to the fraction of dextrins of lowest MW without attempting to model detailed hydrolysis patterns.

The model was based on the three pore model for the transport of fluid, small solutes and icodextrin fractions across the peritoneal transport barrier between blood and dialysis fluid in the peritoneal cavity. The kinetics of each icodextrin fraction in dialysis fluid was in addition supplemented by a dynamics related to the cleavage clearance of the fraction, dependent on the concentration of alpha-amylase in dialysis fluid, with the degradation to the lowest MW fraction, cf. [1, 2] for alternative description. The data from clinical study on 16 hour peritoneal dwells with icodextrin-based dialysis fluid in 11 PD patients were used for the estimation of the model parameters [2]. Fluid volume (using a macromolecular volume marker), small solute concentrations and concentrations of seven icodextrin fractions (calculated from chromatograms with the following MW cut-off values: up to 1.08 kDa (Fraction 1), 4.44 kDa (Fraction 2), 9.89 kDa (Fraction 3), 21.4 kDa (Fraction 4), 43.5 kDa (Fraction 5), 66.7 kDa (Fraction 6), and over 66.7 kDa (Fraction 7) were frequently measured [2]. Besides the transport parameters, the time dependent cleavage clearances $K_i = k_i * V_D(t) * C_{am}(t)$ (in mL/parameters) with the estimated constant degradation rates k_i, calculated dialysis fluid volume $V_D(t)$, and measured alpha-amylase concentration $C_{am}(t)$ in dialysis fluid, were assessed for $i = 1, \ldots, 7$. It was assumed that cleavage products accumulated only in Fraction 1.

The minimal model provided a good fit of the modelled profiles of fluid volume and solute concentrations to the clinical data. The cleavage clearances K_i substantially increased with dwell time for all icodextrin fractions $i = 1, \ldots, 7$. The highest parameters k_i were estimated for fractions $i = 7, 6, 5$ and 1, whereas the cleavage clearances for fractions $i = 2, 3$, and 4 were considerably lower than for the other fractions. The diffusive transport coefficient for fraction 4 was lower than that expected based on its molecular weight.

We conclude that the minimal model can describe the measured profiles of fluid, solutes and icodextrin fractions with high accuracy in spite of much simplified description of the activity of alpha-amylase in dialysis fluid.

[1] Akonur, A., Holmes, C. J. & Leypoldt, J. K. Predicting the peritoneal absorption of icodextrin in rats and humans including the effect of alpha-amylase activity in dialysate. Perit. Dial. Int. (2015) 35, 288–296. https://doi.org/10. 3747/pdi.2012.00247
[2] Stachowska-Pietka, J., Waniewski, J., Olszowska, A., Garcia-Lopez, E., Wankowicz, Z., Lindholm, B. Modelling of icodextrin hydrolysis and kinetics during peritoneal dialysis. Sci. Rep. (2023) 13:6526 https://doi.org/10.1038/s41598-023-33480-w

Modelling and finite element analysis of HAP-Ti FGM material for biomedical applications

Krzysztof Szymkiewicz
Cracow University of Technology,
Department of Applied Mechanics and Biomechanics, 24 Warszawska st., 31-155 Kraków, Poland
krzysztof.szymkiewicz@pk.edu.pl

Introduction

Pure titanium (Ti) belongs to the material with high specific strength and corrosion resistance, as well as high biocompatibility, therefore, it is successfully applied in medicine as implants. Such elements are usually coated with a biocompatible hydroxyapatite (HAP) layer in order to improve adhesion of bone to implant and support bone self-healing processes. Nevertheless titanium has relatively high Young's modulus compared to bone tissue, which could contribute to formation of stress shielding and as a consequence implant loosening. It seems to be that the appropriate way to limit this drawback might be production of functionally graded materials (FGM) constituting the group of unhomogenous composites, which exhibit outstanding properties. The FGM are composed of at least two materials with variable chemical composition thereby different properties in a given direction. FGM materials are characterized by better mechanical and functional properties than each component considered separately. The suitable candidate for biomedical application could be functionally graded HAP/Titanium material. The proposed FGM material might interact better with surrounding tissue. Nevertheless, the knowledge of generating stresses and strains under the influence of loads during work of such parts is necessary. Therefore, the aim of the presented work was micromechanical modeling of HAP-Ti FGM plate and then analysis of stress, strain and deformation with the help of finite element method (FEM). The investigations were performed assuming loads and boundary conditions similar to elements used as medical implant.

Methods

The properties of modelled FG material like density, Young's modulus, Poisson's coefficient were determined with the help of rule of mixture. The HAP-Ti plate was rectangular in shape with dimensions 100, 10[mm] and 4[mm] of thickness. The plate had layered structure and was composed from 10 up to 20 layers. The element was subjected to a force applied in a perpendicular direction to the plate surface. The FEA analysis was carried out with the use of Ansys Workbench 2021 software. The analysis was performed for different mesh density values (number of elements), aimed to validations convergence of obtained results.

Results and conlusions

The preliminary results of studies helped to establish that stress in HAP/Ti plate increases along the cross section of the element. The maximum values of stress was observed at the bottom part of element. Strain deformations occur on the bottom edges of the plate. FEA analysis did not reveal significant deformations of the HAP-Ti part and the obtained values of total deformation were low. To sum up, the finite element analysis allowed to reveal the effect of gradation degree of materials, boundary conditions, volume fraction distribution and geometry on stress and deformation of considered HAP-Ti FGM plate.

References
[1] U.K. Kar, J.Srinivas, Material modelling and analysis of hydroxyapatite/titanium FGM plate under thermo-mechanical loading conditions, *Materials Today: Proceedings*, 2019, 33, 5498-5504
[2] S.N.S. Jamaludin et al., Three-Dimensional Finite Element Modeling of Thermomechanical Problems in Functionally Graded Hydroxyapatite-Titanium Plate, *Mathematical Problems in Engineering*, 2014, 371462

Tympanic membrane displacement may non-invasively measure a rise in intracranial pressure

Agnieszka Uryga[1], Agnieszka Kazimierska[1], Arkadiusz Ziółkowski[1], Klaudia Kalinowska[1], Mateusz Popek[1], Marek Czosnyka[2,3], Magdalena Kasprowicz[1]

1. Department of Biomedical Engineering, Wroclaw University of Science and Technology, Wybrzeże Wyspiańskiego 27, 50-370 Wroclaw, Poland
2. Brain Physics Laboratory, Division of Neurosurgery, Department of Clinical Neurosciences, Addenbrooke's Hospital, University of Cambridge, Cambridge, UK
3. Institute of Electronic Systems, Faculty of Electronics and Information Technology, Warsaw University of Technology, Warsaw, Poland
agnieszka.uryga@pwr.edu.pl

Invasive intracranial pressure (ICP) monitoring is restricted to patients with severe neurological diseases. The observation of tympanic membrane displacement (TMD) opens up the possibility of indirect ICP estimation [1]. When the conventional technique for TMD assessment requires sealing of the ear in an air-tight fashion for the displacements to be detected, a promising method could be a phase-based video motion magnification (VMM) algorithm. This study presents a proof-of-concept for monitoring TMD during jugular vein compression in healthy volunteers using the VMM method.

15 healthy volunteers (8 females, 7 males, median age: 24, range 18–35 years) were included in the analysis. The video recording of the tympanic membrane was captured using a portable videoscope (Hearscope, HearX group, Pretoria, South Africa) with a framerate of 30 fps. The videoscope was stabilized using a custom-made fixation system to avoid auto-focus adjustments. Jugular vein compression has been achieved during Queckenstedt's manoeuvre, which by obstructing the cephalic venous return, increases the ICP. Non-invasive arterial blood pressure (ABP) measurement was performed using a photoplethysmograph (Finometer MIDI, FMS Medical Systems, Amsterdam, The Netherlands). Heart rate (HR) was calculated using the spectral position of the peak associated with the first harmonic of ABP. During the measurement, a volunteer was sitting on a chair in a straight-back position. First, a 5 min baseline recording was made with the volunteer. Then the sphygmomanometer cuff attached to the neck was inflated to 30 mm Hg for the next 5 minutes. After that, the cuff was deflated and the signals were measured for 5 minutes. During each stage, a single 15-second-long video recording of the tympanic membrane was performed. VMM analysis was performed using a custom-written algorithm based on open-source code [2]. The spectral amplitude of TMD (Amp_TMD) was estimated using Fast Fourier Transform in the HR-related frequency range (0.66-3.0 Hz). The Bioethics Committee approved the research protocol (approval no. KB-635/2022). This work was supported by the National Science Centre, Poland (grant no. UMO-2019/35/B/ST7/00500).

The Amp_TMD waveform changed during a neck-cuff test ($p < 0.001$) and was as follows [um]: baseline: 1.0 ± 2.0, cuff inflated: 3.6 ± 4.5, cuff deflated: 1.5 ± 1.4. In comparison with the baseline, the Amp_TMD waveform increased significantly during the inflation of the neck cuff ($p < 0.001$) and returned to the basic level during cuff deflation ($p = 0.529$). In the whole group, jugular vein compression did not influence significantly ABP [mm Hg] (baseline: 70 ± 31, cuff inflated: 53 ± 16, cuff deflated: 60 ± 18, $p = 0.410$), and HR [bpm] (baseline: 77 ± 30, cuff inflated: 80 ± 24, cuff deflated: 79 ± 18; $p = 0.105$).

Our pilot study demonstrates the potential of using the VMM technique to estimate changes in TMD caused by impaired venous return increasing ICP. If this method were to be confirmed on a larger group of healthy volunteers and patients with intracranial pathologies, it could be used as a low-cost diagnostic tool for screening patients with a risk of intracranial hypertension.

References:
[1] Lang EW, Paulat K, Witte C, Zolondz J, Mehdorn HM. Noninvasive intracranial compliance monitoring. Technical note and clinical results. J Neurosurg. 2003; 98(1):214-8.
[2] Popek, M. P., Danielewska, M. E., & Iskander, D. R. (2017). Assessing the feasibility of the use of video motion magnification for measuring microdisplacements. IEEE Transactions on Instrumentation and Measurement, 66(9), 2329–2336.

Generalized Gibbs-Donnan factors for equilibrium in permselective membrane systems

Jacek Waniewski

Nalecz Institute of Biocybernetics and Biomedical Engineering, Polish Academy of Sciences, Ks. Trojdena 4, 02-109 Warsaw, Poland

jwaniewski@ibib.waw.pl

The Gibbs-Donnan (G-D) factors describe the ratio of permeating ion concentrations (in general different from 1) at both sides of the permselective membrane if the solutions contain also ions that do not permeate the membrane (non-permeating ions). The standard approach relates the equilibrium difference in permeating ions concentrations to the electrostatic (Nernst) potential, see [1] for the general formulation. However, the presence in the solutions of non-permeating ions evokes also osmotic pressure, and the similar problem may be formulated for electrically neutral solutes. We present here a general approach that is valid for any number of charged and neutral solutes and provides equations that allow for the calculation of generalized Gibbs-Donnan factors that take into account both electrostatic field and osmotic pressure.

The theory is based on three principles: 1) the balance of mass (molar fractions of all solutes sum up to 1 at each side of the membrane), 2) the electroneutrality (the total electric charge of the solution at each side of the membrane is equal to 0), and 3) the thermodynamic law of the equilibration of electro-chemical potential of each solute (including solvent) at both sides of the membrane. The application of these principles provides two algebraic equations for two variables $x = \exp(-z_{ref} \cdot F \cdot \Delta F_i / RT)$ and $y = \exp(-V_w \cdot \Delta P / RT)$, where z_{ref} is the charge number of a reference permeating ion, ΔF_i is the intercompartment difference in equilibrium electrostatic potential, V_w is molar partial volume of the solvent (or any reference neutral solute), and ΔP is the intercompartment difference in equilibrium hydrostatic pressure (i.e., – osmotic pressure difference). It is assumed that the activities (molar fractions for ideal solutions), a_{1i}, are known at one side of the membrane (compartment 1) for all species i, and at the other side (compartment 2) we know only the amount of non-permeating species, and want to estimate the activities a_{2i} of the permeating species. The ratio $DF_i = a_{2i}/a_{1i}$ defines the (generalized) Gibbs-Donnan factor for permeating species i, and can be calculated as $DF_i = x^{(z_i/z_1)} \cdot y^{(V_i/V_w)}$ if the equations for x and y are solved.

The theory applied for ideal solutions provides much better approximation for osmotic pressure than the linear van't Hoff rule for concentrations of non-permeating species, for example for the solution of albumin and NaCl in water:
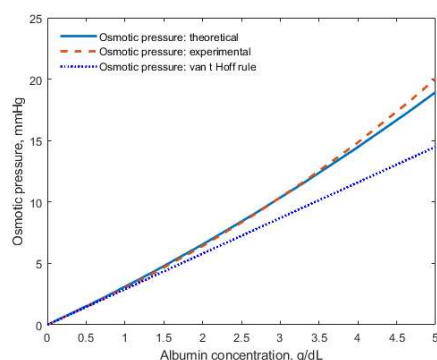
Figure 1. Osmotic pressure of albumin in saline as a function of albumin concentration up to physiological level of albumin in plasma.

In general, the contribution of y term to D-F factors for small ions and osmotic pressure of interest in physiology is negligible, so the standard theory of G-D factors, c.f. [1], is approximately valid, but for small charged proteins permeating across the membrane the y term in D-F factors may get important, especially for higher, pathological or experimental, osmotic pressures of large, non-permeating proteins. The theory provides similar conclusions for neutral solutes of low, middle and large molecular weight.

[1] Waniewski J, Pietribiasi M, Pstras L. Calculation of the Gibbs-Donnan factors for multi-ion solutions with non-permeating charge on both sides of a permselective membrane. Sci Rep 11, 22150 (2021). https://doi.org/10.1038/s41598-021-00899-y

A Model of Cerebral Hemodynamics Incorporating Interstitial Fluid Flow in Cerebral Edema

Kamil Wołos, Jan Poleszczuk

Nalecz Institute of Biocybernetics and Biomedical Engineering, Księcia Trojdena 4 st, Warsaw

Email of Corresponding Author: kwolos@ibib.waw.pl

Aims

Cerebral edema is a pathological state which occurs after brain injuries. We traditionally distinguish two major sub-types of cerebral edemas, vasogenic and cytotoxic. Vasogenic edema is related to the disruption of the blood-brain barrier and extracellular accumulation of fluid in extracellular space in the brain tissue, while cytotoxic edema is linked with cell swelling due to cerebral ischemia. Both cases cause an increase in the brain volume. According to the Monro-Kellie doctrine sum of the volumes of the brain, cerebrospinal fluid, and intracranial blood remains constant and thus, an increase in one should cause a decrease in one or both of the remaining two. This also has an influence on pressures in the intracranial space. Mathematical modeling can help to explain relations between these quantities, very often not measurable using standard medical devices.

There are many models in the literature describing cerebrovascular hemodynamics, [1], [2]. However, most of them do not incorporate edemas-related increase of brain volume. Zadka et. al. proposed a 0-dimensional model of intracranial hemodynamics, including such a type of mechanism but without autoregulation, [3]. Moreover, this model does not describe the pressure gradients, which may occur in different brain compartments. In our study, we sought to propose a model without above mentioned limitations based on the model previously developed by Ryu, [4].

Methods

The autoregulatory, six-regions model developed by Ryu has been connected with a 1D bifurcation tree describing blood flow in the human main systemic arteries up to the arteries placed in the circle of Willis. We added to the capillary compartment the 3-element Windkessel model characterizing flow between capillaries and brain tissue, bulk flow in the brain tissue, and compliance of the brain. We also proposed equations describing the dependence between brain volume and resistance against the flow in capillaries, veins, and interstitial fluid.

Results

For the intact brain, intracranial pressure (ICP) is about 8 mmHg for each compartment. Pressure at the arterioles, capillaries, and veins agrees with the data in the literature. The model can reproduce changes in ICP caused by cytotoxic and vasogenic edema. In both cases, we observe an abrupt rise in the ICP after occurring of the trauma. Moreover, it is possible to follow gradients of the pressures, flows, and changes in the brain volume between the six independent compartments. It is also possible to induce edemas at the different stages of pathological severity   by manipulating resistances describing blood brain barrier and bulk flow in the brain tissue.

Conclusion

Model is physiologically consistent with physiological knowledge, versatile and easily extensible to implement additional features like CO2 reactivity. It is able to reproduce vasogenic and cytotoxic edema, but also stable state of healthy patient. Model also allows individualization of parameters for a given patient. Due to that fact, after thorough validation with clinical data, it can be a helpful tool in assessing the patient's condition.

[1]   M. Ursino and M. Giannessi, "A model of cerebrovascular reactivity including the circle of willis and cortical anastomoses," *Ann Biomed Eng*, vol. 38, no. 3, pp. 955–974, Mar. 2010, doi: 10.1007/S10439-010-9923-7.

[2]   M. Ursino, A. Ter Minassian, C. A. Lodi, A. L. Beydon, A. Ter Minassian, and L. Bey, "Cerebral hemodynamics during arterial and CO 2 pressure changes: in vivo prediction by a mathematical model," 2000, Accessed: Apr. 25, 2023. [Online]. Available: http://www.ajpheart.org

[3]   O. Doron, Y. Zadka, O. Barnea, and G. Rosenthal, "Interactions of brain, blood, and CSF: a novel mathematical model of cerebral edema," *Fluids Barriers CNS*, vol. 18, no. 1, 2021, doi: 10.1186/s12987-021-00274-z.

[4]   J. Ryu, X. Hu, and S. C. Shadden, "A Coupled lumped-parameter and distributed network model for cerebral pulse-wave hemodynamics," *J Biomech Eng*, vol. 137, no. 10, Oct. 2015, doi: 10.1115/1.4031331/422046.

Microsimulation-based investigation of patient stratification strategies for periods of limited healthcare system capacity

Viktor Zaika[1], Jan Poleszczuk[2,*], Benjamin Misselwitz[1]

[1]Department of Visceral Surgery and Medicine, Inselspital Bern University Hospital, University of Bern, Bern, Switzerland

[2]Nalecz Institute of Biocybernetics and Biomedical Engineering, Polish Academy of Sciences, Warsaw, Poland

[*]jpoleszczuk@ibib.waw.pl

Recent global COVID-19 pandemic had a tremendous impact on healthcare systems throughout the world, with negative influence especially visible in non-critical care, such as rehabilitation or various screening programs, for which access was significantly reduced or completely revoked. Assessing the long-term impact of such a drastic temporal change and proposing a strategies that in case of future crises would help to reduce their negative impact, is of utmost importance. The aim of our research was to use mathematical modeling to address both abovementioned needs in case of colorectal cancer screening and follow-up programs, which are crucial for reducing the life years lost to colorectal cancer on a population level.

We advanced our established open-source microsimulation model CMOST [1,2] to simulate the effects of reduced healthcare system capacity and application of various patient stratification strategies on the natural history and medical costs of colorectal cancers. In CMOST, carcinoma develops via early and advanced adenoma precursors. Altogether six adenoma stages and four carcinoma stages are considered in the model. CMOST accounts for the gender- and age-dependent risks for adenoma development, the presence of multiple adenomas, as well as their locations within the colon. CMOST microsimulation tracks the history of a general population from birth until death for a maximum age of 100 years. Adenoma initiation, progression to advanced adenoma and cancer, cancer progression, screening and surveillance are all modeled in time increments of 3 months.

Using extended CMOST we ware able to show that for prolonged crisis which results in significant reduction of the healthcare system capacity the total number of incident colorectal cancers can increase by more than 10% in the long-term observation. However, we show that introducing even the simplest patient stratification scenario which takes into account patient-specific adenoma history and basic clinical characteristics can help to significantly reduce the abovementioned crisis-induced increase in incidence. We interrogated the model for various levels of capacity reduction and various stratification models, showing that introduction of stratification mechanism is always beneficial.

Our results support the need for the development of better patient stratification mechanisms in case when the capacity of the healthcare system is insufficient to perform all required colonoscopies. In the future we plan to use machine leaning models on the model-generated data to propose optimal stratification approaches.

References:
[1] Deibel A, Deng L, Cheng CY, et al. Evaluating key characteristics of ideal colorectal cancer screening modalities: the microsimulation approach. Gastrointest Endosc. 2021 Aug;94(2):379-390.e7. doi: 10.1016/j.gie.2021.02.013. Epub 2021 Feb 16.
[2] Prakash MK, Lang B, Heinrich H, et al. CMOST: an open-source framework for the microsimulation of colorectal cancer screening strategies. BMC Med Inform Decis Mak. 2017 Jun 5;17(1):80. doi: 10.1186/s12911-017-0458-9.

Chapter X

Texture Analysis in Biomedical Imaging

Session organizers:

Prof. Michał Strzelecki, Lodz University of Technology
Prof. Piotr Szczypiński, Lodz University of Technology

The quantification of the radiological features of osteoarthritis using scaled–pixel–counting protocol on the model of spavin in the horse's tarsal joint

Marta Borowska[1,*], Bernard Turek[2], Paweł Lipowicz[1], Tomasz Jasiński[2], Katarzyna Skierbiszewska[2], Małgorzata Domino[2]

[1]Institute of Biomedical Engineering, Faculty of Mechanical Engineering, Białystok University of Technology, ul. Wiejska 45 C, 15-351 Bialystok, Poland

[2]Department of Large Animal Diseases and Clinic, Institute of Veterinary Medicine, Warsaw University of Life Sciences, ul. Nowourynowska 166, 02-787 Warsaw, Poland

*Corresponding Author: m.borowska@pb.edu.pl

Aims: Joint disease, mostly osteoarthritis (OA), is one of the main causes of lameness failing the sports career in equine athletes [1]. As in the course of OA joint cartilage and underlying bone destruction appear, radiography is commonly used to identify structural changes in affected joints [2]. Although visual evaluation of radiographs is essential for OA diagnosis, there is a need to introduce radiographic rating systems to be able to quantify and thus track disease progression [3]. Therefore this study aims to quantify the radiological features of osteoarthritis using the new self–designed scaled–pixel–counting protocol.

Methods: The protocol was implemented on the model of spavin in the horse's tarsal joint. The dorso–plantar radiographs (60 keV, 1.26 mAs, 80 cm distance) of the tarsal joint were taken from twelve horses. Based on the visual evaluation of radiographs, six horses were classified into the healthy group and six horses into the spavin group. On each radiograph, II tarsal bone (II TB), III tarsal bone (III TB), IV tarsal bone (IV TB), central tarsal bone (CTB), proximal intertarsal joint (PIJ), distal intertarsal joint (DIJ), and tarsometatarsal joint (TMJ) were manually annotated. Thus seven regions of interest (ROIs) were selected for calculation. The irregular cuboid density standard (DS; Al; 95.20–98,88 Mass%; 92.71–98.92 Atom%) attached to the radiographic cassette was used as a ten steps (S1–S10) reference for pixel brightness (PB) counting. For each ROI, the percentage of pixels (% of NP) from each range was calculated. The % of NP was then compared between the healthy and the spavin groups for II TB, III TB, IV TB, CTB, PIJ, DIJ, and TMJ, separately using the Mann-Whitney test in Graph Pad Prism 6 software. The alpha value was established as $\alpha = 0.05$.

Results:
Considering the assessed bones, the % of NP in IITB, IIITB, and CTB was higher in the healthy than spavin group in S8 and S9 as well as higher in the spavin than the healthy group in S10. The % of NP in IVTB was higher in the healthy than the spavin group in S9 and higher in the spavin than the healthy group in S10. Considering the assessed joints, the % of NP in PIJ was higher in the healthy than the spavin group in S1, S3, and S4 as well as higher in the spavin than the healthy group in S10. The % of NP in DIJ was higher in the healthy than the spavin group in S8 and higher in spavin than the healthy group in S10. No other differences were found in II TB, III TB, IV TB, CTB, PIJ, DIJ, and TMJ.

Discussion and Conclusion:
The implemented self–designed scaled–pixel–counting protocol provides the quantitative radiological features of the healthy and spavin-affected structures in the horse's tarsal joint. The obtained differences in the % of NP correspond to the radiological features of osteoarthritis. A higher % of NP of the highest density (S10) indicates sclerosis of subchondral bone and mineralization front defects of the affected tarsal bones. Whereas, a lower % of NP of the lowest densities (S1, S3, and S4) together with a higher % of NP of the highest density (S10) suggests joint space narrowing of the affected joints. One may observe that the proximal intertarsal joint is affected more than the distal, whereas, no pathological changes are noted in the tarsometatarsal joint.

References:
[1] Baccarin R.Y.A., Seidel S.R.T., Michelacci Y.M., Tokawa P.K.A., Oliveira T.M. Osteoarthritis: a common disease that should be avoided in the athletic horse's life, *Animal Frontiers*, 2022, vol. 12, no.3, pp. 25-36
[2] Ley C. J., Björnsdóttir S., Ekman S., Boyde A., Hansson K. Detection of early osteoarthritis in the centrodistal joints of Icelandic horses: Evaluation of radiography and low‑field magnetic resonance imaging, *Equine Veterinary Journal*, 2016, vol. 48, no. 1, pp. 57-64
[3] Zubrod C.J., Schneider R.K., Hague B.A., Ragle C.A., Gavin P.R., Kawcak C.E. Comparison of three methods for arthrodesis of the distal intertarsal and tarsometatarsal joints in horses, 2005, *Veterinary Surgery*, vol. 34, no. 4, pp. 372–382

Texture Directionality Detection by means of Convolutional Neural Networks and interpolated Gray Level Co-occurrence Matrix

Marcin Kociołek

Institute of Electronics, Lodz University of Technology, Al. Politechniki 10, 93-590 Łódź, Poland
marcin.kociolek@p.lodz.pl

Texture is a rich source of information about the content of images from various modalities. One of the most important characteristics of an image texture is its directionality. The analysis of local directionality in the image finds a wide spectrum of applications ranging from cellular biology and medicine through materials science to astronomy. The two currently most popular methods of texture directionality analysis, based on the Fourier transform and local gradient orientation (LGO), have their limitations.

We propose the use of two relatively novel methods of directionality analysis in the image developed by us, one using an interpolated gray level co-occurrence matrix (iGLCM) [1] and the other based on convolutional neural networks (CNN) [2]. The iGLCM method is accurate, immune to noise and image blur, and allows for directionality analysis in arbitrary-shaped regions of interest (ROI). The method based on CNNs is extremely fast, still accurate and relatively resistant to noise and image blur, and limited to rectangular ROIs.

We have conducted extensive tests of the effectiveness of our methods, quantitative on artificial directional images and qualitative on real images. Our methods outperforms both the Fourier and the LGO based methods as it is shown in the table below [2][3] In addition, the methods developed by us work nicely on real images.

Gaussian noise std	CNN RMSE [°]	iGLCM RMSE [°]	Fourier RMSE [°]	LGO RMSE [°]
none	**0.00**	**0.00**	1.58	2.03
2000	0.01	**0.00**	1.70	2.11
4000	**0.06**	0.07	2.11	2.11
6000	0.23	**0.16**	2.93	2.43
8000	0.48	**0.31**	5.64	2.69
Blur kernel size	CNN RMSE [°]	iGLCM RMSE [°]	Fourier RMSE [°]	LGO RMSE [°]
none	**0.00**	**0.00**	1.58	2.03
3x3	**0.01**	**0.00**	2.42	2.61
5x5	0.07	**0.00**	3.16	1.27
7x7	2.79	**2.86**	4.41	3.41
9x9	5.81	6.00	5.29	**3.91**
# tiles tested	CNN [tiles/s]	iGLCM [tiles/s]	Fourier [tiles/s]	LGO [tiles/s]
178 605	**6613.3**	34.4	902.2	902.1

Our presentation at the PCBBE conference is aimed at offering cooperation in research works where directionality analysis is important. We offer our in-depth knowledge in this field allowing us to adapt our methods to your individual needs.

References:
[1] M. Kociolek, P. Bajcsy, M. Brady, and A. Cardone, "Interpolation-based gray-level co-occurrence matrix computation for texture directionality estimation," Signal Processing - Algorithms, Architectures, Arrangements, and Applications Conference Proceedings, SPA, vol. 2018-September, pp. 146–151, Dec. 2018, doi: 10.23919/SPA.2018.8563413.
[2] M. Kociołek, M. Kozłowski, and A. Cardone, "A Convolutional Neural Networks-Based Approach for Texture Directionality Detection," Sensors 2022, Vol. 22, Page 562, vol. 22, no. 2, p. 562, Jan. 2022, doi: 10.3390/S22020562.
[3] https://creativecommons.org/licenses/by/4.0/

List of Reviewers

The numbers in brackets indicate the number of reviews completed.

Piotr Augustyniak (5)

Paweł Badura (2)

Ryszard Białecki (4)

Dorota Bociąga (8)

Michał Bujacz (1)

Gerard Cybulski (4)

Marek Darowski (3)

Urszula Foryś (4)

Krzysztof Fujarewicz (5)

Marek Krzysztof Gzik (2)

Krzysztof Jastrzębski (1)

Mariusz Kaczmarek (5)

Bogdan Kaźmierczak (3)

Krzysztof Kędzior (1)

Artur Klepaczko (26)

Marcin Kociołek (2)

Piotr Korbel (3)

Józef Korbicz (4)

Małgorzata Kotulska (5)

Marek Kowal (4)

Aleksandra Królak (2)

Marzanna Kurzawa (4)

Marek Kurzyński (5)

Maciej Kusy (1)

Piotr Ładyżyński (3)

Katarzyna Lewandowska (6)

Roman Major (3)

Roman Maniewski (2)

Andrzej Materka (4)

Olivier Meste (5)

Marcel Młyńczak (2)

Tomasz Moskalewicz (1)

Zbigniew Nahorski (4)

Piotr Niedzielski (8)

Karolina Nurzyńska (2)

Damian Obidowski (1)

Andrzej Obuchowicz (4)

Mariusz Oszust (3)

Elżbieta Pamuła (9)

Krzysztof Patan (2)

Jolanta Pauk (5)

Wojciech Penczek (4)

Kazimierz Pęczalski (2)

Ewa Piętka (3)

Adam Piorkowski (3)

Leszek Podsędkowski (1)

Jan Poleszczuk (5)

Ketul Popat (4)

Valentine Provaznik (1)

Jacek Rumiński (4)

Alina Sionkowska (7)

Paweł Strumiłło (9)

Michał Strzelecki (10)

Andrzej Świerniak (4)

Piotr Szczypiński (7)

Jarosław Śmieja (5)

Zbisław Tabor (3)

Ryszard Tadeusiewicz (4)

Ewaryst Tkacz (2)

Bogdan Walkowiak (10)

Jacek Waniewski (4)

Jerzy Wtorek (4)

Bartłomiej Zagrodny (1)

Krzysztof Zielinski (5)